**Investigating the Potential of a Plasma-Activated Hydrogel Treatment for Infected Diabetic Foot Ulcers**

**Dominic Beith**

**35424506**

This thesis is submitted for the degree of Medical Sciences MSc by Research

Lancaster University

Lancaster Medical School

August 2021

# Abstract

**Introduction**: Diabetes mellitus is a metabolic disorder leading to multiple health conditions including diabetic foot ulcers (DFUs), which often become infected. Current therapies are ineffective and contribute to antimicrobial resistance (AMR). Therefore, new non-antibiotic treatments are required. Cold Atmospheric Plasma (CAP), an ionised gas, has the potential to resolve infection by delivering reactive species (RS) such as hydrogen peroxide ($H_2O_2$) deep into the wound. CAP can also be used to deliver antimicrobial drugs from a hydrogel dressing also known as plasma-activated hydrogel therapy (PAHT).

**Aim:** To investigate the potential of a PAHT for the treatment of infected DFUs.

**Methods:** A systematic review compared two bacterial detection techniques – 16S rRNA gene sequencing and conventional culture. The physical (electrical and optical) and chemical (RS delivery) characteristics of CAP jet were studied. Povidone-iodine (PVP-I) solution and PVP-I from a hydrogel (i.e. PVP-I–PAHT) exposed to CAP were assessed using UV-visible spectroscopy and agarose-starch assays. The antibacterial efficiency of PVP-I–PAHT was assessed using checkerboard synergy assay, Kirby-Bauer Assay, and a wound biofilm model.

**Results:** The review demonstrated the *Staphylococcal spp.* and *Pseudomonas spp.* predominance in DFUs. A low-power CAP jet, which can deliver up to 1.91 mM of $H_2O_2$ in solution was established. A potential formation of hypoiodous acid (HOI) was shown upon the interaction of PVP-I with CAP-produced $H_2O_2$. Complete eradication of an immature biofilm and a log 2 reduction against 1 hour incubated mature biofilms were observed with PVP-I–PAHT.

**Conclusion:** This is the first study to investigate the properties of plasma-activated PVP-I and the anti-microbial activity of PVP-I–PAHT against the bacteria specific to DFUs. It also highlights the role of $H_2O_2$ and HOI in CAP–PVP-I treatment of DFUs. An existing antimicrobial (PVP-I) was repurposed with non-antibiotic CAP technology which is important to combat the growing problem of AMR.

# Acknowledgements

To my supervisor's Dr Bhagirath Ghimire, Dr Nishtha Gaur, Dr Jemma Kerns, and Professor Rob Short. Thank you for all of your time and continued support given to me over the course of this MSc by Research. Bhagirath and Nishtha, thank you both for your guidance throughout this project and teaching me all of my laboratory skills that I have to date. Jemma and Rob, thank you both for this amazing opportunity to undertake a project under your supervision. But also, thank you for inviting me to be part of both of your lab groups of which you made me feel especially welcome. I feel my time this year under your guidance has been an invaluable for my academic and professional development.

I would also like to thank both Dr Bethany Patenall and Professor Toby Jenkins at the University of Bath for hosting me for my bacterial experiments and the mentorship that followed with learning new laboratory techniques.

# Declarations

The work in this thesis is as a result of my own work and where work has been undertaken in collaboration, it is stated here and explicitly in the text.

**Chapter 6**

Table 6.4: Minimum Inhibitory Concentrations for PAO1 and H560 against $H_2O_2$ and PVP-I. PAO1 results are reproduced from Dr B Patenall at the University of Bath.

# Dissemination of Research

- **Poster Presentation –** Cold atmospheric plasma as a potential treatment for diabetic foot osteomyelitis**,** Bone Research Society Annual Meeting, June 2021, Virtual. Abstract pending publication in Journal of Bone and Mineral Research Plus (JBMRPLUS).

# Table of Contents

# List of Tables

# List of Figures

XIII

# Acronyms and Abbreviations

| Full Name | Abbreviation |
|---|---|
| Accessory Gene Regulator | *arg* |
| Antibiotic Resistant Genes | ARGs |
| Antimicrobial Resistance | AMR |
| Argon | Ar |
| Artificial Wound Fluid | AWF |
| Brain-Heart Infusion Agar | BHIA |
| Cold Atmospheric Plasma | CAP |
| Colony Forming Unit | CFU |
| Critical Colonisation Threshold | CCT |
| Diabetic Foot Infection | DFI |
| Diabetic Foot Osteomyelitis | DFO |
| Diabetic Foot Ulcers | DFUs |
| Diabetes Mellitus | DM |
| Dielectric Barrier Discharge | DBD |
| Distilled Water | DIW |
| Elemental Iodine | $I_2$ |
| *Escherichia coli* | *E. coli* |
| Extracellular DNA | eDNA |
| Extracellular Polymeric Substance | EPS |
| Fine Needle Aspirate | FNA |
| Fractional Inhibitory Concentration | FIC |
| Functional Equivalent Pathogroup | FEP |
| High Voltage | HV |
| Horizontal Gene Transfer | HGT |
| Horseradish Peroxidase | HRP |
| Hour | h |
| Hydrogen Ion | $H^+$ |
| Hydrogen Peroxide | $H_2O_2$ |
| Hydroxyl Radical | OH• |
| Hypoiodous Acid | HOI |

| | |
|---|---|
| Inner Diameter | ID |
| Integrating Quorum Sensing Signal | IQS |
| Iodide | $I^-$ |
| Luria Bertani | LB |
| Luria Bertani Agar | LBA |
| Messenger RNA | mRNA |
| Methicillin-resistant *Staphylococcal aureus* | MRSA |
| Minimum Inhibitory Concentration | MIC |
| Muller Hinton | MH |
| National Health Service | NHS |
| National Institute for Health and Care Excellence | NICE |
| Nicotinamide Adenine Dinucleotide Phosphate | NADPH |
| Nitrate Ion | $NO_3^-$ |
| Nitric Acid | $HNO_3$ |
| Nitric Oxide | NO |
| Nitrogen Dioxide | $NO_2$ |
| Nitrogen Second Positive System | $N_2SPS$ |
| Operational Taxonomic Units | OTUs |
| Optical Emission Spectroscopy | OES |
| Outer Diameter | OD |
| Overnight | ON |
| Ozone | $O_3$ |
| o-phenylenediamine | ODP |
| Penicillin Binding Protein | PBP |
| Peroxinitrite | $ONOO^-$ |
| Peroxynitrous acid | NOOH |
| Phosphate Buffer Solution | PBS |
| Plasma-Activated Hydrogel Therapy | PAHT |
| Plasma-Activated Water | PAW |
| Polymerase Chain Reaction | PCR |
| Polysaccharide Intercellular Antigen | PIA |
| Polyvinylpyrrolidone | Povidone |
| Polyvinyl Alcohol | PVA |
| Potassium Iodide | KI |

| | |
|---|---|
| Povidone-Iodine | PVP-I |
| *Pseudomonas Aeruginosa* | *P. aeruginosa* |
| Pseudomonas Quinolone Signal | PQS |
| Quorum Sensing | QS |
| Radical | $\bullet$ |
| Randomised Control Trial | RCT |
| Reactive Nitrogen Species | RNS |
| Reactive Oxygen and Nitrogen Species | RONS |
| Reactive Oxygen Species | ROS |
| Ribosomal RNA | rRNA |
| Singlet Oxygen | $^1O_2$ |
| Sodium Nitrite | $NaNO_2$ |
| Standard Litres Per Minute | SLPM |
| *Staphylococcal aureus* | *S. aureus* |
| Staphylococcal Accessory Regulator | *sarA* |
| Superoxide | $O_2^-$ |
| Triiodide | $I_3^-$ |
| Trypticase Soy Agar | TSA |
| Trypticase Soy Broth | TSB |
| Ultraviolet | UV |
| Ultraviolet Visible Spectroscopy | UV-VIS |
| United Kingdom | UK |
| United States of America | USA |
| University of Texas Classification | UT |
| Whatman®nuclepore™ track-etched membrane discs | WM |

# 1  Chapter 1 : Introduction

## 1.1  The Clinical Problem - Diabetes Mellitus and Diabetic Foot Ulcers

Diabetes Mellitus (DM) defines a collection of metabolic disorders featuring a chronic state of hyperglycaemia. They are caused by a defect in the anabolic hormone, insulin, which alters its secretion, its activity, or both. DM can be broadly classified based on its pathology as shown in Table 1.1. Polyuria, polydipsia, weight-loss, polyphagia and blurred vision are all symptoms of chronic hyperglycaemia. If left uncontrolled, DM is a life-threatening illness, with the development of symptoms such as stupor or coma from sequalae such as ketoacidosis or hyperosmolar hyperglycaemic nonketotic syndrome.[1, 2] As a consequence of DM, the marked hyperglycaemic state produces a myriad of multi-systemic damage leading to diabetic foot ulcers (DFUs), atherosclerosis, and neuropathy among many others.[1] This chapter aims to review the clinical problem of DM and DFUs, its pathophysiology and classification, as well as discuss the available and upcoming adjuvant treatment options.

*Table 1.1: General classification of DM. [3]*

| Category | Definition |
|---|---|
| Type 1 | Autoimmune β-cell destruction causing complete insulin deficiency. |
| Type 2 | Progressive loss in β-cell insulin secretion following resistance. |
| Gestational DM | DM presenting from the start of the second trimester of pregnancy that did not exist pre-gestation. |
| Specific Types | Neonatal diabetes; maturity-onset diabetes of the young; diseases of the exocrine pancreas; chemical induced diabetes |

Unfortunately, although advances have been made in the management of hyperglycaemia with the advent of exogenous insulin, the incidence of complications such as DFUs is forever increasing as patients are able to live longer with DM. The formation of DFUs is thought to be triggered by a triad of causes: neuropathy, ischaemia and infection.[4]

In the most recent prevalence model of the disease[5], it was estimated that 4.7 million people in the United Kingdom (UK) were living with DM, with an estimated 900,000 living asymptomatically with the Type 2 DM.[6, 7] By 2030, the number of cases in the UK is expected to be at 5.5 million. Type 2 DM constitutes 90% of the total number of cases, with Type 1 and other forms at 8% and 2% respectively.[6] Not only is the prevalence of DM increasing, but there is also a huge economic burden

associated with this disease for all health services, and of most relevance, the National Health Service (NHS). Hex, N *et al.*[8] reports that the management of DM costs £27 million per day, accounting for 10% of the total spending for the NHS as well as the cost of DFUs alone at £650 million per year. Otherwise put, £1 in every £150 spent by the NHS is attributed to the management of DFU.[9]

DM is not only a problem for the UK, but is now considered a worldwide pandemic. The International Diabetes Federation[10] reported that the worldwide prevalence of DM in 2019 was 463 million, equating to 9.3% of adults aged 20-79. Of the 463 million cases, 79% of cases were found in low- to middle-income countries with 87% of the deaths. Worryingly, in less than 20 years, the number of people worldwide diagnosed with DM has more than tripled, already surpassing the 2025 estimation set back in 2000 of 438 million.

The aetiology of DM has a strong genetic element with ethnicity reported as a large variable. South Asian and black ethnicities are estimated to have up to a four-fold increase in the risk of developing Type 2 DM when compared to white people.[11] DMs' aetiology extends beyond strict biological causes; with environmental, demographic, and socioeconomic factors playing crucial roles in its pathogenesis. The large increase in cases could be attributed to an increase in Type 2 DM as lifestyles have changed in order to facilitate less active and unhealthy lifestyles; and an increase in childhood-onset Type 1 DM is also now being reported. The International Diabetes Federation[10] reports that by 2030, an expected 578 million adults could be living with DM and an estimated 700 million by 2045. The continuing exponential increase in prevalence of DM will only put further pressures on health services worldwide to treat the complications of this disease and of most interest in this work, DFU.

## 1.2 The Pathophysiology of DFUs

DFUs are one of the highest risk complications with DM,[12] with the lifetime risk of developing a foot ulcer between 10-25%.[9, 13, 14] DFUs are also a major risk factor for non-traumatic lower limb amputation, with 85% of all lower limb amputations attributable to them.[9, 15, 16] The life expectancy for individuals with DM is reported to be shortened by up to 15 years with 75% of deaths attributable to macro vascular pathology. As the acquisition of a DFU is a marker of DM chronicity,[17] the 5-year mortality rate following an ulcer development is 50%. Following amputation, the 5-year mortality rate is 70%.[9] According to Pendsey, S[18], the formation of a DFU is a consequence of the triad of peripheral neuropathy, peripheral vascular disease, and infection occurring simultaneously. It is such that a DFU can be defined as a break in the cutaneous surface, associated with neuropathy and vascular disease within a diabetic.[19]
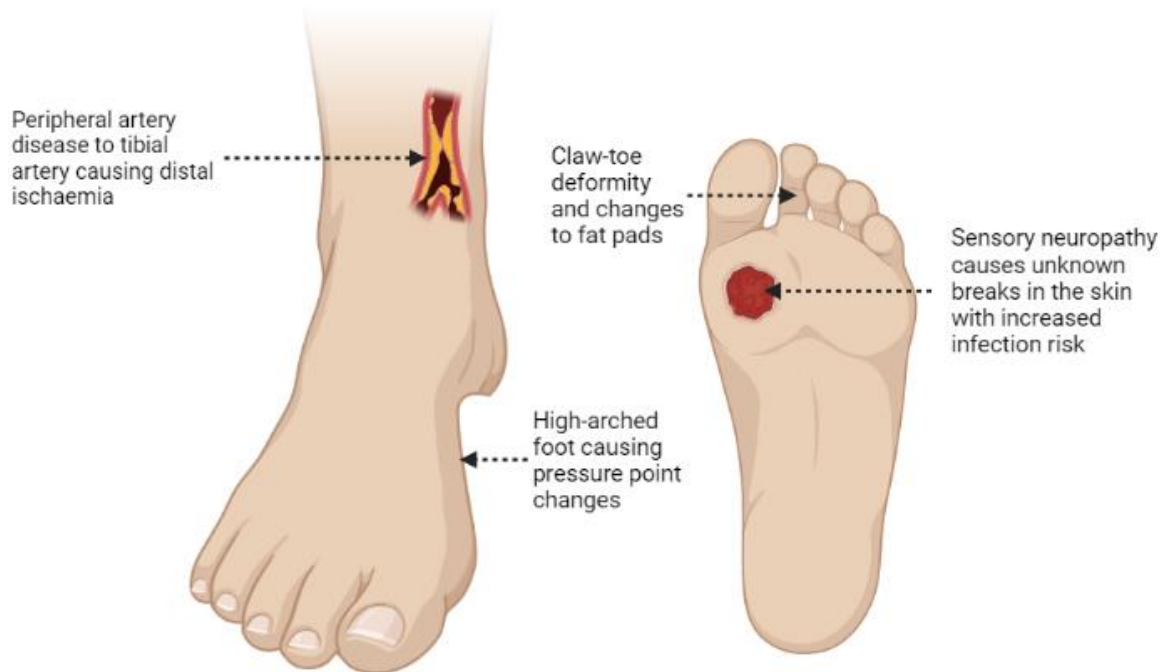
*Figure 1.1: Schematic of the changes caused in DFUs by peripheral neuropathy, peripheral vascular disease and infection. (Created by D Beith, in BioRender.com).*

## 1.2.1.1 Peripheral Neuropathy

DM causes chaos within the nervous system of the body, leading to axonal degeneration[20] and manifesting clinically as motor, autonomic and sensory dysfunction.[18] It is estimated that up to 60% of DFUs are complicated by neuropathy.[17, 21]

The polyol pathway has been described as the mechanism for diabetic neuropathy.[22] Hyperglycaemia leads to an increase in carbohydrates, sorbitol and fructose, from intracellular glucose through the upregulation of aldose reductase and sorbitol dehydrogenase. As sorbitol and fructose accrue within the neuron, there is disruption to the synthesis of myoinositol[21] which is crucial for axonal propagation.[23] Disruption also causes a decrease in nitric oxide as well as an increase in reactive oxygen species (ROS). Together, the oxidative stress through ROS and apparent vasoconstriction from the depleted nitric oxide ultimately leads to neuronal damage.[21]

As a result of neuronal damage, motor dysfunction leads to de-innervation of the small muscles of the foot, causing permanent architectural changes to the foot. Development of a high-arched foot and a claw-toe deformity mean that pressure points of load are shifted and new bony prominences are formed[18], otherwise known as Charcot's neuroarthropathy.[24] It is also reported that as a result of atrophy within the foot, positions of important cushioning fat-pads are altered such that new areas now pose a threat to cutaneous breakdown.[25]

Secondly, autonomic damage causes the downregulation of sweat and oil glands leading to anhidrosis or the absence of sweating.[25] Absence of sweating causes cracks to appear as the skin becomes more keratinised, increasing the chance of bacterial infection.[26] Autonomic dysfunction also causes loss of lower limb peripheral vascular resistance, and thus increasing the arterial pressure and subsequent damage to the capillary basement membrane. The result is peripheral oedema, whereby patients are forced to wear ill-fitting shoes in order to ambulate, and adding to the risk of a new ulceration.[25]

Lastly, sensory neuropathy is additive to the aforementioned motor and autonomic dysfunction. Loss of sensation of the foot exacerbates pre-existing damage as patients are unable to sense pain and take reactive precautions.[21] The patients with sensory dysfunction are seven times more likely to develop a foot ulcer than those without.[27]

## 1.2.1.2 Peripheral Vascular Disease

Along with neuronal damage, peripheral vascular disease leads to vessel wall thickening or atherosclerosis within the foot.[15] Atherosclerosis is more generalised in diabetic patients and has accelerated disease progression. Occlusion of crucial arteries such as the tibial artery, peroneal artery, as well as the smaller blood vessels that supply the toes mean that any DFUs present on the foot, may not only be triggered through ischaemic causes, but the apparent ischaemia will enhance already delayed wound healing.[28] The vasoconstrictor and platelet aggregation agonist, Thromboxane A2, facilitates a hypercoagulable state within diabetes. Potential thrombus formation coupled with vasoconstriction on already narrow arteries is a perfect storm for widespread peripheral ischaemia.[21]

## 1.2.1.3 Infection

A diabetic foot infection (DFI) is defined as an infection in soft tissue below the malleolus (ankle). Patients with DFUs are at a high risk of infection and it is the most frequent cause of hospital attendance in diabetics, with a yearly infection risk of 7% for those with foot ulcers.[26]

Infection starts when there is a break in the cutaneous surface, either through trauma or through ulceration from the aforementioned peripheral neuropathy or peripheral vascular disease. DFI are often polymicrobial in nature, with Gram-positive cocci such as *Staphylococcus aureus* (*S. aureus*) and Gram-negative bacilli such as *Pseudomonas aeruginosa* (*P. aeruginosa*) and *Escherichia coli* (*E. coli*) most common.[26, 29] Chapter 2 of this work aims to explore the bacteriology of DFUs in greater detail.

DFIs are particularly disastrous to the patient due to the communicating anatomical compartments within the foot and ankle. There are several indefensible structures within the foot, such as the plantar aponeurosis and associated tendons which provide limited resistance towards the contiguous spread of bacteria.[18] It is as such, that DFI pose a spectrum of risk, from uncomplicated to limb-threatening disease from resistant strains such as methicillin-resistant *Staphylococcus aureus* (MRSA).[24]

## 1.2.1.4 Osteomyelitis

The etymology of the word osteomyelitis is from the Greek language with the combination of *Osteon, myelon* and *itis*. Together, it can be defined as the spread of bacteria into the bony compartments of the foot, otherwise known as diabetic foot osteomyelitis (DFO). DFO is a common disease within DFIs. An estimated 10-15% of moderate and 50% of severe infections are complicated by DFO.[24, 30] The risk of amputation for those with DFO is four-fold higher than those with a DFI[31] and it most commonly complicates the forefoot in 90% of cases[24] with the first and fifth metatarsal heads being prime targets.[31]

## 1.3  Classification of DFUs

Classification systems are used within healthcare to facilitate accurate descriptions of a disease, and in this case DFUs, between health-care professionals. This can then inform important choices about suitable investigations and treatment options for the individual. They can also be an integral part of research methodology whereby inclusion and exclusion criteria for participants are based upon these.[32] This work aims to provide an overview of the three commonly used classification tools to grade DFUs: Wagner Classification (Table 1.2), and the University of Texas Classification (UT) (Table 1.3).

The first tool, Wagner Classification, utilises the grade the DFUs (0 through 5) to describe depth and presence of infection or ischaemia.[33] Grade 0 describes a patient who has DM and may exhibit a peripheral neuropathy or evidence of peripheral vascular disease, but there is no cutaneous breakage yet. Grade 3 describes the first evidence of DFI, either as a simple infection or as DFO. Grade 4 and 5 describes DFU with ischaemia.

UT[34] is the second tool and is currently suggested to use for the classification of DFUs by National Institute for Health and Care Excellence, UK[9] (NICE). UT provides a similar grading experience for DFUs, 0 through 3. But unlike the Wagner Classification[33], the assessment of depth of the ulcer is

independent to the presence of infection and ischaemia. It therefore allows for a more in-depth description of DFUs, where a Wagner Grade 1 may exist with infection, but unable to communicate it unlike a UT Grade IB. Both UT and Wagner Classifications grade the existence of ischaemia as a worse prognostic factor than the presence of infection, be it DFI or DFO.[35]

*Table 1.2: Wagner Classification for Diabetic Foot Ulcers.[33]*

| Wagner Classification | |
|---|---|
| **Grade 0** | Pre-Ulcer. Skin intact, no open lesion. |
| **Grade 1** | A superficial ulcer without penetration of subcutaneous fat layer. |
| **Grade 2** | A full thickness ulcer which penetrates through fat and tendon. |
| **Grade 3** | A deep ulcer which may or may not probe to bone, with abscess, osteomyelitis or joint sepsis. |
| **Grade 4** | Gangrene of a geographical area of the foot. Not limb-threatening. |
| **Grade 5** | Gangrene to the extent that foot is beyond salvage. |

*Table 1.3: University of Texas Classification for Diabetic Foot Ulcers.[34]*

| University of Texas Classification | | | |
|---|---|---|---|
| **Grade** | | | |
| **0** | **I** | **II** | **III** |
| Pre- or post-ulcerative lesion completely epithelialized | Superficial wound not involving tendon, capsule or bone | Wound penetrating to tendon or capsule, not bone | Wound penetrating to bone or joint |

| | |
|---|---|
| **A** | Absence of Infection and Ischaemia |
| **B** | Grade A0-III + Infection |
| **C** | Grade A0-III + Ischaemia |
| **D** | Grade A0-III + Infection and Ischaemia |

## 1.4 Treatment of DFUs

Treatment for DFUs continue to remain difficult despite the established long-standing principles of standard wound care.[36] And even after treatment, patients still have a high recurrence rate of 40% within a year.[37] Arguably the father of management, Dr Frederick Treves[38], reported a new way to treat DFUs in 1884: (i) surgical debridement; (ii) wound irrigation; (iii) infection prevention; and (iv)

supportive footwear. This would be later recognised as the three pillars of standard care: off-loading, sharp debridement, and patient education.[39]

NICE National Guideline 19[9] for DFUs without infection or ischaemia recommends a non-removable cast as an off-loading device. Alternatively, wound debridement and appropriate wound dressing are also recommended where needed. If infection is present, wound or bone samples are collected from the base of a debrided DFU before identification and subsequent commencement of antibiotic therapy (Section 1.5).[40]

Because of the difficulty in association with the treatment of DFUs, one of the major challenges patients and clinicians face is their long exposure to broad-spectrum antibiotics following infection for anywhere up to 6 months. Alongside the patient-centred challenge of drug concordance over the long period of time, there is the accompanying risk of widespread contribution to antimicrobial resistance (AMR). *S. aureus* already exists within DFUs as one of the most predominant organisms, extensive exposure to powerful antibiotics may promote further resistance, such as MRSA, which has shown to prevent wound healing through biofilm formation.[41] Long antibiotic courses and the growing risk of resistant strains may mean that surgical management is preferred thus increasing the amputation rate in DFUs in the future.[42] Currently, there is still no effective treatment that prevents the amputations seen in 15% of DFU patients.[43] This has encouraged research into alternative novel or repurposed therapies for DFUs.

Of particular interest to this piece of work is Plasma Medicine. Plasma Medicine is an evolving field of research combining plasma physics, life science and clinical medicine in order to facilitate the use of physical plasma in novel therapeutic applications.[44] Cold Atmospheric Plasma (CAP) generated using plasma jets and directed onto the wound has the potential to resolve infection and improve vascularisation; both needed for wound healing. Within the literature, it has been hypothesised that CAP has the ability to destroy complex diabetic foot biofilms through the generation of reactive oxygen and nitrogen species (RONS) along with other plasma components such as electrons, ions, ultra-violet radiation, electromagnetic field etc. Of importance to DFO, Tominami, K[45] reported that when CAP was directed onto osteoblasts, alkaline phosphatase was upregulated as well as increasing mineralisation of bone. Although the randomised clinical trial landscape is sparse within Plasma Medicine, early studies within humans[43, 46, 47] have shown promising results. CAP eradicates infection, upregulates beneficial mediators of wound healing such as growth factors, increases cellular proliferation, and promotes angiogenesis.[48] Chapter 3 aims to outline the field of CAP and its mechanisms against relevant bacteria.

## 1.5 Antibiotics

Antibiotics are used readily within modern-day healthcare and are substances aimed to stop infections and eradicate bacteria.[49] The first written evidence of the use of an antibiotic-producing microbe to treat disease was noted in 1550 BC whereby mouldy bread was used as a treatment for chronic wounds. Early in the 20th century, Paul Ehrlich developed the first anti-infective chemotherapy drug, salvarsan, which is a synthetic arsenic-based pro-drug used to treat the cause of syphilis, *Treponema pallidum*.[50] Almost two decades later in 1929, the serendipitous series of events that would lead Fleming to discover penicillin, would mark the start of the antibiotic age.[51, 52]

Antibiotic mechanisms can be grouped into three main categories based on their mechanisms of action: cell wall synthesis disruption, nucleic acid synthesis disruption and disruption of protein synthesis, as shown in Figure 1.2.
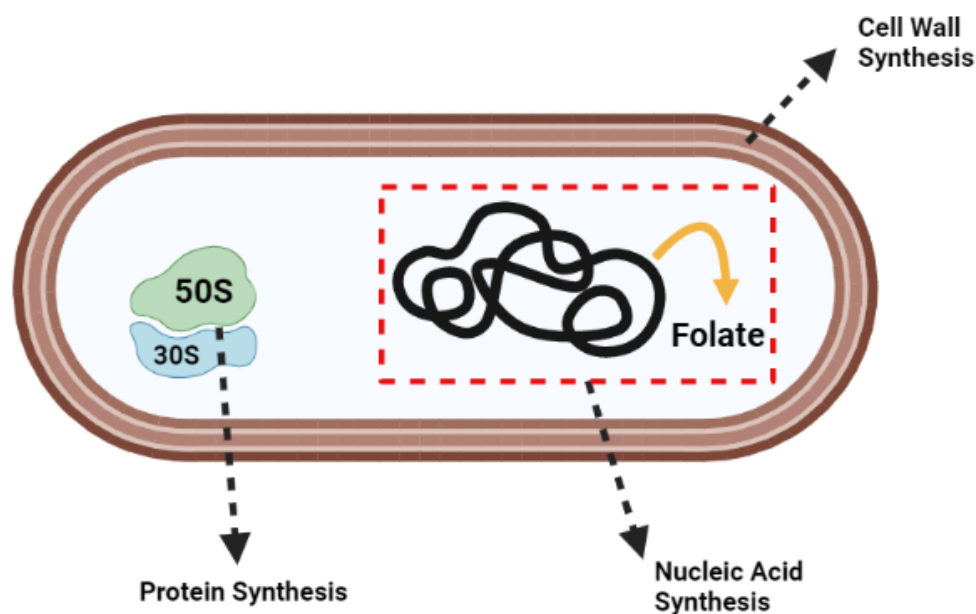


*Figure 1.2: Antibiotic Targets. (Created by D Beith, in BioRender.com).*

The first category of antibiotics cause disruption to the synthesis of the cell wall. The enzyme transglycosidase is an important enzyme in the maintenance of cell wall rigidity within bacteria. It cross-links the glycan strands by connecting the peptide chains to the polymer sugars. Within the added peptide chain, the D-alanyl-alanine portion later becomes cross-linked with a penicillin binding protein (PBP) in order to increase the cell wall strength.[53]

Of the first category, two main groups of antibiotics disrupt cell wall synthesis, β-lactams and glycopeptides. β-lactams, such as penicillin, cephalosporins and carbapenems, target PBP. The β-lactam ring of the antibiotic interrupts cell wall synthesis through replacement of the D-alanyl-D-

alanine portion with its ring and inhibiting peptide bond formation with the PBP. In doing so, the terminal stage of peptidoglycan synthesis cannot occur. Glycopeptides, such as Vancomycin, aim to inhibit cell wall synthesis through binding to the D-alanyl-alanine portion of the peptide chain and blocking the action of transglycosidase. The resultant of both β-lactams and glycopeptides is a cellular stress leading to lysis.[54]

The second category of antibiotics disrupt nucleic acid synthesis by inhibiting the process of folic acid synthesis or DNA replication. Antibiotics such as sulphonamides and trimethoprim are both folic acid synthesis inhibitors, which inhibit the synthesis of p-amino benzoic acid and enzyme dihydrofolate reductase, respectively, which are important to folate synthesis pathway.[55] Antibiotics such as fluoroquinolones disrupt DNA replication by inhibiting the function of enzyme DNA gyrase, which is important to prevent excessive positive coiling in the ds-DNA. DNA gyrase consists of subunits A and B. Subunit A is inhibited when fluoroquinolones are bound and consequently are unable to cut the ds-DNA before supercoiling and strands are unable to replicate or transcribe affectively.[56]

The last of the antibiotic category are those that disrupt protein synthesis. Protein synthesis transforms messenger RNA (mRNA) into a polypeptide chain through a four-stage process: initiation, elongation, termination, and recycling. Within prokaryotes, protein synthesis occurs within 70S ribosomes, comprised of 50S and 30S ribonucleoprotein subunits.[55] The larger 50S subunit is responsible for the elongation process within protein synthesis and the 30S subunit contains 16S ribosomal RNA (rRNA) which initiates protein synthesis through binding with mRNA.[57] Individual classes of antibiotics affect each ribosomal subunit to disrupt either of the four stages of protein synthesis. All the antibiotics above are summarised in Table 1.4.

One of the issues surrounding the use of antibiotics for the treatment is the development of resistance against them, decreasing their efficacy to resolve infection. Their overuse within medicine and decrease in the rate of discovery has meant that resistance is a striking concern which will covered in the next section.[58]

*Table 1.4: Examples of antibiotics that inhibit protein synthesis and mechanism of action.*

| Class of Antibiotic | Subunit Target | Mechanism of action | Reference |
|---|---|---|---|
| Macrolides<br><br>Lincosamides<br><br>Streptogramin B | 50S | Targets the 23S rRNA contained within the 50S subunit and causes detachment of the peptide chain and incomplete translation, thus inhibition. | 57 |
| Chloramphenicol | 50S | Prevents the binding of tRNA to the A-site of the 50S ribosome, thus affecting translation. | 55 |
| Oxazolidinone | 50S | Binds to the 50S subunit and prevents t-RNA binding to the A-site. Also, globally supresses the 70S ribosome. | 59 |
| Aminoglycoside | 30S | Aminoglycosides create a pore and penetrate into the bacterium to interact with the 16S rRNA causing misreads and termination of mRNA translation | 60 |
| Tetracyclines | 30S | Prevents tRNA binding to the A-site of 16S rRNA. | 61 |

# 1.6 Antimicrobial Resistance (AMR)

AMR describes a process of change where micro-organisms develop traits over time making current treatments such as antibiotics less effective or completely ineffective.[62] It is a huge concern globally with an ever-increasing incidence of patients dying from common bacterial infections.[63] An economics report published in 2016 by O'Neill[64] confirmed this with a worrying projection for the death toll attributable to resistant bacterial infections in 2014 at 700,000 deaths. Unless AMR is tackled by 2050, it is thought that we could expect to see AMR-complicated bacterial infections be the biggest killer globally and attributable for 10 million deaths per year, ahead of cancer as a cause of death. Alongside the grave risk of AMR is the economic burden associated with it. It is estimated that by 2050, the cost of AMR will be at 100 trillion USD per year as current therapies now offer diminishing returns.[64]

AMR is not a new concept. Antibiotic resistant genes (ARGs) have existed for millions of years, slowly accruing over time with the agricultural environment acting as an important reservoir for the transfer of these genes.[65] The use of antibiotics within agricultural foods has been linked with AMR-related infections within humans. It is reported in the literature that the ingestion and exposure to animals treated with antibiotics promotes resistant colonisation in the gut and on the skin (Figure 1.3).[66]
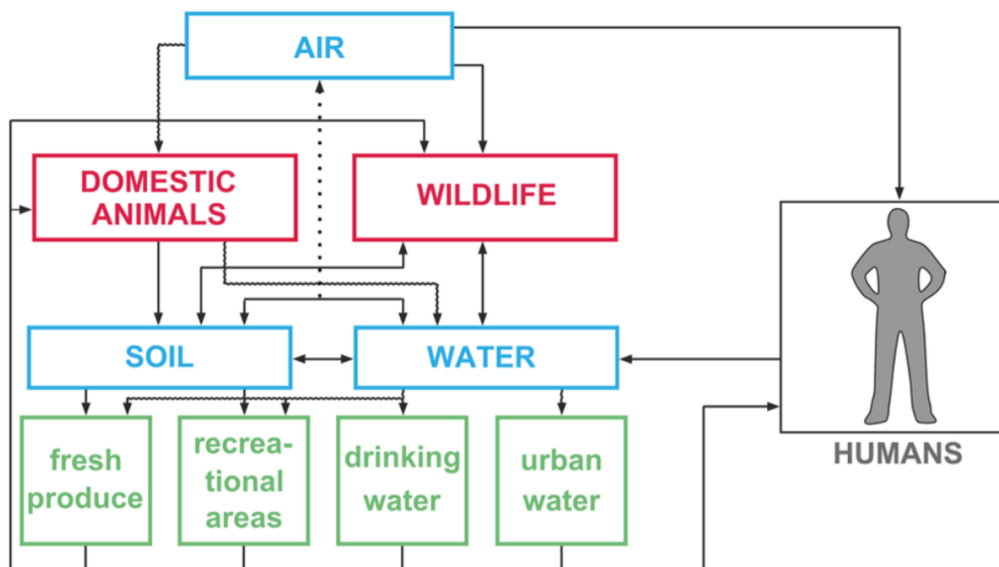


*Figure 1.3: Schematic of the transfer of AMR between humans and the environment. (Reproduced with permission from Environmental Science & Technology).[67]*

The first reported case of human-intervention induced AMR occurred in 1941 following the introduction of penicillin into clinical medicine the previous year. Strains of *Escherichia. Coli* were detected in 1941 to be producing penicillinase, an intracellular enzyme, which inactivates penicillin. Of more importance to DFUs, Rammelkamp[68] observed one of the first cases of penicillin-resistant *S. aureus* in 1942. By 1960, it was reported that in excess of 80% of all *S. aureus* were resistant.[51]

The origins of AMR in bacteria can be split into natural resistance and acquired resistance. Natural resistance of an organism can be defined as a trait which is constantly expressed by the species, irrespective of exposure to antibiotics. For example, in Gram-negative bacteria, the lipid-rich nature of their cell membrane infers resistance to antibiotic penetration.

Acquired resistance of a bacterium is through the horizontal gene transfer (HGT) which facilitates the transfer of ARGs between species or through genetic mutations. Mutations resulting in AMR act through a variety of mechanisms.[69] A mutational resistance in a bacterium is identified when a bacterium survives after the administration of an antibiotic (at a concentration above a normal killing threshold). Those microorganisms who have survived are known to have ARGs which alters the response of the microorganism to the drug and hence enhance the capacity of the microorganism to survive mechanism of action of the drug.[70]

For instance, the mutations can change the drug-binding site on the bacteria surface/membrane, which leads to decreased drug affinity. One example of this is the *mecA* gene. The initial mechanism behind methicillin resistance was not discovered until 1981 where it was found that the *mecA* gene located on staphylococcal cassette chromosome *mec* was responsible for a change in the penicillin-binding protein-2a which causes reduced affinity for penicillin. This is one of the first examples illustrating the effect of AMR and through mechanisms such as HGT, the binding site has changed.[51, 71] Other resistance mutations are through decreased penetration or active efflux of the antibiotic out of the bacteria. Finally, the most drastic mutation is a change in metabolic pathway so that the antibiotic no longer targets it [70, 72].

Differences in the genes expressed by the bacteria within a biofilm compared with a planktonic bacterium can change their therapeutic characteristics.[73-75] Biofilms show decreased susceptibility to antibiotics leading to inadequate bacterial resolution and treatment failure. One of the mechanisms by which decreased susceptibility occurs is due to the extracellular polymeric substance (EPS), which prevents the penetration of antibiotics. A therapeutic dose does therefore not accumulate inside the bacteria, for example from active efflux of the antibiotic via channels in the cell membrane, and thus treatment failure.[76] The decreased metabolic state of bacteria within the biofilms mean that they are able to withstand the antibiotic for much longer than planktonic bacteria.[77]

# 2 Chapter 2: Bacteriology of DFUs

## 2.1 Aim

In order to develop a novel treatment for DFUs, the first issue faced is to determine the bacteriology of their wounds. Therefore, the aim of this chapter is to (i) provide an overview of bacteria and detection methods and (ii) determine the predominant bacteria found within DFUs through the completion of a systematic review comparing two diagnostic techniques. Bacteria and the mechanisms behind bacterial infections will be outlined in Section 2.2. A systematic review of broad-range 16S rRNA gene polymerase chain reaction (PCR) compared to conventional microbiological culture will then be performed using the operators outlined in Section 2.3 in PubMed and Web of Science databases. Section 2.4 investigates the characteristics of each dataset and compares the predominant aerobic species or genera as well as the predominate obligate anaerobes found within DFUs. Outcomes from this systematic review will later inform the experiments and result carried out in Chapter 6 using the predominant bacteria found in DFUs. Outcomes between broad-range 16S rRNA gene PCR differences in bacteria detected and to postulate how both diagnostic modalities could be used within a clinical environment.

## 2.2 Introduction

DFIs are often chronic with a polymicrobial predominance. Up to 70% of all DFIs are polymicrobial and where monomicrobial infections are seen, it is often in an acute infection only.[1] Monomicrobial infections are most commonly complicated by *S. aureus* or *Streptococci* organisms whereas polymicrobial infections see an increase the predominance of Gram-positive cocci, and Gram-negative bacilli such as *Pseudomonas spp.*, as well as anaerobes. Polymicrobial infections are highly prevalent in prolonged infection and in high Wagner grade wounds.[78, 79] The bacterial species cultured are affected by a variety of conditions, such as foot hygiene, previous antibiotic use and lower limb flora. Although data for DFUs with bacterial infections is readily available, there is a distinct lack of research surrounding the effect of fungal infections in DFIs despite being readily cultured. [80] There are many microbes to study but covering all of them is beyond the scope of this study. Therefore, this thesis will focus only on bacteria found in DFUs.

The morphology of bacteria can be determined by their shapes (cocci, rods, spirals) and through their patterns of aggregates (pairs, chains, tetrads, clusters). Unlike human eukaryotic cells, bacteria contain no membrane-bound organelles. Bacterial traits such as presence of flagella, and number of fimbriae are typical of a genus, and so are used diagnostically alongside important staining techniques.[81] A schematic of the structure of a bacterium is shown in Figure 2.1.
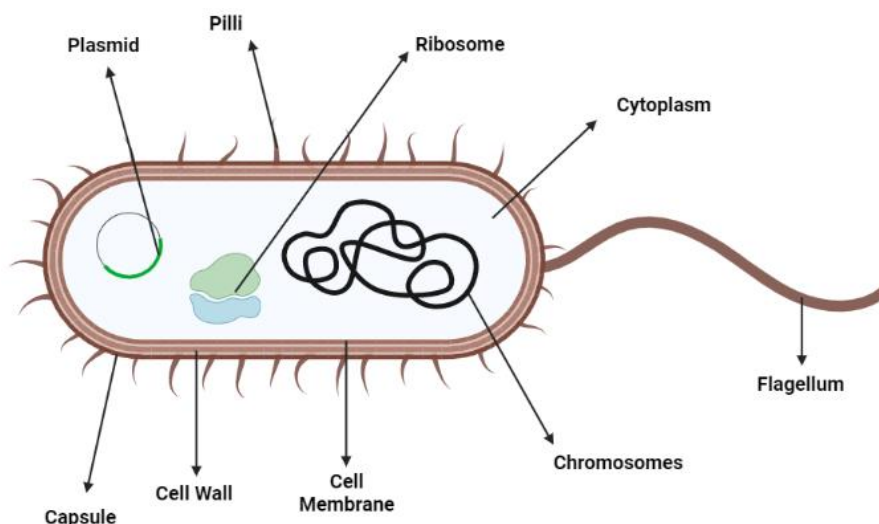


*Figure 2.1: Diagram of the structure of a bacterium. (Created D Beith in BioRender.com).*

Christian Gram[82] developed the gram staining technique for light microscopy, initially to identify organisms that caused pneumonia. Gram-staining allows for the identification of bacteria into two main groups: Gram-positive (such as *S. aureus*) and Gram-negative (such as *E. coli* or *P. aeruginosa*)

bacteria. The basis for these differences lies within the structural differences of their cell envelope.[83, 84] Bacterial cell walls are layers of peptidoglycan which lie externally to their plasma membrane. Compared to their Gram-positive counterparts, Gram-negative bacteria have much a thinner and more lipid-rich peptidoglycan cell wall containing a periplasmic space.[85]

## 2.2.1  Bacterial Infections

A wound infection is defined as the presence of a sufficient number of bacteria or bacteria of sufficient virulence to trigger a host response, determined from the critical colonisation threshold (CCT).[86] The concept of the CCT has was first presented by Davis, E[87] in 1996. Davis initially described the four stages for a wound to become infected: sterile, colonised, critically colonised, and infected. This concept was later revised into five phases to better correlate with clinical progress and interventions and now includes the fifth, systemic infection. The CCT describes a pivotal stage within wound infection by which bacteria colonise the wound in the absence of invoking a host response. The different phases of CCT are described in Table 2.[88]

It is the interface between the second and third phase which determines CCT. From this point onwards, the planktonic bacteria that previously inhabited the wound have now transformed into thick aggregates (a biofilm) exceeding $10^4$ colony forming units (CFU) and an intervention is required in order to resolve the infection.[88] The role of biofilms in DFI are discussed in detail below (Section 2.2.2)

| Phase | Description |
|---|---|
| Phase 1: Contamination | Microorganisms from the surrounding normal flora can be detected in the new wound. Bacterial numbers are neither sufficient nor virulent enough to invoke a host response and so may resolve at any time. |
| Phase 2: Colonisation | Growth of the microorganisms within the wound, but still in the absence of an immune response or interrupted healing. |
| Phase 3: Critical Colonisation | Proliferation and maturation of bacteria causes mild symptoms of infection such as fever. |
| Phase 4: Infection | Increase in bacterial count coupled with an increase in the strength of virulence causes the patient to exhibit more obvious signs of infection such as delayed wound healing and wound erythema (redness). |
| Phase 5: Systemic infection | Infection spreads via vascular and lymphatic routes, leading to sepsis and organ dysfunction |

## 2.2.2 Biofilms

DFIs are more commonly caused through a biofilm model of infection.[73] A biofilm is defined as an aggregation of microbes irreversibly attached to a surface, covered in a exopolysaccharide matrix.[89] Up to 78.2% of chronic wounds infections are populated by biofilms as opposed to 9% in acute infections.[90, 91] As diabetic wounds often remain unhealed and thus chronic, the focus of future medical therapies aims to eradicate biofilms.[72] The stages of biofilm formation are illustrated in Figure 2.2.

An infection will start when there is a disruption in the cutaneous surface. In the case of DFIs, disruption to the foot is either through direct trauma or through ulceration.[26, 73] Potentially pathogenic planktonic bacteria then enter the wound. Planktonic bacteria are defined as freely suspended bacteria that are reversibly attached to their surface with the ability to divide exponentially inside the wound and this is shown as Stage 1, Figure 2.2.[92] The second stage involves multiplication of the planktonic bacteria and irreversible attachment of the bacteria to the wound bed through the production of the EPS occurs.[72, 73] Stage 3 involves further growth of the immature biofilm before maturation and

aggregation in Stage 4. In the final stage, planktonic bacteria are dispensed from the biofilm, forming new niches at distant wound sites.[93]
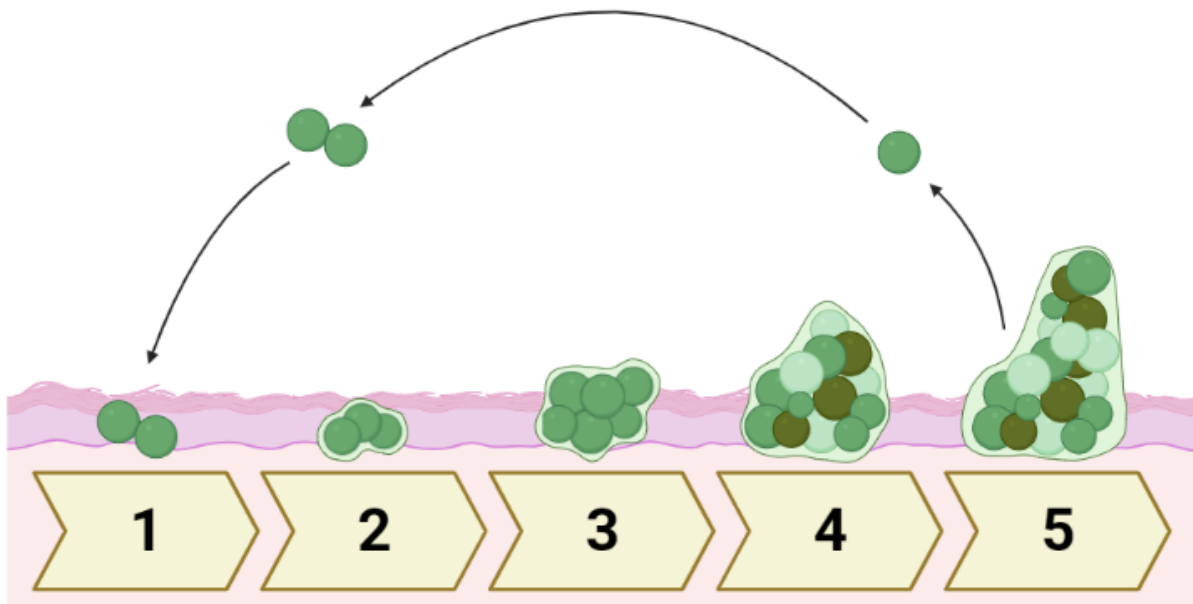


*Figure 2.2: Schematic of the formation of a biofilm. 1) Reversible attachment of planktonic bacteria. 2) EPM matrix formation results in irreversible adhesion. 3) Growth of immature biofilm. 4) Further growth and maturation of the biofilm. 5) Release of planktonic bacteria to create new niches. (Created D Beith in BioRender.com)*

In the process of biofilm formation, quorum sensing (QS) also plays a key role. QS refers to the process of communication and coordination of cellular processes within groups of bacteria and is observed during biofilm formation as it matures. The number of bacteria in a biofilm are determined by the concentration of QS signalling molecules, which starts to be produced during stage 1.[89] Examples of such QS signalling molecules include peptides, unsaturated fatty acids, acyl homoserine lactones and furanosyl borate diesters.[94] It is at the final stage where QS signalling molecules are responsible for the orchestration of processes to enable the production of satellite niches.[94, 95]

A newer concept for the organisation and pathogenicity of bacteria in a biofilm was suggested by Dowd *et al.*[96] The authors commented on the role of a Function Equivalent Pathogroup (FEP), which is a group of genotypically different bacteria that work in synergy to be pathogenic, in the organisation and pathogenicity of biofilms. By working in synergy, they are able to collectively alter the conditions of the environment in order ensure survival. He also hypothesised that individual bacteria are not pathogenic, but when consorted in an FEP they are able to maintain chronic biofilm infections and mimic bacterial properties, such as those seen in *S. aureus*.[97]

Biofilms formed within DFUs often form complex polymicrobial biofilms that intercommunicate through QS signalling molecules. Interactions between the species change their virulence and the

properties of the biofilms. *S. aureus* and *P. aeruginosa* are the commonly investigated bacteria within DFIs and as such, the following subsections will describe these biofilms only.[72, 98]

## 2.2.2.1 Biofilms with *S. aureus*

*S. aureus* is a Gram-positive coccus and is typically detected in infected DFUs. *Staphylococci* are of particular interest to this work as they have been identified as one of the most common causes of biofilm-related infections, and reported in one study to be responsible for 60% of DFU biofilm isolates.[99] The ability of *S. aureus* to form multi-layered biofilms within wounds is credited to the production of polysaccharide intercellular antigen (PIA) which is made from β-1,6-linked- *N*-acetylglycosamine and facilitates the production of the structural pericellular matrix.[100]

Biofilms and planktonic bacteria of the same species can express different genes through up- and down-regulation.[101] Important to the regulation of *S. aureus* biofilms is staphylococcal accessory regulator (*sarA*), and accessory gene regulator (*agr*).[102] *sarA* induction is needed to prevent proteolytic enzyme damage and initiate immature biofilm attachment. Once matured, the *agr* quorum sensing system in the biofilm is activated. *Agr* is responsible for the increase in biofilm virulence, as well as decreasing cell wall adhesion thus facilitating the release of satellite planktonic bacteria. Together sarA and agr form a dynamic two gene locus system *arlRS, which* if left unregulated, it has been shown to prevent biofilm formation.[27]

## 2.2.2.2 Biofilms with *P. aeruginosa*

*P. aeruginosa* is the second bacteria of interest within this piece of work and reported to be one of the most virulent microbes due to its complex genome.[103] In a study conducted by Banu, A *et al.*, it was reported that 26.5% of DFU biofilms were caused by *P. aeruginosa.*[104] It is also is an important cause of acute and chronic wound infections but can also be found respiratory conditions such as cystic fibrosis, urinary tract infections and medical device-related infections.[105] The control of conditions within the EPS of *P. aeruginosa* biofilms is controlled through a variety of similar abovementioned QS systems. Within *P. aeruginosa* biofilms, there are four key QS systems responsible the adaptation and development of the biofilm within the wound environment and are all interconnected: Las, Rhl, pseudomonas quinolone signal (PQS), and integrating quorum sensing signal (IQS).[106] The Las system is activated in the very beginning of biofilm formation and is responsible for the production of EPS. Later, the Rhl system is activated and is responsible for the survival of mature biofilms through

preventing nitric oxide (NO) from accumulating within the biofilm, as well as controlling the production of biosurfactants. The PQS system is responsible for the development of extracellular DNA as well as being involved in both Rhl and Las systems. Finally, the IQS system prevents biofilm inhibition in phosphate-limited environments, often seen in wound infections.[107] These four QS systems work to produce biosurfactants, such as rhamnolipid and pyocyanin, which are responsible for the preservation of pores and channels between microcolonies and cell lysis needed for mature biofilms.[108] The QS systems also lead to the release of extracellular DNA (eDNA), important for biofilm aggregation and survival.[109]

## 2.2.3  Methods of Bacterial Detection

## 2.2.3.1 Conventional Microbiological Culture

Employing conventional microbiological culture methods is a key detection method used for DFUs. Cultures are considered gold-standard detection method, should they be positive. Once the clinical sample is obtained, a suitable growth media such as blood agar is chosen based on expected growth. The sample is then inoculated onto the culture media and incubated. It is important that samples are obtained pre-antibiotic therapy as it can increase the chance of the culture-negative outcome. Following incubation and growth of the bacteria, a range of basic biochemical tests including identification of species using the aforementioned Gram staining, and antimicrobial susceptibility testing through a dilution series is performed.[110]

Unfortunately, conventional culture methods have poor sensitivity, and harder fastidious organisms such as those found in blood cultures and anaerobic bacteria, only produce culture-positive results in up to 15% of samples, thus failing to detect these species. This is complicated further by previous antibiotic exposure. Another inherent problem of the conventional culture methods is that the results are not instantaneous nor timely. From inoculation, incubation of the agar plate may require up to 5 days before an outcome, providing it's not negative, however most are achieved between 24-48 hours (h). Fast identification of bacteria is needed in serious disease as time delayed before correct treatment could seriously affect the patient's outcome. New molecular methods should seek to provide timely outcomes to limit patient deterioration in the context of systemic disease.[111, 112]

The advantages of conventional culture as a detection method is that when a culture-positive result is obtained, susceptibility to an arsenal of antimicrobials through disk diffusion such as the Kirby-Bauer assay is easily tested for, to inform the clinical treatment. One disadvantage of the following detection method, broad-range 16S rRNA gene PCR, is its inability to determine antimicrobial sensitivity.[110, 113]

## 2.2.3.2 Broad-Range 16S rRNA Gene PCR

Previous research has indicated that less than 1% of bacterial species can be grown under culture conditions, potentially limiting the detection of the true pathogenic microbe of the sample. Broad-range 16S rRNA gene PCR, herein referred to as 16S rRNA, is also used for the detection of microbes and is particularly useful for difficult cultures which have previously been unidentified, such as the causative organism of Whipple's disease, *Tropheryma whipplei*.[114, 115]

The 16S rRNA gene is found within the 30S subunit of the 70S ribosome. Newer gene-sequencing methods such as 16S rRNA now have the possibility upon comparison with a gene bank to characterise the diversity and the evolutionary distance of cultured bacteria through production of a phylogenetic tree at the species and genus level.[96]

For 16S rRNA, initially, the DNA is extracted from the bacterial colonises before adding specific primers to the sample that attach only to the 16S rRNA encoding gene. The sample is then amplified through PCR and sequenced before analysis by comparing sample-sequence to a reference-sequence on a database such as GenBank.[113]

The niche of 16S rRNA is in the detection of harder, fastidious organisms. Where the conventional culture method is unable to detect bacteria in clinically infected patients, the importance of other techniques such as 16S rRNA is crucial. Rampini, S K *et al.* conducted a study comparing conventional culture to the newer molecular method, 16S rRNA in order to determine the bacterial profile of DFUs. 130 of 186 samples analysed were from patients without microbiological evidence of infection i.e. positive culture. Using 16S rRNA, bacteria were identified in 42.9% of the culture-negative samples highlighting its potential use in a potential culture-negative diagnostic algorithm.*[116]*

The downsides of broad-range 16S rRNA is the breadth of information available and the method by which it detects bacteria. For non-sterile samples, such as stool samples, the result is uninterpretable. Using 16S rRNA, all bacteria detected are amplified and so it is unable to distinguish which bacteria is dominant and pathogenic due to the result merely indicating presence of the species. Another obvious downside to molecular methods such as 16S rRNA is the availability of equipment. Although identification of bacteria is quicker using 16S rRNA, smaller hospitals may not have access to the expensive equipment needed for this technique, and as a result, samples may need to be sent away, adding to clinical delay and cost.[117]

The subsequent aim of the rest of this chapter is to determine the most common pathogenic bacteria within DFU through a comparative systematic review of two pools of literature for the bacteriology of DFUs detected. One search criteria focused on detection with conventional culture methods versus a search criteria for 16S rRNA. Through identification of the core bacteria, this will then later inform

the experiments applied to bacterial species (Chapter 6). A further aim was also to determine if there were any differences in bacteria detected and to postulate how both diagnostic modalities could be used within a clinical environment.

## 2.3  Methods

Two different search criteria were used in order to determine the bacteriology of DFUs using 16S rRNA and conventional culture. For conventional microbiological culture, a search was conducted using PubMed and the ISI Web of Science databases using the following operator: "(diabetic foot infection OR DFI OR Diabetic foot ulcer OR DFU) AND (culture) AND (bacterial profile)". 86 papers were identified before any exclusion. Figure 2.3 shows a flow diagram for the selection of papers in this analysis. The second search criteria for 16S rRNA utilised PubMed and the ISI Web of with the following search terms were used: "(diabetic foot infection OR DFI OR Diabetic foot ulcer OR DFU) AND (bacteria) AND (16S rRNA)" yielding 56 papers before exclusion. Titles and abstracts of each paper were then screened by the author of this work for their eligibility. Figure 2.4 shows the flow diagram towards the final 10 papers included.

Papers selected for inclusion within this review were those whose aim aligned with the study and reporting of bacterial compositions within DFUs using either conventional culture methods or 16S rRNA. Eligible papers must have been primary studies and be with a prospective or retrospective cohort, observational or be cross-sectional in design. In both search criteria, studies were excluded if duplicated, no full text, not written or translated into English, *in Vivo/Vitro* studies, reviews, letters, abstracts, and any studies not focused on DFUs.

Paper characteristic data concerning author, year, country, type of study, and specimen collection method was collected from each paper by the author. Subsequent core microbiological data varied between search criteria due to the variation in result outputs between each method. For conventional microbiological culture, data was extracted on the following categories: total specimen number, number of culture-positive specimens, total number of bacterial isolates, percentage of polymicrobial samples, Gram-positive bacteria prevalence, Gram-negative bacteria prevalence, and predominant aerobe or facultative anaerobic species. Additional information was collected from each paper on predominant anaerobe species and percentage prevalence if cultured; this information was non-essential and papers without this information would not be excluded if absent. 16S rRNA had core microbiological data extracted on the following: predominant aerobe/facultative anaerobe genus, predominant obligate anaerobic genus. Extra methodological information was extracted for 16S rRNA outside of specimen type: DNA extraction method and sequencing platform used.

In both search criteria, the included studies were analysed initially with equal weighting. Unequal weighting was subsequently applied to the included studies by weighting each study by the number of specimens sequenced or cultured as a proportion of the total number of specimens.
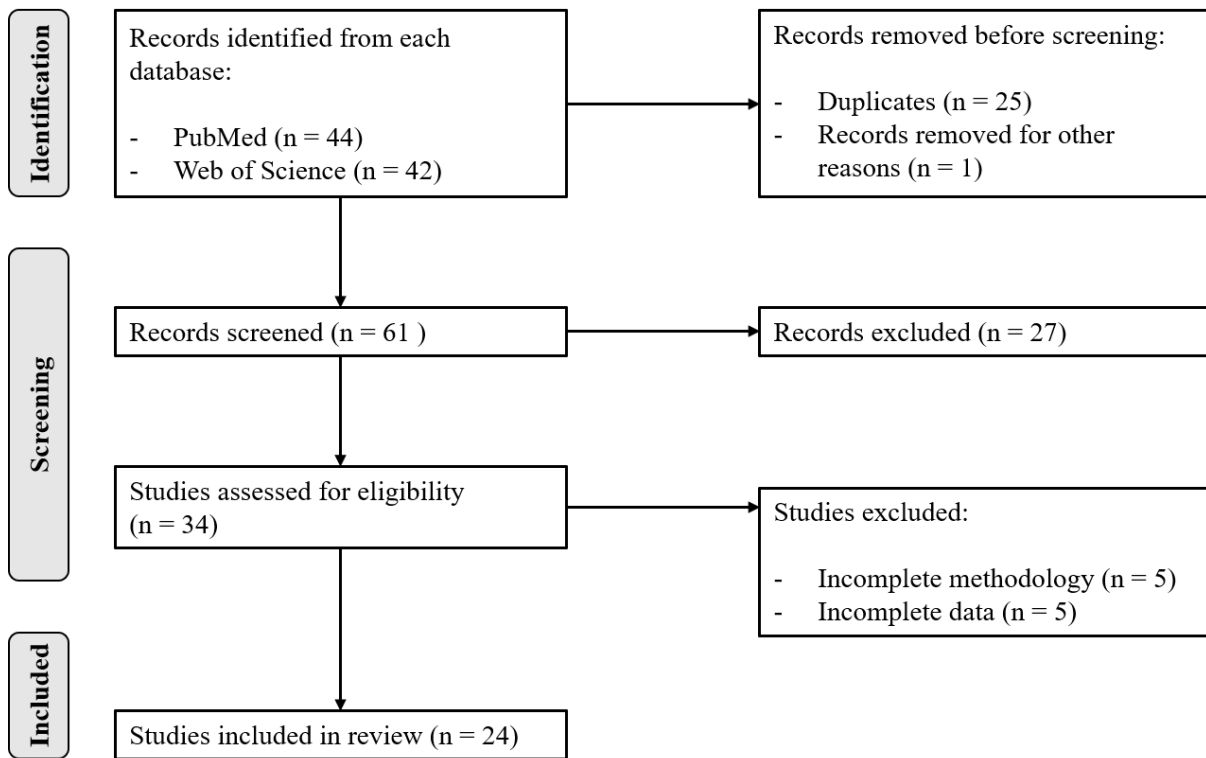
*Figure 2.3: Search criteria flow diagram for convention microbiological culture.*
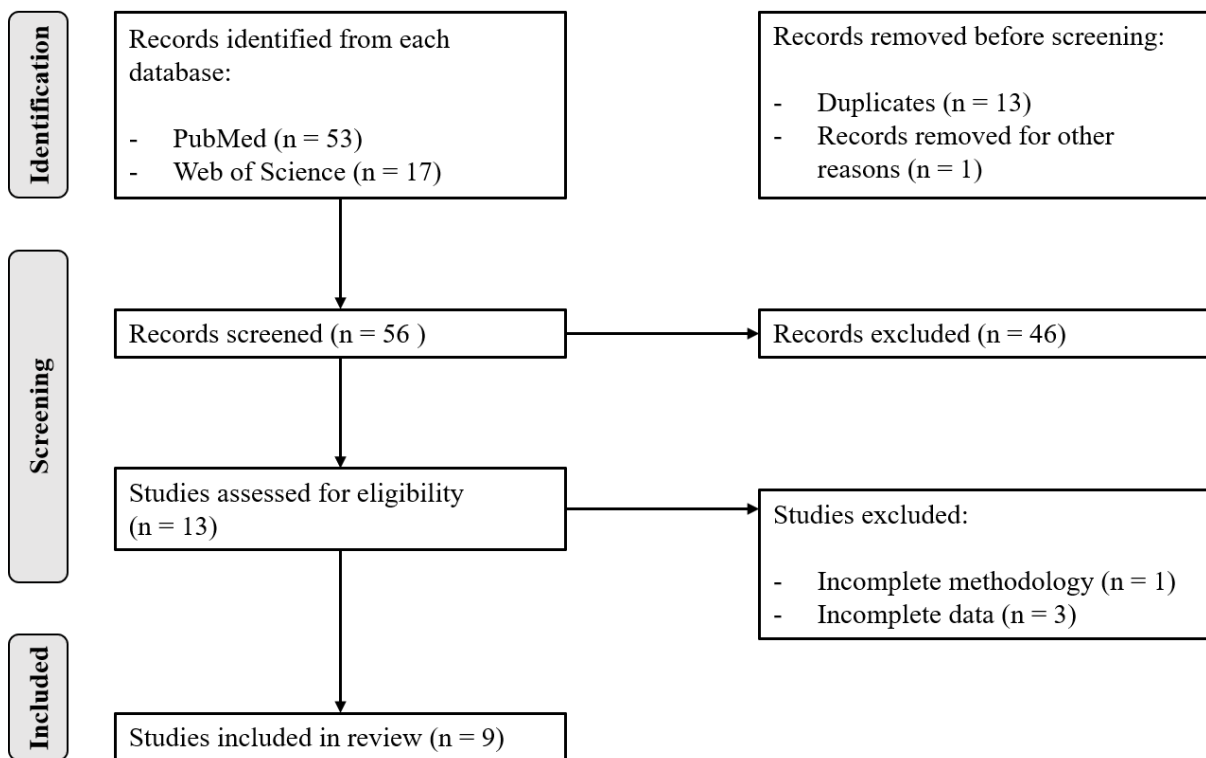


*Figure 2.4: Search criteria flow diagram for 16S rRNA gene PCR.*

## 2.4 Results and Discussion
## 2.4.1 Conventional Microbiological Culture

The results of 24 studies using conventional microbiological culture have been corroborated in order to determine the most abundant microorganism within DFUs. Table 2.2 illustrates the basic characteristics of each study. There was a spread of study designs in the included papers: retrospective or prospective cohort (n = 21), cross-sectional (n = 2) and transverse observational studies (n = 1). Figure 2.5 shows the distribution of origin country for each study. With 29.2% (n = 7) of the papers, the most common was India, followed by South and Central America (n = 4) where 2 papers were conducted in Brazil, 1 paper in Trinidad and Tobago and finally, 1 multi-national study across South and Central America. Interestingly, only 4 studies were conducted in Europe, with the majority of the rest residing in the Middle Eastern countries.

*Table 2.2: Characteristics of included studies (n = 24) in the conventional culture arm from PubMed and Web of Science databases. Fine needle aspirate (FNA).*

| Author (Year) | Country | Study Design | Specimen Type | Total No. of Specimens |
|---|---|---|---|---|
| Akhi, M T *et al.*[118] (2015) | Iran | Prospective | FNA | 60 |
| Al Ayed, M Y *et al.*[119] (2018) | Saudi Arabia | Retrospective | Swab | 126 |
| Al Benwan, K *et al.*[120] (2012) | Kuwait | Retrospective | Swab, Tissue, Pus, Bone | 440 |
| Aysert, Y *et al.*[121] (2018) | Turkey | Retrospective | Tissue | 112 |
| Birra, V *et al.*[122] (2016) | Brazil | Prospective | Swab | 41 |
| Carro, G *et al.*[123] (2020) | South and Central America | Prospective | Tissue, Bone | 382 |
| Gadepalli, R *et al.*[124] (2006) | India | Retrospective | Pus | 80 |
| Islam, S *et al.*[125] (2013) | Trinidad and Tobago | Retrospective | Swab, Tissue, Pus | 139 |

| | | | | |
|---|---|---|---|---|
| Jaju, K et al.[126] (2019) | India | Cross-Sectional | Swab | 140 |
| Jouhar, L et al.[29] (2020) | Lebanon | Retrospective | Tissue | 179 |
| Kow, R et al.[127] (2019) | Malaysia | Retrospective | Tissue, Bone | 173 |
| Kunjappan, S and Saju, I[128] (2017) | India | Prospective | Swab, Pus | 550 |
| Li, X et al.[129] (2018) | China | Retrospective | Swab, Tissue | 456 |
| Macdonald, K et al.[130] (2020) | Scotland | Retrospective | Swab, Bone | 200 |
| Machado, C et al.[131] (2020) | Portugal | Retrospective | Swab, Tissue, Bone | 243 |
| Mendes, J et al.[132] (2012) | Portugal | Transversal Observational | Tissue, FNA | 49 |
| Neves, J et al.[133] (2019) | Portugal | Cross-Sectional | Swab, Tissue | 87 |
| Perim, M et al.[134] (2015) | Brazil | Prospective | Swab | 41 |
| Ramakant, P et al.[135] (2011) | India | Retrospective | Swab, Tissue, Pus | 1632 |
| Shankar, E et al.[136] (2005) | India | Prospective | Swab, Pus | 77 |
| Appapalam, S T et al.[137] (2019) | India | Prospective | Swab, Pus | 50 |
| Turhan, V et al.[138] (2013) | Turkey | Retrospective | Swab, Tissue, Bone | 298 |
| Wu, M et al.[139] (2018) | China | Retrospective | Swab | 428 |
| Zubair, M et al.[140] (2011) | India | Retrospective | Swab, Tissue | 102 |
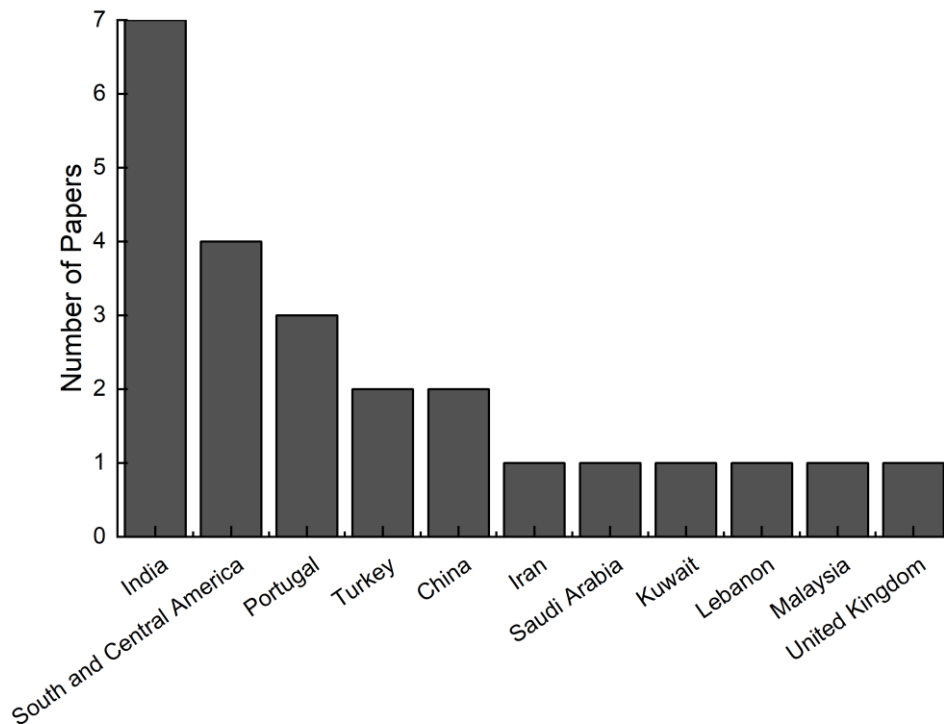
*Figure 2.5: Distribution of Countries for conventional culture (n = 24) search criteria from PubMed and Web of Science databases.*

Out of the 24 papers included, when equally weighted, 70.83% (n = 17) identified *S. aureus* as the predominant bacterial isolate in the cultures, Figure 2.6. Interestingly, although *S. aureus* was predominant in these papers, the average percentage Gram-positive prevalence across all papers was less than Gram-negative prevalence, with 45.94% and 47.29% respectively. The other predominant bacteria reported were *Enterobacteriaceae spp.* 8% (n = 2)*,* and *Pseudomonas spp.*, 20% (n = 5).

When the papers included were weighted (Figure 2.6) by the number of specimens analysed per study as a proportion of the total number of samples (n = 6085), herein called unequal weighting, there was an observed shift in the percentage for each of the species. Although *S. aureus* decreased, it still remained the predominant bacteria in 52.54% of samples. The proportion of samples containing *Pseudomonas spp.* increased more than two-fold from 20.83% to 42.84%, and the proportion of *Enterobacteriaceae spp.* dropped to 4.62%. One explanation for the doubling of *Pseudomonas spp.* could be due to a bias within the included papers by Ramakant, P *et al.* not highlighted when equally weighting.[135] This paper represents 26.82% of the total number samples, and from their samples (n = 1632) it was reported that *Pseudomonas spp.* were the predominant bacteria.
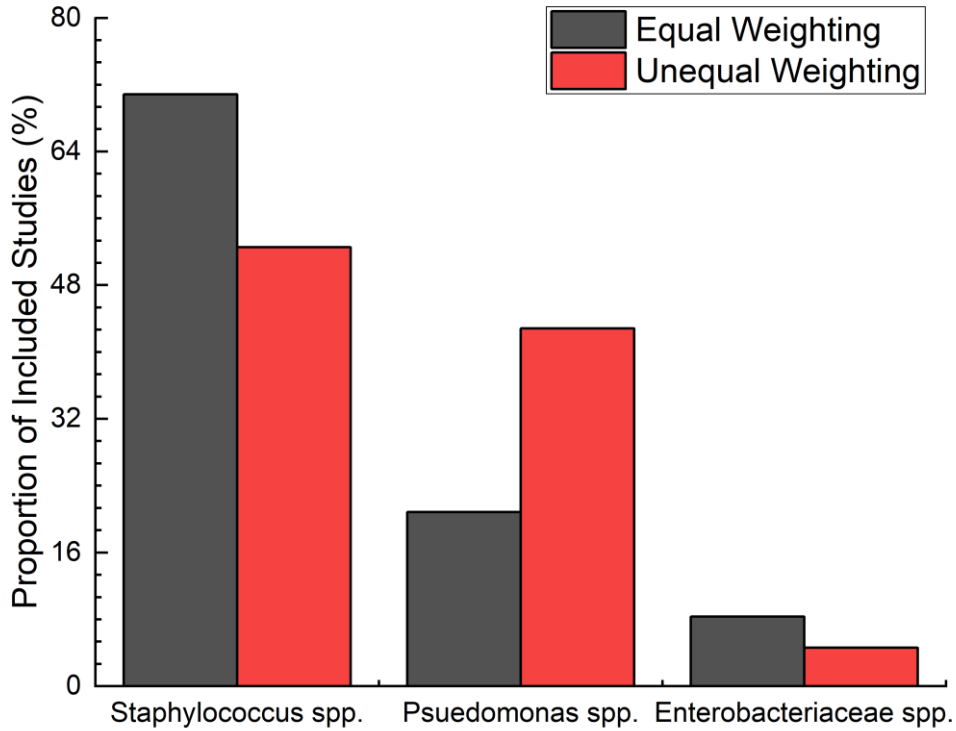
*Figure 2.6: Bar chart indicating the predominant species of bacteria using conventional culture when equally-weighted and weighted by the proportion of samples per paper (n = 24) as a proportion of the total number of samples (n = 6085).*

Additional to the primary aim of the paper by Aysert, Y *et al.*[121], they also reported a change in microbiome due to complicating factors of DFUs such as peripheral vascular disease. Out of the 112 specimens studied, 76.79% (n = 86) had peripheral vascular disease within this retrospective cohort. A statistically significant (p = 0.020) increase in detected *Pseudomonas spp.* was observed in DFUs with peripheral vascular disease versus without peripheral vascular disease.

A pooled total of 7908 bacterial isolates were detected in this systematic review of conventional microbiological culture. From this, an average of 1.72 bacterial isolates were detected per positive specimen (n = 5474) and an average of 48.14% of samples classified as polymicrobial. Polymicrobial is defined as >2 bacterial species detected per sample. Figure 2.7 shows the average prevalence of Gram-positive and Gram-negative bacteria from the 24 included papers; equally weighted. When unequal weighting is applied, the percentage Gram-positive to Gram-negative changed to become more Gram-negative (49.49%), and 39.98% Gram-positive bacteria producing the opposite result in terms of bacteria predominance.
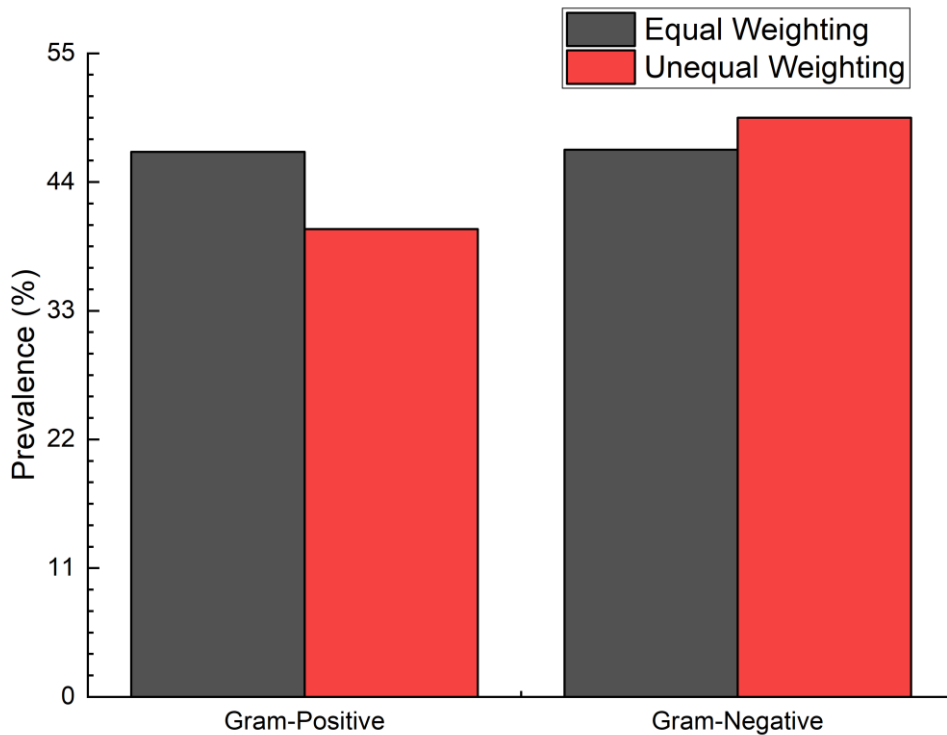
*Figure 2.7: Comparison of Gram-positive versus Gram-negative Bacteria detected with equal and unequal weighting.*

Of the 24 included studies, a major limitation of this systematic review is that only 29.17% (n = 7) of studies conducted cultures suitable for obligate anaerobic organisms. An average relative abundance of 6.73% of detected bacterial isolates were due to obligate anaerobes, of which the most commonly detected species were *Bacteroides spp.* (n = 4) followed by *Peptostreptococcus spp.* (n = 3).

Akhi, M T *et al.*[141] reported that obligate anaerobes contributed to 4% of the total isolates and the most abundant obligate anaerobic bacteria was *Bacteroides fragilis* when using conventional microbiological culture. Another paper to report on the proportion of obligate anaerobes was Al Benwan *et al.*.[120] This prospective cohort study based in Kuwait reported that anaerobes represented 15.3% of detected bacterial isolates (n = 777). Again, *Bacteroides spp.* were the most abundant obligate anaerobe at 10.81% (n = 84). The difference in result could be due to the location of the ulcer as bacterial load varies based on its temporality. It has been hypothesised that the proportion of anaerobes within a DFU may correlate with its chronicity, with increasing numbers of anaerobes detected as ulcer duration increases.

Conventional microbiological culture techniques have been shown to produce a selective bias for microorganisms that thrive under pre-determined laboratory conditions. Differences in culture media such as inoculating bacteria on chocolate versus blood agar leads to selection pressures and misrepresentation of true microorganisms within wounds. Although not frequently detected in

conventional microbiological culture, the literature reports that obligate anaerobes are implicated in DFUs with varying claims on their importance in infection.[68]

## 2.4.2 Broad-Range 16S rRNA Gene PCR

Unlike the results of the cultured-based methods which reported results at a mainly at species-level, the output of 16S rRNA depends on operational taxonomic units (OTUs). Following the creation of sequences, the 16S rRNA technique creates clusters of sequences by similarity in order to create OTUs. Clustering of sequences with >95% similarity is the same genus and >97% similarity between sequences for the same species. The most common output of these 16S rRNA studies was the identification of the most predominant genera.

Table 2.3: Characteristics of included studies (n = 9) in the 16S rRNA gene PCR from PubMed and Web of Science databases.

| Author (Year) | Country | Study Design | Specimen Type | Total No. of Specimens |
|---|---|---|---|---|
| Akyshbayeva, K *et al.*[142] (2018) | Kazakhstan | Prospective | Tissue | 34 |
| Gardner, S E *et al.*[143] (2013) | USA | Cross-Sectional | Swab | 52 |
| Hu, P *et al.*[144] (2017) | China | Prospective | Tissue | 16 |
| Malone, M *et al.*[145] (2017) | Australia | Prospective | Tissue | 39 |
| Min, K *et al.*[146] (2020) | USA | Prospective | Tissue | 50 |
| Sloan, T *et al.*[147] (2019) | UK | Prospective | Swab | 256 |
| Smith, K *et al.*[148] (2016) | Scotland | Prospective | Swab | 20 |
| van Asten, S *et al.*[149] (2016) | USA | Prospective | Bone | 26 |
| Zou, M *et al.*[150] (2020) | China | Prospective | Bone | 17 |

This second search criteria aimed to determine the most common genera generated from 16S rRNA. Later comparisons will aim to determine if there are any similarities or differences between 16S rRNA and the previous search criteria for conventional microbiological culture. The paper characteristics differed slightly: the most common countries were United States of America (USA) (n = 3) and China (n = 2), as illustrated in Table 2.3.

Of the papers reviewed, a total of 510 specimens were sequenced. 83% of studies (n = 5) had the presence of *Staphylococcal spp.* as the predominant genera in DFUs. In one paper, it was reported that their *Staphylococcal Spp., Corynebacterium Spp., Anaerococcus Spp.* and *Finegoldia Spp.* were present in every sample they took from their bone and tissue swabs of DFI.

Results in Figure 2.8, specifically that *Staphylococcus spp.* are the most common genera present are analogous to the abovementioned findings detected by conventional microbiological culture which showed that Gram-positive cocci such as *Staphylococcus aureus* were the most commonly cultured bacteria.

A similar review done in 2018 found analogous results from their analysis, confirming that the genera *Staphylococcus spp.*, and specifically *S. aureus* were most abundant in diabetic wounds.[73] It has also been confirmed that this result is consistent with most findings from studies in North America and Europe.[149] This systematic review has found that 75% of studies carried out in North American and European countries (n = 4) detected *Staphylococcal spp.* as the predominant genera and 1 paper which detected *Corynebacterium spp.*. The implications of *Corynebacterium spp.* predominant DFUs are poorly understood. It is hypothesised that they are a contaminant of a wound rather than being clinically significant. Further studies may wish to measure the abundance of *Corynebacterium spp.* detected between specimen collection methods to establish the best method for detecting clinically relevant bacteria only.

Not included within the data due to its aim not aligning with the systematic review criteria, Wolcott *et al.* carried out a study which has sequenced the highest number of DFUs to date alongside other chronic ulcerative diseases. From the 910 DFUs sequenced, the relative abundances of bacteria were calculated through the use of species-level operational taxonomic units, which are a mathematical tool used to describe bacterial communities from 16S rRNA. [151, 152] Firmicutes and Proteobacteria contributed to 64% and 26% of the most abundant phyla respectively, with *S. aureus* being the most abundant species-level OTU with a 48% relative abundance.[151]
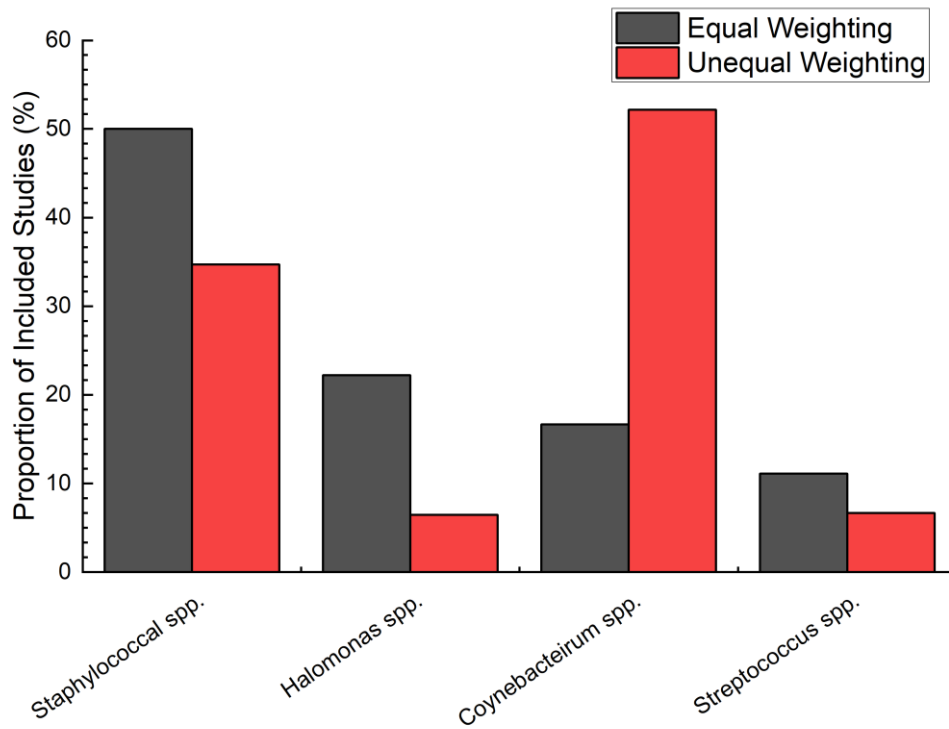
*Figure 2.8: Bar chart indicating the predominant genera of DFUs from the broad-range 16S rRNA gene PCR search criteria (n = 9) with both equal and unequal weighting.*

Using 16S rRNA, every paper included reported the detection of anaerobes. The Gardner, S E[143] study was excluded from Figure 1.10 because, although anaerobes were detected in 100% of their samples, they did not identify these anaerobes at a genus- or species-level despite clustering >95% similarity and reporting facultative genera such as *Staphylococcus*. The pooled results from the remaining 8 papers are shown in Figure 2.9 illustrating the most predominant anaerobic genera. Both equal- and unequal-weighting show that *Anaerococcus spp.* are the most predominant obligate anaerobe in this systematic review with 62.50% and 86.24% of studies showing *Anaerococcus spp.* predominance respectively. Other dominant obligate anaerobes that were detected were *Finegoldia spp. and Peptoniphiulus spp.*.
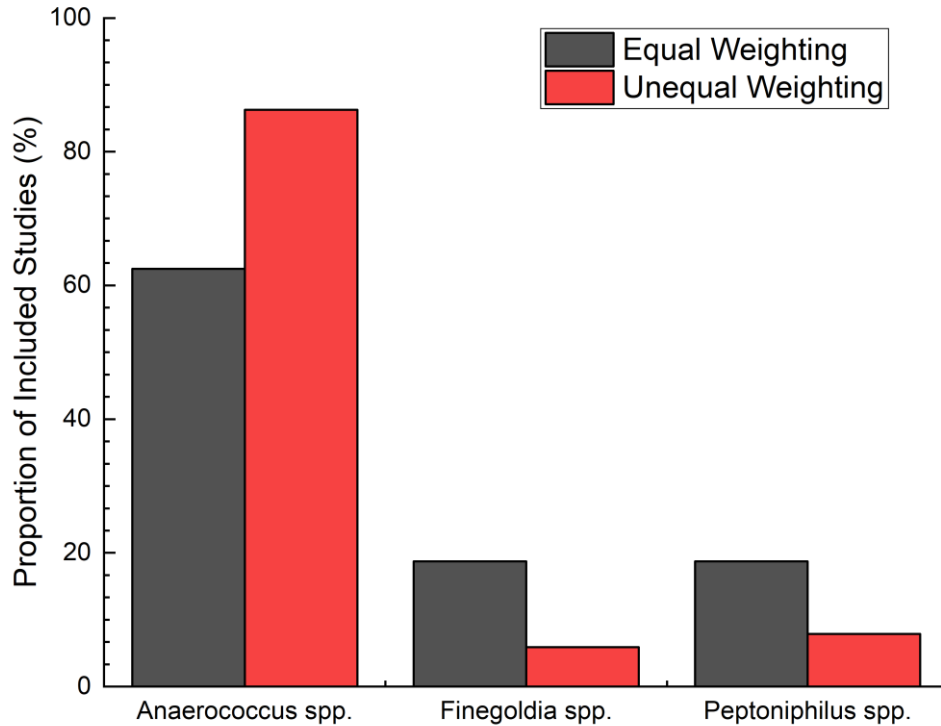
*Figure 2.9: Bar chart indicating the percentage of predominant obligate anaerobic genera.*

## 2.4.3  Comparing Techniques

As abovementioned, depending on the laboratory setup, conventional microbiological culture displays a high level of selection bias. A phenomenon described in the literature known as the "great plate count anomaly" describes the results from conventional culture by which only a fraction of the true bacterial picture is grown on the selected agar media under laboratory conditions and the outcome may necessarily correlate with the clinical picture. [149, 153] By default, this phenomenon is completely eliminated with the use of 16S rRNA making it an advantage of this technique and means that in the event of a culture-negative result, the 16S rRNA technique will facilitate detection of fastidious bacteria within these samples.[154]

Conventional culture methods have become threatened with the advent and accessibility of molecular techniques.[155] One large advantage of 16S rRNA is its rapid determination of bacteria. Historically, a large drawback associated with the conventional microbiological culture method has been the time required for the growth of organisms and further biochemical analysis for microbiological determination. This is not the case with 16S rRNA gene sequencing and will facilitate a faster therapeutic response to patients upon presentation, whereby it is reported that 16S rRNA will yield a result within 10 h compared to 24 h using conventional culture methods.[156] However, although the

determination of organisms is achieved faster with 16S rRNA, there is a large time cost associated with it in the form of the microbiology technicians time as they must record and compare the coded sequences.[157]

Comparison of the outputs between the two modalities has shown that 16S rRNA detects a large number of otherwise undetectable microorganisms within the same wound. The findings of this systematic review are in keeping with similar studies comparing bacteriology.[158] For example, a much greater number of obligate anaerobes were detected using 16S rRNA gene sequencing whereby only 7 out of 24 papers cultured for anaerobic bacteria and 100% of 16S rRNA studies detected anaerobic species. 16S rRNA studies such as van Asten *et al.*[149] reports that anaerobes were detected in 86.9% of samples compared to the 4% of samples reported in 3.4.1 by Akhi *et al.*[141] using conventional culture.

Additional to the problem of undetected species with conventional culture, Gardner, S E *et al.* conducted a study and directly compared conventional culture with 16S rRNA in DFUs within the same cohort. Not only was there a greater diversity detected with 16S rRNA, conventional culture was found to have over-represented the relative abundance of *Staphylococcal spp.* by >15% and underrepresented the abundance of anaerobes by 7.3%.*[143]* This could be one explanation for the above differences in anaerobic detection even when cultured.

16S rRNA is not without limitations. Although not the focus of this work, due to the very nature of the technique, DFUs caused by fungi or viruses will not be detected as this technique can only detect bacteria.[143] One of the main disadvantages of molecular techniques such as 16S rRNA is the quantity of information that it generates. The added information is invaluable when determining relative abundance of organisms within an infected wound. But, the fundamental method of sequencing the 16S rRNA gene means that many of the bacteria detected could in fact be dead or dormant. It is challenging to ascertain which of the detected bacteria is causing the clinical picture.[159] Possible pairing of 16S rRNA with conventional culture methods may alleviate this problem.

Within the 16S gene are conserved and hypervariable regions. Conserved regions allow for the development of primers used in PCR whereas the hypervariable region allows for identification and determination between species of bacteria.[160, 161] The true microbial diversity of a wound is also never entirely captured using variable 16S rRNA regions as they rely on two assumption: (i) genus identification requires a greater than 95% match in the 16S rRNA sequence ; and (ii) a greater than 97% match allows for the determination of species. This means that errors in sequencing may cause changes to the identified genus or species.[162]

None of the included papers for 16S rRNA sequenced the full 16S gene, rather they amplified common hypervariable regions such as V4, often to a greater than 95% match, and as such, comparisons between 16S rRNA and conventional culture was only available at the genus level. To

overcome this problem, it has become recently possible to sequence the full 16S gene which provides greater accuracy, up to one nucleotide differentiation in the full gene, than just sequencing variable regions and as such future bacteriology studies should aim to investigate the use of this technology in DFU bacteria determination.[163]

One inherent drawback of this systematic review is the absence of homogeneity between the aetiology of DFUs in the included papers for each search criteria. The microbiota found in DFUs has been reported to be influenced by patient characteristics such as glycaemic control, country of origin, previous or current antibiotic treatment, and spatial differences in ulcer location.[134, 141, 157] For example, Abdulrazak, A *et al.* reports an increase in Gram-positive organisms in low-grade DFUs compared to a Gram-negative predominance in severe ulcers.[164] It has also been reported that increasing ulcer depth is associated with an increase in anaerobic bacteria.[143]

As Wagner grade has not been controlled for between the cohorts, difference in detected bacteria could be due to these confounding variables rather than differences purely based on the detection methods. In one review whereby, the samples had been made to be homogenous, the pooled literature still showed that *Staphylococcal spp.* are most common and therefore agreeing with the findings reported in this systematic review.[143]

Weighting was applied to the included papers as to remove the risk of bias potentially present by the unequal number of specimens sequenced or cultured in each included study.[165] An alternative avenue for weighting individual papers which also removes the risk of bias is to calculate is to first calculate a z-scores for each study and then, as has already been performed in this work, weight by the sample size of each study.[166]

## 2.5 Conclusions

Both conventional culture-based methods and 16S rRNA studies have shown that the predominant species in DFUs are *Staphylococcal spp.*, despite the Gram-negative preponderance. It has been shown that at a species level, *S. aureus* is the most abundant isolate from conventional culture-based methods. Knowledge generated through microbiological culture, 16S rRNA studies and other detection methods are crucial not only to reduce the burden of disease associated with DFUs for patients but also to retard emerging resistance and limit the economic stress for healthcare systems such as the NHS.

New molecular methods such as 16S rRNA studies show a promising insight into detecting and gathering information on these hard to culture bacteria. 16S rRNA has already revealed a greater diversity of bacteria than previously thought. Detection of these bacteria, including obligate anaerobes may be key to understanding their role in DFU and therapeutic interventions. A new investigation algorithm for DFUs could be proposed whereby in the event of a culture-negative sample, 16S rRNA could be deployed. Not only would this allow for the detection of bacteria in an otherwise negative sample, it would also help to stop the prescribing of incorrect and potentially contributory antibiotics to the ongoing problem of AMR.

The aim of this chapter was to an overview of bacteria and the detection methods (Section 2.2), and through the completion of the systematic review determine (i) the bacteriology of DFUs and (ii) consider the role of newer molecular techniques such as 16S rRNA as opposed to conventional microbiological culture. The systematic review has informed future work within this thesis. As such, it has determined that the focus of the laboratory experiments in Chapter 6 should be on *Staphylococcal spp.* and *Pseudomonas spp.*

# 3   Chapter 3 : An Alternative Treatment: CAP

## 3.1   Introduction

In 1879, Sir William Crookes experimented with the ionisation of a gas through applying a high voltage to an electrical discharge tube whilst the gas passed through it. A substance known as radiant matter was produced, which was later coined plasma thanks to the descriptions of Irving Langmuir[167] in 1927. Plasma can be defined as an ionised gas, but not all ionised gases can be considered as plasma. In order to be a plasma, it has to exhibit the following: (1) it must be quasi-neutral, i.e. the resultant electrical charge must be zero, (2) plasma must have Debye shielding, which is where the particles become arranged to block electrostatic fields, and (3) plasma must exhibit plasma frequency, whereby disruptions in the equilibrium condition cause particles to restore the neutrality.[168] Plasma is known as the fourth state of matter and is claimed to make up 99% of the visible universe, such as in polar aurora, lightning and within the stars.[169, 170] Plasma is composed of charged particles such as ions and electrons, electromagnetic fields, ultraviolet (UV) radiation, heat and a variety of RONS (Figure 3.1).[171]
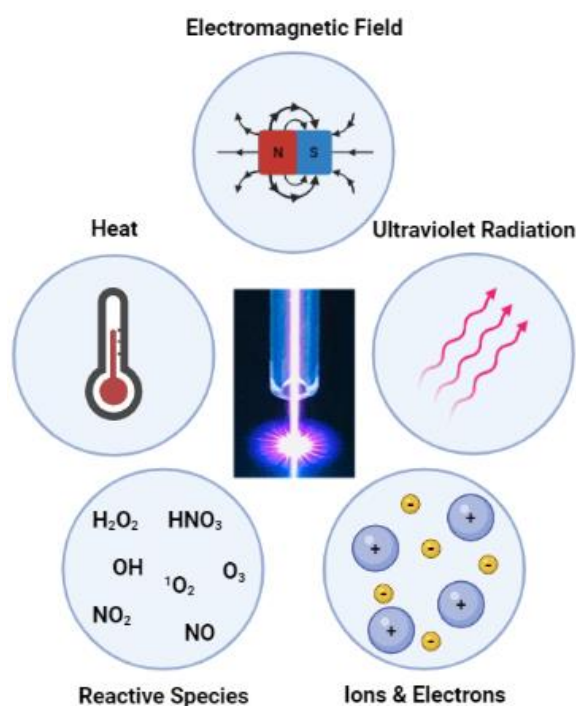


*Figure 3.1: Components of Plasma. (Created by D Beith, in BioRender.com).*

There are two types of plasmas that exist, thermal and non-thermal plasma. Thermal plasmas are the most common within nature and are as a result of both electrons and ions occupying the same high energy state. In non-thermal plasma, however, the electrons have a high energy and the ions and neutral species are deemed cold, and hence called CAP.[44] Plasmas may also be operated at either low-pressure, operated between 1 Pa and 100 Pa, or operated at atmospheric pressure.[172] The advantages of atmospheric plasma are they are cheaper than low-pressure plasma systems, can be ignited in air, and can be handheld facilitating ease of use for use against thermally-sensitive tissues due to a lower operating temperature at temperatures below 50°C.[173, 174]

One of the first uses of non-thermal plasma was in the 1960s using a low-pressure setup to decontaminate surfaces. Later in 1996, Mounir Laroussi was the first to demonstrate the bactericidal properties of.CAP.[168, 175, 176] Since then, CAP has proven to be to be a useful modality for a variety of biomedical applications besides wound healing and wound decontamination, such as dental hygiene, cancer treatment, and food decontamination.[173, 177, 178]

More is now known about plasma medicine as research continues to study its promising biological effects and new CE certified CAP jets such as the kINPen®MED and Adtec SteriPlas offer a real-world solution to chronic wounds. Within the field of chronic wounds such as DFUs, three different types of plasma sources: direct, atmospheric pressure plasma jets, and hybrid plasma sources are used, as described in Table 3.1[179, 180]

*Table 3.1: Types, descriptions, and examples of each plasma source.[170, 181]*

| Type of Plasma Source | Description | Examples |
|---|---|---|
| Direct plasma sources | A carrier gas moves between a floating high-voltage electrode and the skin/tissue which is used as a ground electrode. | Floating-electrode dielectric barrier discharge device |
| CAP jets | Plasma is generated between two electrodes, one high-voltage and the other a ground electrode. | kINPen® MED, Adtec SteriPlas |
| Hybrid plasma sources | A combination of the two plasma sources. It uses a wire-mesh ground electrode, offering less resistance than tissue. | Surface-micro discharge (e.g. MiniFlatPlaSter) |

### 3.1.1.1 Plasma Sources
### 3.1.1.2 Dielectric Barrier Discharge

Dielectric Barrier Discharge (DBD) was first created in 1857 as a device to create ozone.[182] The high-voltage electrode in DBD systems are covered with a dielectric material such as glass or alumina. Upon switching on the high voltage alternating current power supply, charge amasses on the surface of the dielectric material. It creates an opposing electric potential to that produced by the power supply and thus creates a current waveform and plasma formation (Figure 3.2). The DBD system is typically operated at kHz of frequencies and voltage amplitudes between 1 and 100 kV. They have widespread applications, ranging from the aforementioned creation of ozone, surface sterilisation due to their large plasma footprint as well as use biomedically for wound healing, and cancer cell and tumour destruction.[179, 183]
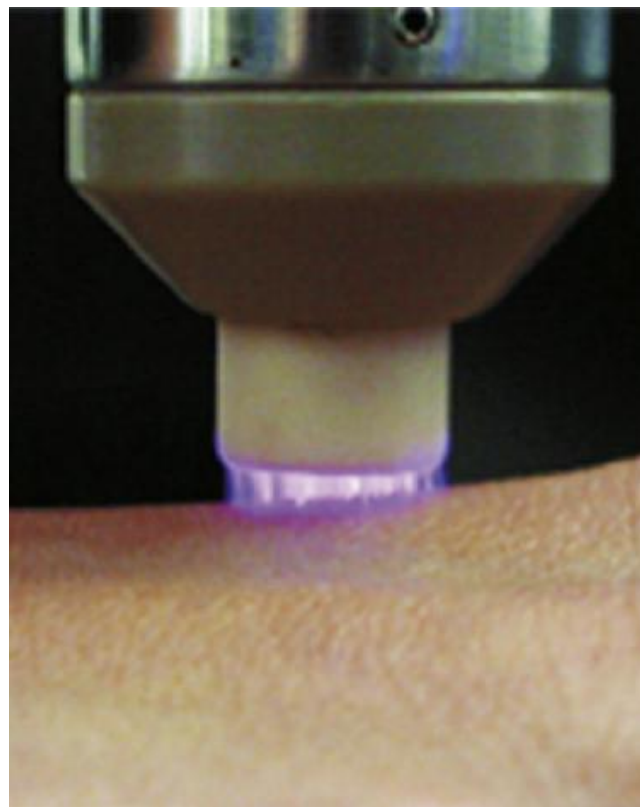


*Figure 3.2: A floating-electrode DBD device on skin. Reprinted from Clinical Plasma Medicine, Volume 1, Emmert, S et al., Atmospheric pressure plasma in dermatology: Ulcer treatment and much more, Copyright (2012), with permission from Elsevier.*

### 3.1.1.3 CAP jets

CAP jets were much later to field of plasma medicine in terms of use for biomedical applications, having and began to be developed in the 1990s.[184] Upon ignition, CAP jets emit a non-thermal plasma plume which are reported to operate below 40°C, conferring their safety for use with biological tissue such as skin, without risk of thermal damage.[185] The generation of CAP occurs in three stages: (i) electrical energy excites a neutral gas such as argon (Ar); (ii) electrons and atoms within the Ar in high energy states interact generate reactive species; and (iii) Heat, UV, electromagnetic field, and visible light in the form of photons are emitted upon successful ignition.[186]

CAP jet designs vary in terms of electrode configuration, inert gas used, and their characteristics: optical, physical, and electrical.[179] For example, as show in Figure 3.3, the kINPen®MED device and the Adtec SteriPlas device, are CAP jets but have different designs and generate plasma differently. A kINPen®MED (Figure 3.3A) utilises an argon gas to generate a plasma plume of 8-12 mm in length and 1mm in diameter. The device is a handheld unit (Figure 3.3B) that utilises a central pin high-voltage electrode design and operates at 2-6 kV and 1 MHz frequency from the high voltage alternating current power supply. The device uses 3 to 5 standard litres per minute (SLPM).[187]

The second commonly used CAP jet is the Adtec SteriPlas device uses a 6-electrode system through a microwave-induced plasma discharge. Because of this design, the Adtec SteriPlas has a wider plume diameter of 3.5 cm, compared to 1 mm with kINPen®MED, and can operate over a wound size of 4 to 5 cm$^2$ (Figure 3.3C) the clinical significance of this being that it is able to treat a larger area of wound at any one time.[179] The electrical characteristics of the Adtec SteriPlas are as follows: 2.45 GHz microwave frequency and 85 W power (Figure 3.3D), with a Ar gas feed of 2.2 SLPM to produce a plasma plume with a temperature of 320K.[188]

*Figure 3.3: Two examples of atmospheric pressure plasma sources. A, B kINPen®MED, C, D Adtec SteriPlas. Reprinted from Clinical Plasma Medicine, Volume 9, Arndt, S et al., Comparing two different plasma devices kINPen and Adtec SteriPlas regarding their molecular and cellular effects on wound healing, Copyright (2018), with permission from Elsevier.[189]*

## 3.2  Mechanisms of action of CAP devices

CAP is composed of a cocktail of reactive species, ions and electrons that induce biological, physical and chemical changes on surfaces of the target upon plasma-activation. RONS are important intracellular molecules which are regulated by a host of antioxidants and enzymes.[181] One mechanism implicated in the mechanism of action of CAP against cells is lipid peroxidation, causing penetration of the RONS into the cytoplasm. ROS are known to be important cellular messengers, and it has been reported that the ROS interact with calcium cascades which are ultimately responsible for cellular death.[190] With respect to reactive nitrogen species (RNS), their mechanism of action is not confirmed, however they have been shown to cause mitochondrial death through binding to cytochrome c and increasing ROS levels by apoptosis of the cell.[191, 192]

At a low CAP-treatment doses, RONS are implicated in bacterial eradication through promotion of macrophages and vasodilation of vessels within the target tissue through endothelial nitric oxide ($NO_2$) production. Beneficial to this piece of work, at high CAP-treatment doses, RONS cause oxidative stress leading to cytotoxicity and cellular death.

### 3.2.1  CAP-generation of RONS

CAP jets produce a variety of RONS species upon activation of a solution or target tissue. Of note, RNS such as nitric oxide (NO) and nitrogen dioxide ($NO_2$) and peroxinitrite ($ONOO^-$) and ROS such as hydroxyl radicals ($\bullet OH$), super oxide ($O_2^-$), ozone ($O_3$), and singlet oxygen ($^1O_2$) are formed, with varying species lengths. [193]

### 3.2.2  Role of RONS in Wound Healing

Wound healing relies on the succession of three stages after platelets aggregate on exposed collagen following epithelial damage. Table 3.2 describes these stages. As aforementioned, RONS act via a wide range of pathways within the cell and the production of hydrogen peroxide ($H_2O_2$) through CAP is one of the most influential molecules for the bacterial eradication properties displayed by plasma jets. RONS are essential messengers used to supply the increased energy demand during the epithelial insult caused by DFUs. They also facilitate cellular division and the migration of crucial cells such a keratinocytes, fibroblasts, and endothelial cells leading to angiogenesis, and collagen fibre formation.

*Table 3.2: Descriptions of the three stages of wound healing.[194]*

| Stage | Description |
|---|---|
| 1: Inflammation | Macrophages and granulocytes are recruited to the wound and create an antibacterial site. There is also increased excretion of blood plasma from the wound bed. |
| 2: Proliferation | Granulation tissue is formed on the wound bed, accompanied by neovascularisation. |
| 3: Remodelling | Collagen maturation, and recruitment of the epithelial cells from wound edge allow for closure of the site. |

Mentioned above in Section 3.2 is how high RONS levels lead to cellular death. In wound healing, RONS-related cellular death can be advantageous and used for bacterial eradication. However sustained high levels of RONS lead to delayed healing and further wound damage.[195] In the development of plasma-activated hydrogel therapy (PAHT), accurate determination of concentrations of RONS will prevent "over-dosing" the wound, potentially adding to existing wound damage.[196]

In lower-doses, the destructive properties of RONS are harnessed whereby neutrophils and phagocytes trigger nicotinamide adenine dinucleotide phosphate (NADPH) oxidase and creates ROS from reduction of $O_2$. The result is either $O_2^-$ or $H_2O_2$ which then destroys the bacteria creating a sterile wound site.[197] Production of longer-acting species via CAP jet such as $H_2O_2$ also encourages an acidic wound environment, thus again promoting wound healing.[43]

## 3.3 CAP jet for DFU treatment

Chronic wounds, such as DFUs, being polymicrobial in nature lead to a chronic inflammatory state which prevents healing.[198, 199] Therefore, there is a need for a multi-modal solution with the ability to eradicate polymicrobial biofilms as well as induce the healing process. The future of chronic wound resolution could lie with CAP, known for its bacteria eradication and healing properties, as discussed below.[200]

Both animal[201] and human[43, 46, 47] studies of chronic wounds, including DFUs, have shown that CAP is antimicrobial with additional pro-wound benefits and limited side-effects reported on the local healthy tissue.[43] As mentioned in Section 1.2.5, AMR is a massive problem within chronic wounds. Zimmermann, J L *et al.[202]* reports following the use of CAP on MRSA and *E. coli* in a bacterial resistance build-up study, that no resistance had been identified. CAP combats the problem of the ever-growing threat of AMR due to over/mal-prescription of antibiotics within hospitals and could be used both as a treatment method in DFUs and also in a post-debridement scenario.

CAP has also been shown to transform chronic wounds into an acute healing wound through decreasing inflammation, up-regulation of growth factors related to angiogenesis and neovascularisation. [200] Expression of inflammatory cytokines IL-6 and IL-8 and growth-factor TGF-β1/2 is seen following CAP treatment of fibroblasts. These factors are released after injury to the epithelium and help recruit inflammatory cells. Up-regulation of these factors is thought to contribute to the accelerated wound healing of chronic wounds following CAP.[203]

### 3.3.1 Current Uses of CAP in DFUs

The aforementioned Adtec SteriPlas was the first device to be trialled in a clinical phase II study.[204] The outcomes of the study showed that in the randomised control trial (RCT) of 36 patients, with a combined total of 291 plasma-treatments, that there was a statistically significant decrease in number of bacteria between plasma-treated wounds and standard-care-treated wounds, with 67% and 34% respectively. Important for the future and safety of CAP, in this cohort of patients, 0 patients reported pain and no observed complications.
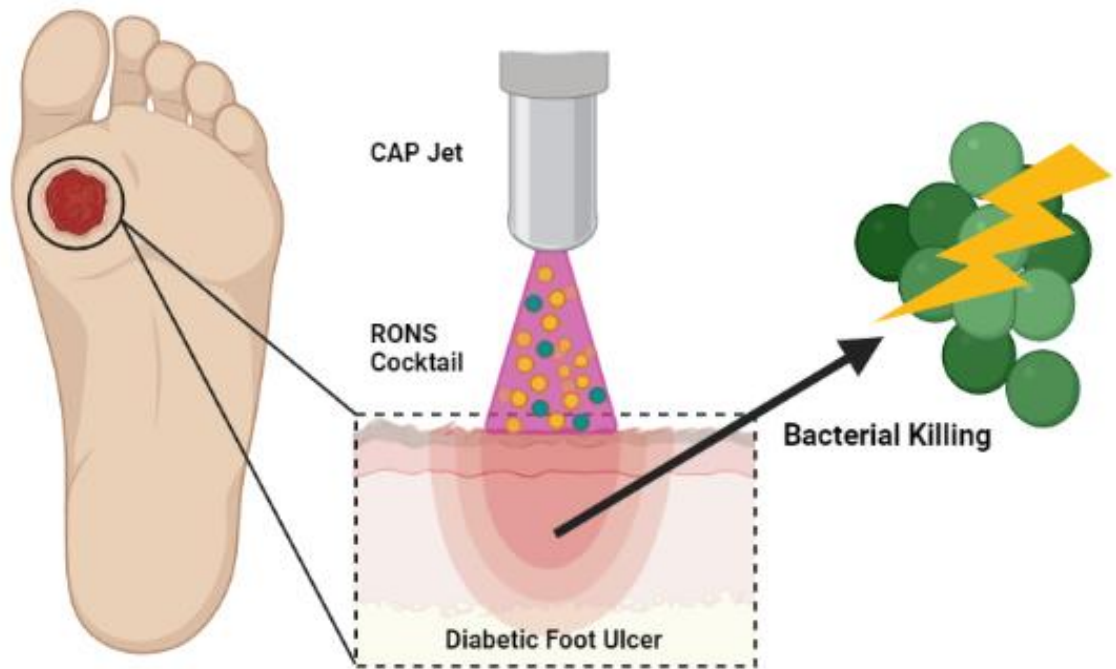
*Figure 3.4: Schematic of direct CAP treatment for DFUs. (Created by D Beith, in BioRender.com)*

The RCT landscape for CAP is sparse, but even more so for studies on DFUs and to date, only three RCT have been conducted on diabetic wounds. [43, 46, 47] The results from Stratmann, B *et al.*[47] and Mirpour, S *et al.*[43] both showed statistically significant fractional decreases in DFU wound size compared with standard care or placebo treatment. Amini, M *et al.*[46] reported a decrease in DFU size, but also a statistically significant decrease in inflammatory cytokines when standard care was combined with CAP, as opposed to standard care on its own. To date there hasn't been a RCT study to investigate the effect of CAP on complex DFUs of Wagner Grade 3 and above, otherwise known as a DFO.

### 3.3.2 PAHT

The above-mentioned techniques all use direct methods of CAP treatment for DFUs i.e. the plasma plume is moved directly on top of the wound surface (Figure 3.4). As a result, CAP has the potential to cause DNA damage and mitochondrial dysfunction.[179] One study reported that on the WIL2-NS B lymphoblastoid cell line, plasma-treatment via a CAP jet had a 10 fold increase in the number of micro-nuclei compared to no CAP as detected by the CBMN-Cyt assay.[205]
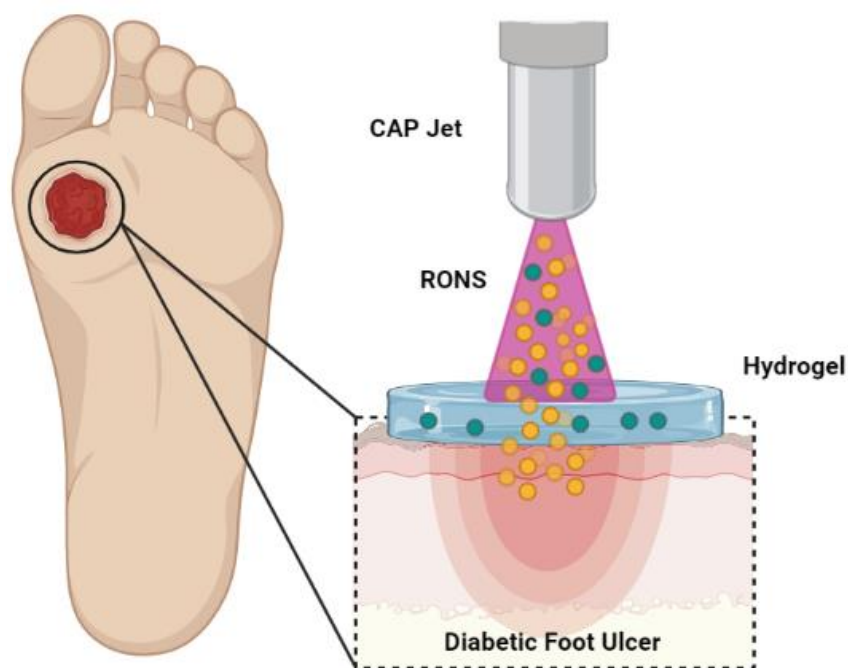
*Figure 3.5: Schematic of Plasma Activated Hydrogel Therapy (PAHT) for the treatment of DFUs showing the delivery of "good" RONS into the DFU (yellow) and the trapping of "bad" RONS (green). (Created by D Beith, in Biorender.com)*

In this study, we propose an alternative novel system for CAP-based treatments of chronic wounds such as diabetic ulcers. As previously highlighted, CAP has the potential to produce large amounts of RONS as well as cytotoxic radicals chiefly •OH. The proposed PAHT system is shown in Figure 3.5 whereby we create a suitable hydrogel to be placed upon a diabetic wound in order to filter the highly-reactive and short-lived species such as •OH (green) whilst still allowing bactericidal species such as $H_2O_2$ (yellow) to penetrate into the wound bed. As part of DFU pathogenesis, explored in Chapter 1, DFU formation could be attributed to the presence of hypoxia. [19] Results from Szili, EJ *et al.*[206] have shown an improvement in oxygen levels beneath a hydrogel, thus combating hypoxia within DFUs which is associated with delayed healing.[28] Progression of this system would allow for integration and repurposing of antibiotics within the hydrogel that would be subsequently and released into the wound upon activated via CAP treatment.

## 3.4  Aims and Objectives

CAP as a potential treatment for DFUs has shown promising results in the form of the included RCTs in Section 3.3.1. However, potential genotoxic and cytotoxic components mean that direct plasma treatment of DFUs is not suitable and as such, alternative applications of CAP must be developed. Initial work with plasma-activated hydrogel systems have eliminated these drawbacks and as such, the subsequent remaining aim of this study is to investigate the effect of a PAHT treatment against common bacteria found in DFUs within the experimental chapters. Chapter 2 describes the first aim, (i) investigating the bacteriology of DFUs, and has determined that application of the PAHT should be against both *Pseudomonas spp.* and *Staphylococcus spp.* In order to develop the PAHT, Chapters 4 and 5 describe the second aim, (ii) characterisation of the CAP jet and plasma-activated solutions; and Chapter 6 describes the third, (iii) optimisation the PAHT treatment parameters for optimal RONS delivery. Chapter 4 characterises the plasma source through physical (electrically, optically) and chemically (RONS delivery), and Chapter 5 studies the characteristics of plasma-activated Povidone-Iodine (PVP-I), a common antimicrobial. Completing both chapters yielded the crucial understanding of the CAP jet, facilitating optimum PAHT treatment, and identification of potentially beneficial products. Chapter 6 therefore focuses on the optimisation of (iii), before PAHT with PVP-I was tested against the aforementioned *Staphylococcal spp.* and *Pseudomonas spp.*.

# 4 Chapter 4 : Characterisation of Argon Driven CAP jet and Plasma-Activated Solutions

## 4.1 Aims

The aim of the work described in this chapter was to characterise the operating parameters of the Ar driven CAP jet used in this study. Herein, this will be referred to as CAP jet. Understanding the operating parameters of the CAP jet as well as quantification of RONS fits into the overall aim of the project. This chapter will fulfil the second aim needed for the development of PAHT as it is important to understand the reaction of plasma with solutions. Activation of povidone iodine and hydrogels was investigated followed by the application to bacterial growth, Chapter 6. Section 4.2 characterises the CAP jet using electrical and optical diagnostics tools. Section 4.4 describes the production of RONS, specifically $H_2O_2$ and $NO_2^-$ using chemical analysis techniques. Changes in the pH of the plasma-activated solution may have a beneficial effect for wound healing. Thus, the pH of plasma-activated water was determined in Section 4.4.5 following varied plasma treatment time. The plasma characterisation in this chapter is in the absence of an overlying screen or hydrogel.

## 4.2 Background

CAP is composed of a cocktail of chemically active species such as ions and electrons that induce biological, physical, and chemical changes on surfaces of the target upon plasma-activation. One mechanism of action is oxidative stress caused by CAP. RONS are important intracellular molecules which are regulated by a host of antioxidants and enzymes.[207] Examples of RONS in intracellular signalling cascades are mitochondrial ROS which have been linked to inflammation and their role in insulin signalling.[208, 209] When used for in short treatment doses, CAP-produced-RONS cause bacterial eradication and vasodilation through increased $NO_2$ production. At higher doses, RONS have been reported to cause cytotoxicity and cellular death.[181]

### 4.2.1 CAP-generation of RONS

CAP produces a variety of RONS species upon activation of a solution or target tissue. Of note, RNS such as NO, $NO_2$, and ROS such as $O_2^-$, $O_3$, and $^1O_2$ are formed, and radicals (•) such as •OH with varying species lengths.[193] RONS act via a wide range of pathways within the cell and the production of $H_2O_2$ through CAP is one of the most influential molecules behind the bactericidal properties exhibited by plasma jets.

Khlyustova, A *et al.* describes the non-equilibrium dissociation of water molecules caused by plasma activation. Short-lived species such as •H, •OH and hydrated electrons (e$^-$solv) are initially formed before longer species such as $O_3$, $H_2$, and $H_2O_2$. Reactions are shown in Equations 4.1 to 4.7 below.[210]

$$2H_2O + e_{solv}^- + e_{solv}^- \rightarrow H_2 + 2OH^-$$

*(Equation 4.1)*

$$H^+ + e_{solv}^- \rightarrow H^{\cdot}$$

*(Equation 4.2)*

$$H^{\cdot} + H^{\cdot} \rightarrow H_2$$

*(Equation 4.3)*

$$OH^{\cdot} + OH^{\cdot} \rightarrow H_2O_2$$

*(Equation 4.4)*

$$H^{\cdot} + O_2 \rightarrow HO_2^{\cdot}$$

*(Equation 4.5)*

$$O_2 + e^-_{solv} \rightarrow O_2^-$$
<div align="right">*(Equation 4.6)*</div>

$$HO_2^{\bullet} + HO_2^{\bullet} \rightarrow H_2O_2 + O_2$$
<div align="right">*(Equation 4.7)*</div>
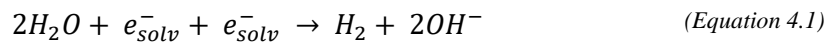
Equations 4.8 through 4.11 occur in gaseous air. The following RNS are also formed in liquid: NO, $NO_2^-$, nitrate ions ($NO_3^-$), and $ONOO^-$. The formation of NO is caused by the dissociation of oxygen and nitrogen in air.

$$O_2 + e^- \rightarrow O + O + e^-$$
<div align="right">*(Equation 4.8)*</div>

$$N_2 + e^- \rightarrow N + N + e^-$$
<div align="right">*(Equation 4.9)*</div>

$$N + O \rightarrow NO$$
<div align="right">*(Equation 4.10)*</div>

$$N + 2O \rightarrow NO_2$$
<div align="right">*(Equation 4.11)*</div>

Following the production of NO, they react with water forming acids (Equations 4.12-16). Depending on the pH of the plasma-activated solution, either $NO_2^-$ or $NO_3^-$ will be formed.

$$3NO_2 + H_2O \rightarrow 2H^+ + 2NO_3^- + NO$$
<div align="right">*(Equation 4.12)*</div>

$$NO_2 + NO_2 + H_2O \rightarrow HNO_3 + HNO_3^+$$
$$\rightarrow NO_3^- + NO_2^- + 2H^+$$
<div align="right">*(Equation 4.13)*</div>

$$NO_2 + NO + H_2O \rightarrow 2HNO_2 \rightarrow 2NO_2^- + 2H^+$$
<div align="right">*(Equation 4.14)*</div>

$$NO_2 + H_2O \rightarrow NO_3^- + H^+$$
<div align="right">*(Equation 4.15)*</div>

$$4NO + O_2 + 2H_2O \rightarrow 4NO_2^- + 4H^+$$
<div align="right">*(Equation 4.16)*</div>
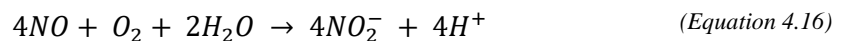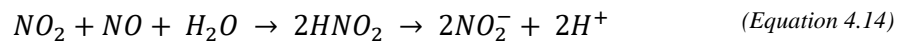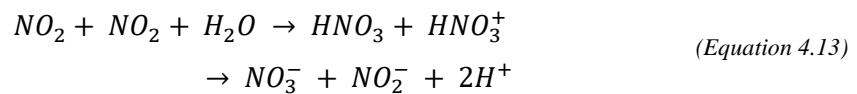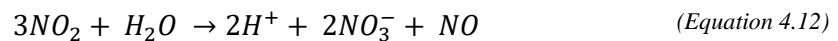
Within plasma-activated solutions, the reaction of •OH with $NO_2$ forms nitric acid ($HNO_3$) (Equation 4.17). Later reactions with a combination of the previous species formed (Equations 4.1-16) within

the plasma-activated solution lead to the formation of either peroxynitrous acid (NOOH) (Equation 4.18) or ONOO⁻ (Equation 4.19), in acid and basic conditions, respectively.

$$NO_2 + OH^\cdot \rightarrow HNO_3$$ *(Equation 4.17)*

$$NO_2^- + H_2O_2 + H^+ \rightarrow O = NOOH + H_2O$$ *(Equation 4.18)*

$$NO_2^- + OH^\cdot \rightarrow O = ONOO^- + H^+$$ *(Equation 4.19)*
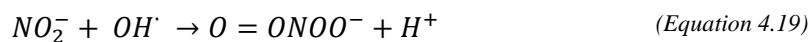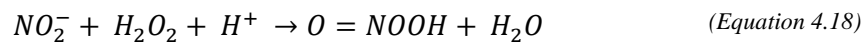
## 4.3 Materials and Methods

### 4.3.1 Plasma Source

Figure 4.1 is a schematic of the novel experimental setup of the CAP jet used throughout this work and has been developed by Ghimire, B *et al.*[211] at Lancaster University. The schematic shows the location of both the high-voltage (HV) and current probes, both attached to an oscilloscope for electrical characterisation (Section 4.4.1). The HV electrode is made up of stainless-steel (outer diameter/OD of 0.9 mm and an inner diameter/ID of 0.6 mm, and length 51 mm). This is then sealed inside the non-tapered quartz tube (ID = 1.5 mm, OD = 3 mm, length below HV electrode = 164 mm) using torr-seal. A longer length of the quartz tube with two ground electrodes was designed in order to maximize the concentration of hydrogen peroxide. The ground electrodes made of copper (length=4 mm, thickness=1 mm) were mounted externally to the quartz tube at positions of 56 mm and 110 mm below the tip of the HV electrode.

All experiments were done using 99.9999% Ar gas (supplier: BOC UK) and were fed into the plasma jet by using a combination of nylon, polytetrafluoroethylene and polyurethane tubing. A mass flow controller (Omega Engineering UK, model: FLDAR3501C) was used to maintain a constant flow of 1 SLPM. An AC power supply (PVM500, amazing1.com) was used to operate the plasma. An oscilloscope (Siglent SDS1102CML, Siglent Technologies Co. Ltd) was used to monitor the voltage and current signals. Voltage signals were measured by using HV probe (PINTEK HVP-39 pro, Pingtek Electronics Co. Ltd) while the current signals were measured by using a current probe (Pearsons Electronics Inc., model 2877). For all experiments, the distance from the end of the quartz tube to the target, denoted d, was 10 mm.
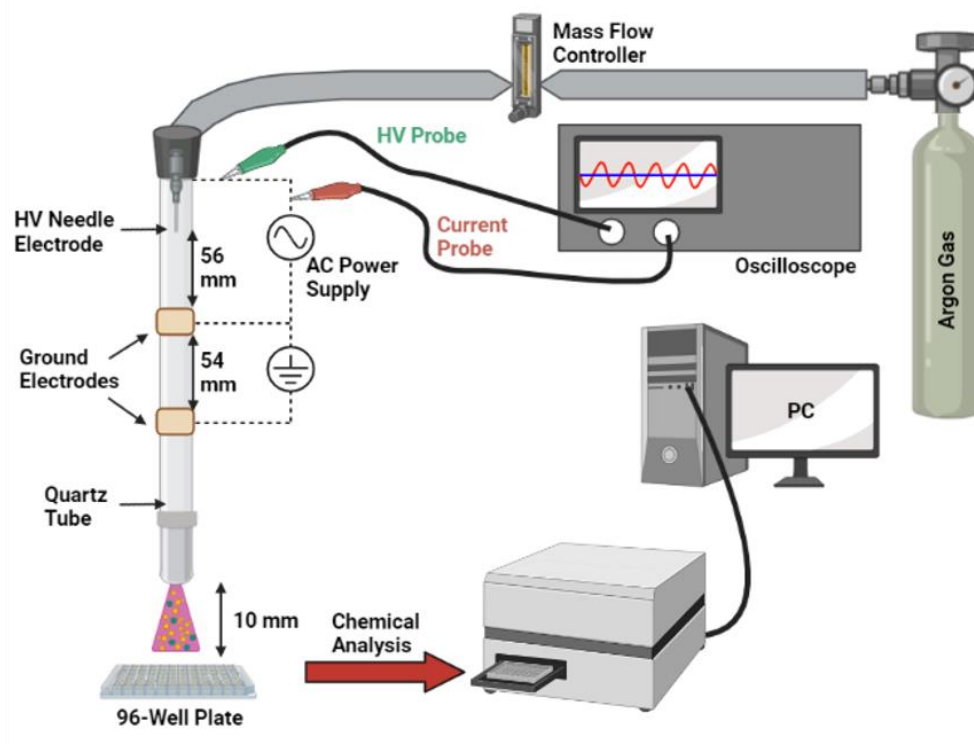
*Figure 4.1: Schematic of the CAP jet showing the techniques for characterisation. (Created by D Beith in BioRender.com).*

## 4.3.1.1 Optical Characterization

Optical emission spectra of the discharge were measured by using optical emission spectroscopy (OES; HR4000CG-UV-NIR, Ocean Optics Inc) at a 4 mm position below the nozzle of the quartz tube. The principal behind OES is that the spectrophotometer, measures the light in the form of photons emitted via excited high energy atoms returning to a lower energy level. The optical fibre is used to detected the emitted photons. The difference in energy state correlates to a specific wavelength, and analysis of the wavelengths enable the determination of CAP composition.[212]
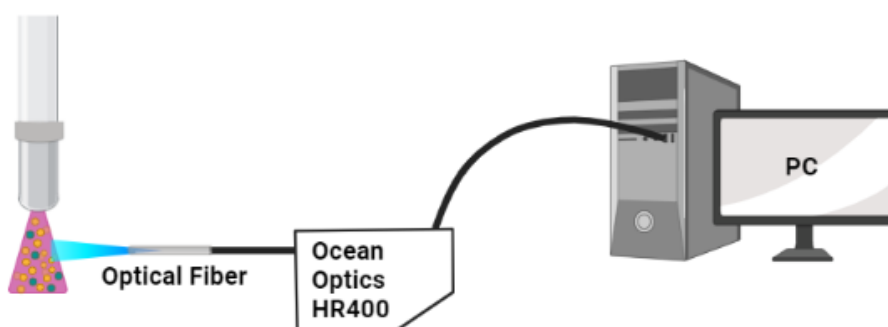


*Figure 4.2: Schematic for optical emission spectroscopy. (Created by D Beith in BioRender.com).*

## 4.3.2  Preparation of Plasma-Activated Water

Plasma-activated water (PAW) was prepared by treating 350 µl of distilled water (DIW) in flat-bottomed wells of 96-well plate (CLS3599, Corning Inc.). Unless otherwise stated, the target nozzle distance in the study was set to 10 mm and plasma exposure time was varied from 1 to 5 minutes. At 10 mm, the plasma jet plume was in contact with the distilled water (DIW) at all times.

## 4.3.2.1 Measurement of $H_2O_2$ concentration

The concentration of $H_2O_2$ delivered by CAP was determined using a reporter system consisting o-phenylenediamine (OPD) and horseradish peroxidase (HRP). In the presence of HRP, OPD reacts with $H_2O_2$ to form a yellow-coloured product – 2-3-diaminophenazine, which has an absorbance maximum at 450 nm. A calibration curve was constructed with known concentrations of $H_2O_2$ (Sigma-Aldrich Catalogue Number: H1009), which was used to measure the formation of $H_2O_2$ in PAW.

Construction of the calibration curve for $H_2O_2$ measurement involved the preparation of the chemical reagents:

(i)     a tablet of OPD (CAS number: 95-54-5, Sigma-Aldrich Corporation) was dissolved in 10 mL of DIW;

(ii)    20 µL of 2 mg/mL HRP (CAS number: 9003-99-0, Sigma-Aldrich Corporation) was added into the solution prepared in (i); and

(iii)   different concentrations of $H_2O_2$ at 10 mM, 5 mM, 4 mM, 2 mM, 1 mM, 0.5 mM, and 0.25 mM (v/v) concentrations were prepared from a stock solution of 9.8 M $H_2O_2$ (CAS number: H1009, Sigma-Aldrich Corporation).

In the next step, 180 µL of OPD/HRP solution prepared in (ii) was transferred to the flat-bottomed well of a 96-well plate (CLS3599, Corning Inc.) and 20 µL of $H_2O_2$ concentration was added. This process was repeated in triplicates for all concentrations of $H_2O_2$ solutions prepared in (iii). The solution was then incubated for 15 minutes at room temperature and absorbance values of 2-3-diaminophenazine were measured at 450 nm in a plate reader (Synergy LX, BioTek). The absorbance values measured for increasing $H_2O_2$ concentrations are proportional to each other (Figure 4.3). The line of best fit derived from Figure 4.3 was used to estimate the $H_2O_2$ concentrations in PAW.

The $R^2$ value for this experiment was at 0.99448 (Figure 4.3), denotating a positive correlation and a strong linear relationship between absorbance and $H_2O_2$ concentration. The experiment was carried

out in triplicates with the means and standard deviations plotted for each of the six concentrations ranging from 0.25 to 10 mM.
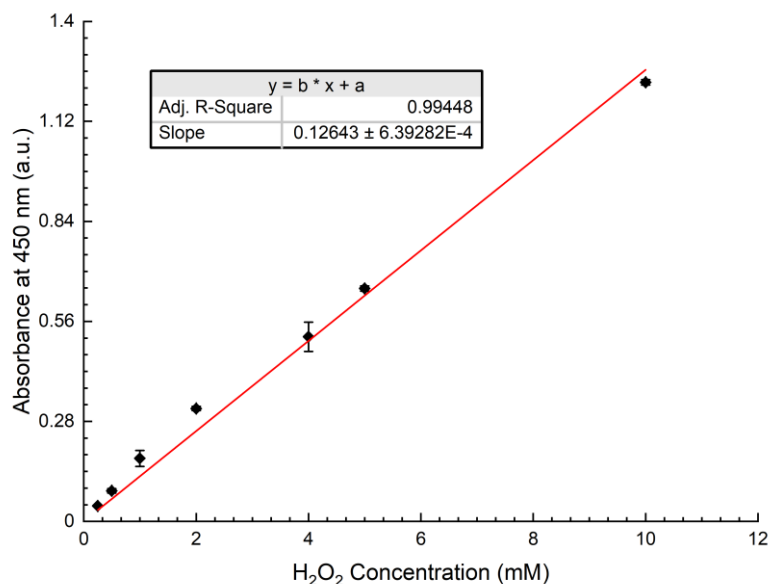


*Figure 4.3: $H_2O_2$ Calibration Curve using an ODP/HRP Reagent system calculated through linear regression. The experiment was performed in triplicate (n = 3) with the mean and standard deviations plotted.*

## 4.3.2.2 Measurement of $NO_2^-$ concentration

$NO_2^-$ concentration in PAW was measured after 1, 2, 3, 4, and 5 minutes CAP treatment times using Griess reagent (G-7921, ThermoFisher Scientific US). The G-7921 kit comprises of N-(1-napthyl)ethylenediamine dihydrochloride, sulfanilic acid, and sodium nitrite ($NaNO_2$). Sulfanilic acid reacts with $NO_2^-$ forming diazonium salt, which further reacts with N-(1-napthyl)ethylenediamine dihydrochloride to form a chromophoric azo dye.[213] An increase in absorbance indicated the production of $NO_2^-$ which can be recorded at a wavelength of 548 nm using a plate reader.

Griess reagent was prepared by mixing 10 µl of N-(1-napthyl)ethylenediamine dihydrochloride and 10 µl of sulfanilic acid. 20 µL of the Griess reagent was transferred to the flat-bottomed well of a 96-well plate (CLS3599, Corning Inc.) before adding 150 µL of DIW and 20 µL of $NaNO_2$ (of various concentrations). To make the calibration curve, stock solutions of $NaNO_2$ were prepared at the concentrations of 40 mM, 30 mM, 20 mM, 10 mM, 5 mM, and 2.5 mM. The calibration curve was carried out in triplicate for all concentrations of $NaNO_2$. The plate was incubated for 30 minutes at room temperature before using the Synergy LX, BioTek plate reader, for absorbance calculation at

wavelength 548 nm. A calibration curve was calculated, Figure 4.3. The gradient of Figure 4.4, 0.00338, was used to calculate the concentrations of $NO_2^-$ (mM) in PAW for each plasma treatment time.

The adjusted $R^2$ value (Figure 4.4) for this experiment is 0.99877 meaning that the relationship between absorbance and $NO_2^-$ concentration is linear. Standard deviations (n = 3) were plotted for each of the six concentrations between 2.5 and 40 µM, with only 10, 30, and 40 µM concentrations visible using the given y-axis scaling. None of the standard deviations between the different $NO_2^-$ concentrations overlapped.
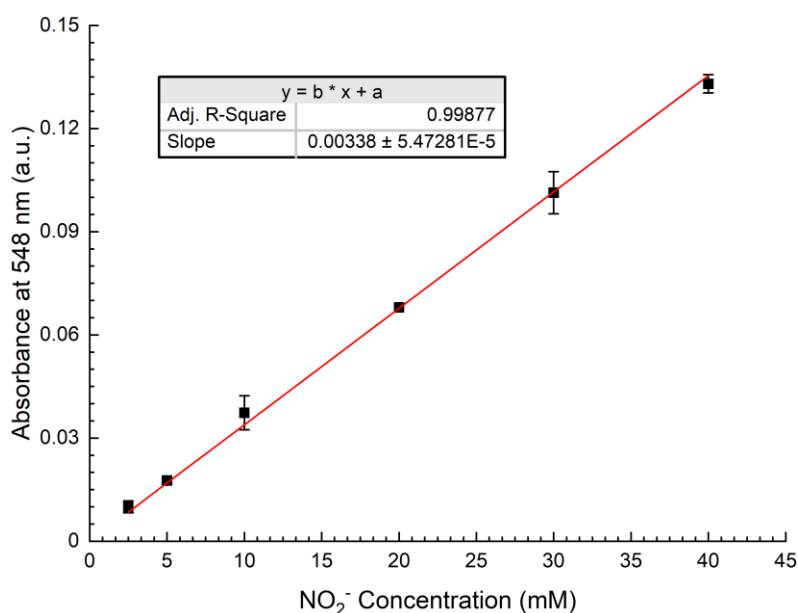


*Figure 4.4: $NO_2^-$ Calibration Curve using a Griess Reagent system calculated through linear regression. The experiment was performed in triplicate with the mean and standard deviations plotted.*

## 4.3.2.3 Temperature Measurement

The temperature of the plasma jet was measured using a thermometer (Fluke 652 Max) in direct contact with the CAP jet.

## 4.3.2.4 pH Measurements

pH of PAW was measured using an indicator paper (catalogue number: 110962, Merck Millipore). The indicator papers were cut into identical sized strips before they were soaked in 50 µl of PAW and a control, DIW. Change in colour of the indicator paper (Appendix 8.2, Figure 8.2) was compared with the colour chart (Appendix 8.2, Figure 8.3) with the naked eye.

## 4.3.3  Data Analysis

OriginPro 2020b (Academic) was used to perform all statistical analysis, using linear regression, One-way ANOVA, Tukey test, and Levene's test. OriginPro 2020b (Academic) and MATLAB R 2016a were both used to plot the graphs in this chapter. A *P*-value of $<0.05$ was used as statistically significant for all cases. Experiments were performed in triplicates and unless otherwise stated, and error bars on respective graphs represent standard deviations unless stated otherwise.

## 4.4 Results

This chapter describes the characteristics of the plasma jet utilised throughout this project. These are subsequently linked to the activation of PVP-I, release of therapeutic agent from the hydrogel and bactericidal effects which will be discussed in subsequent chapters. A change in plasma treatment time has significant impact on RONS generation, which should be optimised moving forward to investigate its bactericidal potential (Chapter 6).

### 4.4.1 Electrical Characteristics

Figure 4.5 depicts the current and voltage waveforms of the CAP jet used in this study. Plasma was generated at an applied voltage peak to peak ($V_{p-p}$) of 6.96 kV at 23.5 kHz, and at a gas flow rate of 1 SLPM. Included in Appendix 8.1 is the CAP jet ignited under these parameters (Figure 8.1). As the applied voltage is increased, two primary current peaks were observed at 2.11 µs and 3.96 µs. These are caused by the accumulation of wall charges inside the quartz tube.[214, 215] As the voltage reaches its peak and starts decreasing, the accumulated charges reverse in polarity giving rise to the appearance of two negative discharge current peaks. The root mean square of current caused by accumulated charges was 7.78 mA and the energy dissipated per cycle is 0.11 mJ.

$$P(t) = f \int_0^t V(t) \, I(t) \, dt \qquad \text{(Equation 4.20)}$$

Equation 4.20 describes the relationship, in generality, between the frequency (f), voltage (V) and current (I) yielding the power of the system over the time period $[0, t]$. Using a basic numerical approximation and the observed data, the power between time $t = 0$ and time $t = 42.5$ µS is calculated to be 2.61E+3 W.
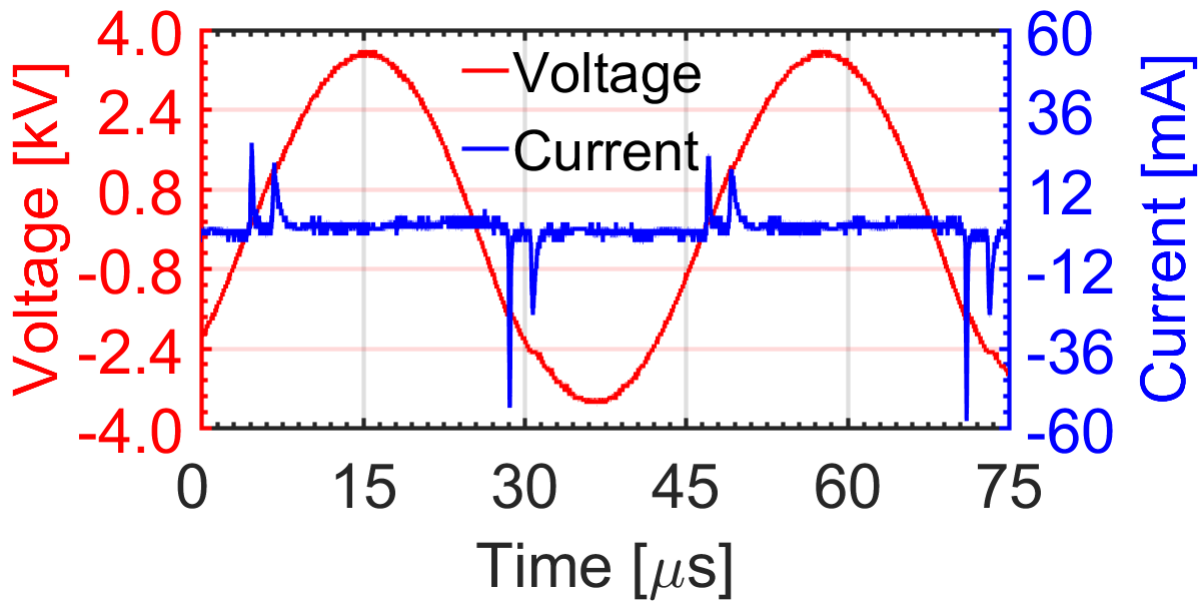
*Figure 4.5: Electrical Characteristics of the CAP jet. Operating parameters: $V_{p-p}$ = 6.96 kV at 23.5 kHz, Ar gas flow rate = 1 SLPM.*

## 4.4.2  Optical characteristics

OES is an important tool to identify the excited and short-lived reactive species generated from the plasma jet and the results are shown in Figure 4.6. The majority of the spectrum consists of emissions from excited argon which occurs between 690 nm and 900 nm. These are created through the collision of electrons with argon atoms present in the feeding gas. The spectrum also consists of emissions from short lived reactive species such as atomic oxygen O, excited nitrogen and •OH. Emission from atomic O is observed at 778 nm (Figure 4.5B).[216] This occurs through the dissociation of oxygen molecules present in the ambient environment. Between 300 to 400 nm, there are emissions from •OH and excited nitrogen species (Figure 4.5C). Emission from •OH occurs at 309 nm and is due to the dissociation of water vapour molecules present in the feeding gas and those present in the ambient environment. Excited nitrogen molecules (mainly bands from nitrogen second positive system, $N_2$SPS) are present between 311 to 380 and they occur through the dissociation of nitrogen molecules present in the ambient environment. These RONS led to the formation of long lived reactive species such as $H_2O_2$, etc. and these will be measured in the next section.[217]
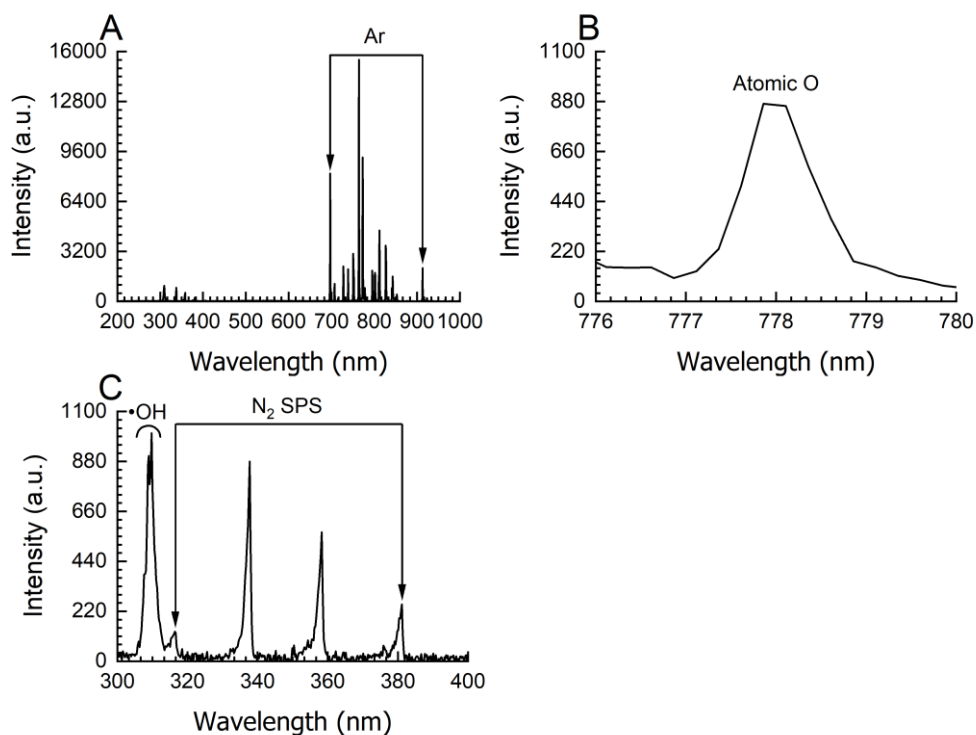
*Figure 4.6: Optical Emission Spectra of the Ar-driven CAP Jet taken at 5 mm position outside of the Quartz Tube: (A) between 200 to 1000 nm, (B) emission from atomic oxygen at 778 nm, (C) emission from •OH and excited nitrogen species between 300-400 nm. Operating parameters: $V_{p-p}$ = 6.96 kV at 23.5 kHz, Ar gas flow rate = 1 SLPM.*

### 4.4.3 Temperature Measurement

For the operation conditions used in this study (Operating parameters: $V_{p-p}$ = 6.96 kV at 23.5 kHz, Ar gas flow rate = 1 SLPM), the gas temperature was found to be cool at ≈40°C.

### 4.4.4 Quantification of long lived RONS in PAW

### 4.4.4.1 $H_2O_2$ concentration in PAW

Formation of $H_2O_2$ (Equation 4.4, section 4.2.1) occurs when OH• recombines at the gas-liquid interface. The $H_2O_2$ calibration curve using the ODP/HRP system is reported in Figure 4.3. As the concentration of $H_2O_2$ increases, the orange colour saturation within the 96-well plate increased in line with the respective increase in the absorbance recorded at 450 nm. UV-VIS is subsequently taken at 450 nm following incubation, and the concentration of $H_2O_2$ is directly proportional to the absorbance of 2-3-diaminophenazine at 450 nm, Figure 4.7.[218]

Figure 4.7 shows the quantification of $H_2O_2$ using an ODP/HRP system and the aforementioned CAP jet operating parameters. It was found that the concentration of $H_2O_2$ increased with increasing plasma treatment time. Mean $H_2O_2$ concentrations for each plasma treatment times are as follows for 1 through 5 minutes respectively: 0.52 mM, 0.81 mM, 1.20 mM, 1.47 mM, and 1.91 mM. A one-way ANOVA test found a statistical significance of $P$-value $<0.05$ between every combination of the means for each condition. Comparison of the means between 4 minutes and 5 minutes plasma treatment times has a $P$-value $<0.001$ illustrating a statistically significant relationship between $H_2O_2$ production and plasma treatment time. The results shown in Figure 4.7 agree with the current literature that demonstrates that an increase in plasma treatment time increases the production of $H_2O_2$ within plasma activated water.[219]
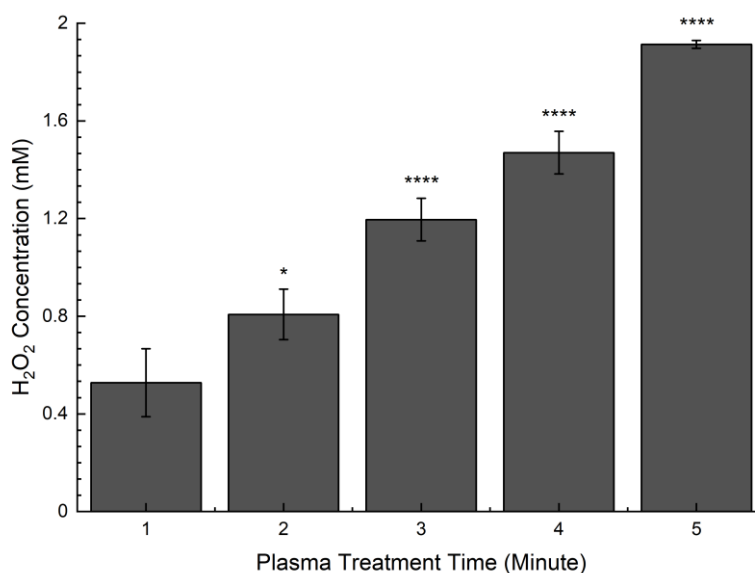


*Figure.4.7: Determination of $H_2O_2$ following varied plasma treatment times of DIW using ODP/HRP assay. Comparison of means between 1-minute plasma treatment time and 2, 3, 4, and 5-minute plasma time performed by Tukey Test: p<0.05 (*), p<0.0001 (****). Error bars represent standard deviations. Experiments carried out in triplicate (n=3). Operating parameters: $V_{p-p}$ = 6.96 kV at 23.5 kHz, Ar gas flow rate = 1 SLPM.*

## 4.4.4.2 $NO_2^-$ concentration in PAW

The $NO_2^-$ calibration curve using the Griess reagent assay is reported in Figure 4.4. A stock $NaNO_2$ solution contained within the commercially available kit was prepared to 40 mM, 30 mM, 20 mM, 10 mM, 5 mM, and 2.5 mM concentrations. As the concentration of $NO_2^-$ increases, the purple colour saturation within the 96-well plate increased in line with the respective increase in the absorbance

recorded at 548 nm before ultraviolet visible spectroscopy (UV-VIS) analysis. NO concentration can be therefore ascertained by UV-VIS of $NO_2^-$ at 548 nm.[220]

Figure 4.8 shows the concentration of $NO_2^-$ with the CAP jet under standard operating parameters. The gradient of the calibration curve has been used to convert the absorbance at 548 nm. When absorbance was recorded at 548 nm, the concentration of $NO_2^-$ decreased with increasing plasma treatment time. Mean $NO_2^-$ concentrations for each plasma treatment times are as follows: 12.13 µM, 11.83 µM, 6.51 µM, 1.48 µM and 0.30 µM for 1 through 5 minutes respectively. A one-way ANOVA test found an overall statistical significance of $P$-value $<0.05$ between the means at a population level. A Tukey Test showed that except 1 minute versus 2 minutes and 4 minutes versus 5 minutes, there was a statistically significant difference ($P$-value $<0.0001$) between the $NO_2^-$ concentrations for all other combinations of mean comparisons. Comparing the $NO_2^-$ concentrations after 1 minutes with 5 minutes, the $P$-value was $<0.001$ showing a statistically significant relationship between $NO_2^-$ production and plasma treatment time.
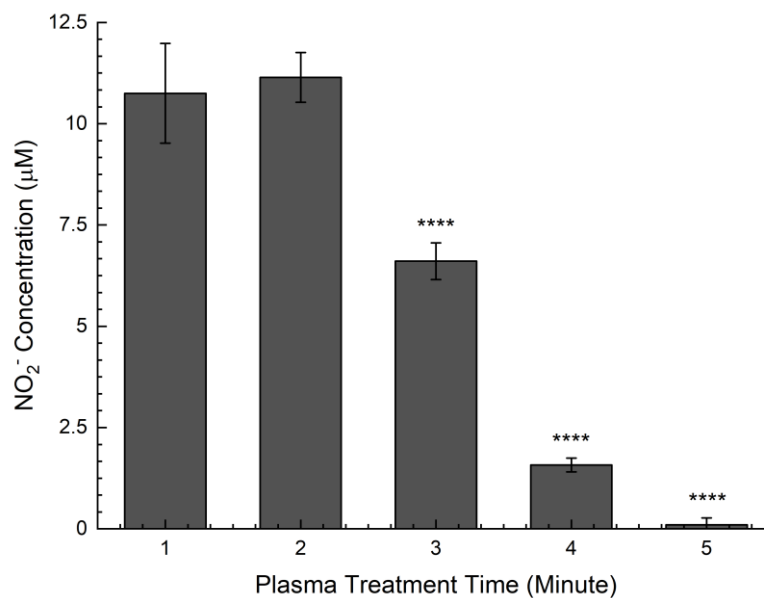


*Figure 4.8: Concentrations of $NO_2^-$ in PAW after 1, 2, 3, 4 and 5 minutes of CAP treatment using Griess reagent assay. Comparison of means between 1-minute plasma treatment time and 2, 3, 4, and 5-minute plasma time performed by Tukey Test: p<0.0001 (****). Error bars represent standard deviations. Experiments carried out in triplicate (n=3). Operating parameters: Vp-p = 6.96 kV at 23.5 kHz, Ar gas flow rate = 1 SLPM.*

## 4.4.4.3 pH of PAW

The pH of PAW was measured following varied CAP treatment times (1, 2, 3, 4, and 5 minutes) using pH indicator paper. The pH decreases with increase in the CAP exposure time, such that after 5 minutes of CAP treatment, the pH was 4.5, compared to 6.5 for untreated DIW (control). Results in Figure 4.9 are confirmed with supporting literature that also reports decreasing pH with longer plasma treatment times.[221] Interestingly, it was reported that the production of RONS associated with the decrease in pH does not occur linearly, and as such a slowing of decreasing pH after 30 minutes of plasma-treatment time was noted.

$$NO_2 + NO_2 + H_2O \rightarrow HNO_3 + HNO_3^+$$
$$\rightarrow NO_3^- + NO_2^- + 2H^+$$

*(Equation 4.21)*

$$NO_2 + NO + H_2O \rightarrow 2HNO_2 \rightarrow 2NO_2^- + 2H^+$$
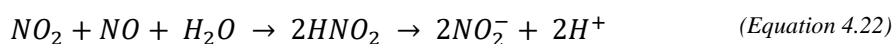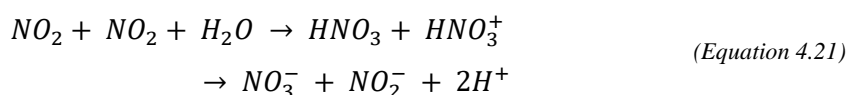
*(Equation 4.22)*

NO formed in water form from the equations (4.21, 4.22) $NO_2^-$ and $NO_3^-$ but also an abundance of hydrogen ion (H$^+$) contributing to the above decrease in pH.[222]
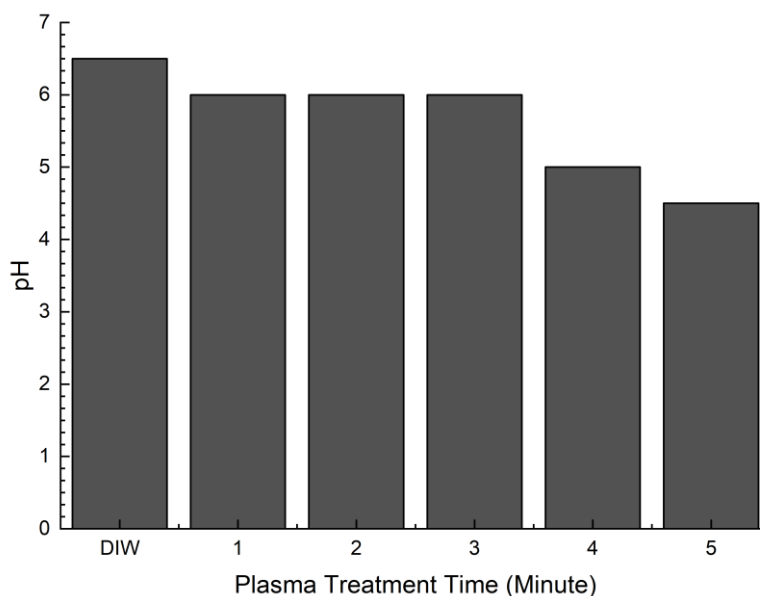


*Figure 4.9: pH of solution following varied plasma treatment times of DIW.*

## 4.5 Discussion and Conclusions

The aim of Chapter 4 was to establish the operating parameters of the CAP jet that are to be used in the subsequent chapters of this thesis. This was done using electrical, optical, pH, temperature and chemical analysis techniques.

Under the operating parameters used in this chapter, a CAP jet with plasma temperature of $\approx 40°C$ was established, thus making it suitable for the treatment of thermally sensitive materials such as tissues or in this thesis, hydrogels.

Observation of the current-voltage waveforms showed the appearance of discharge current peaks with the rise and fall in the spectra of applied voltage. These current peaks are caused by the accumulated charges which, during the discharge collide with neutral gas molecules, undergo dissociation and lead to the formation of excited/short-lived species. These species were observed through the techniques of optical emission spectroscopy. The OES showed the emission from several reactive species such as •OH, excited nitrogen, atomic oxygen, excited argon, etc. The short lived-reactive species are the precursor for the formation of long-lived reactive species. For example, •OH and O lead to the formation of $H_2O_2$, while excited $N_2$ species are responsible for the formation of $NO_2$ and $NO_3^-$.

The formation of long-lived reactive species was carried out using chemical analysis techniques. $H_2O_2$ was measured using OPD/HRP detection kit and it was found to increase with increasing plasma treatment time. Similarly, measurement of nitrite concentration was done using Griess reagent kit. Unlike $H_2O_2$, the concentration of $NO_2^-$ was not directly proportional to plasma exposure time. Initially, the reaction of $H_2O_2$ and $NO_2^-$ will form $ONOO^-$ at higher pH, and as the pH falls, the conversion of $NO_2^-$ to $HNO_2$ at lower pH's which is unstable and will further decompose to $NO_x$ means that the relationship between plasma treatment time and $NO_2^-$ is not directly proportional.[223]

pH of the plasma activated solutions was also measured. It was observed that with increasing plasma treatment time, the pH of the plasma activated solutions decreased. This is due to the formation of longer lived RONS such as such as $H_2O_2$, $ONOOH$, $HNO_2$, $NO_2^-$ which are known to reduce pH.

Further work to characterise the plasma jet should aim to investigate the electrical characteristics of the Ar-driven CAP jet when directed onto different targets such as aqueous solutions and hydrogels. A decrease in $V_{p-p}$ could be beneficial for chronic wound applications. Lower $V_{p-p}$ produce lower temperatures and thus would be more tolerable for the patient without risking thermal damage to the wound. It would be also interesting to study the differences in RONS productions at different distances away from the end of the quartz tube. Optimisation of RONS production is key to producing a CAP-based therapy and thus it is important to develop strategies for accurate and precise quantification of RONS, which can be an area of future study.

# 5 Chapter 5 : Characterisation of Plasma-Activated Povidone-Iodine

## 5.1 Aims

The overall aim of this chapter is to study the characteristics of plasma-activated povidone-iodine (PVP-I) to later incorporate into a PAHT. The initial portion of this chapter, Section 5.2, will provide an overview of the background of PVP-I and its current medical uses as an antimicrobial/antiseptic. Later in Section 5.4, the potential of plasma-activated PVP-I to tackle AMR will be discussed. This will include understanding the interactions of plasma-activated PVP-I with CAP-delivered RONS such as $H_2O_2$ and the subsequent release of reaction products such as hypoiodous acid (HOI). The formation of HOI in plasma-activated PVP-I is measured qualitatively using KI-starch gel assay (Section 5.4.2) and quantitatively using UV-Vis (Section 5.4.3). Changes in the pH of the plasma-activated PVP-I will also be investigated (Section 5.4.4).

## 5.2 Background

DFUs are one of the most dangerous consequences of DM and are the most common cause of non-traumatic lower-limb amputation as discussed in Chapter 1 with a lack of effective treatment methods for severe infections.[224] The current management of DFUs involves wound debridement and, if infected, an appropriate antibiotic therapy, which is determined by its bacteriology. Antibiotic therapy involves the use of systemic antibiotics to resolve infection and can last up to 6 months: drastically contributing to the ongoing problem of AMR (Chapter 1, Section 1.6).[9] As estimated by O'Neil[64] in his report, if not resolved by 2050, AMR could attribute to 10 million deaths per year. To date, there has been no promising development in terms of new antimicrobials.[58] An alternative avenue is now being explored which involves 'repurposing' currently available therapeutic drugs instead of creating a new antimicrobial.[225] One such concept being explored in this project is the enhancement of therapeutic efficacy of the antimicrobial – PVP-I using CAP against known bacteria within DFUs.

PVP-I was first used in 1955 and classified as an antiseptic.[226] PVP-I is a bound complex of polyvinylpyrrolidone (povidone), $H^+$, iodide ($I^-$), elemental iodine ($I_2$), and triiodide ($I_3^-$) as shown in Figure 5.1.[227] Herein, collectively $I^-$, $I_2$, and $I_3^-$ will be referred to as "iodine species". It is one of the most commonly used preparations in order to combat infection within chronic wounds.[228] When compared with antibiotics, antiseptics like PVP-I have a much wider antimicrobial activity with good efficacy against both Gram-positive and Gram-negative bacteria, and as such AMR is less likely to develop with this drug.[226, 227] It is reported to have good biofilm penetration, with low cytotoxicity and no reported impact on wound healing.[227] Common preparations of PVP-I within healthcare settings contain 10% PVP-I as solution or contained within a dressing.[229]
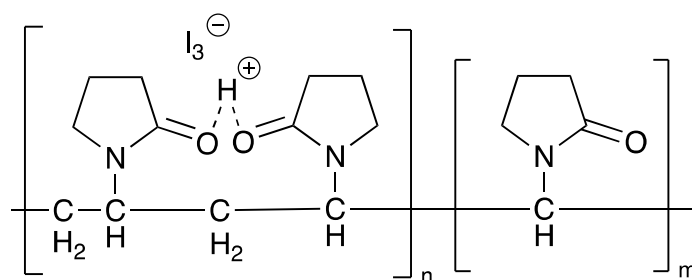


*Figure 5.1: Chemical Structure of PVP-I.*

Equation 5.1 illustrates the $I_3^-$ equilibrium that exists within PVP-I when in aqueous solution, with the point of equilibrium dependent on PVP-I concentrations. The equilibrium occurs such that concentration of free $I_3^-$ increases as $I_2$, and $I^-$ are consumed by a bacterium.[226] Although, the exact

mechanism behind the antimicrobial activity of $I_2$ is unknown , studies suggest that $I_2$ enters the bacteria through oxidation of fatty acids, nucleotides, free-sulphur amino acids, cysteine, and methionine which results in the formation of cell membrane pores causing bacterial death. .[229, 230] The development of bacterial resistance was tested against two strains of *Pseudomonas* with below minimum inhibitory concentration (MIC). It was reported that even after 20 passages, there was no noted change in the MIC or time taken for bacterial death.[229]

$$I_3^- \; \rightleftharpoons \; I_2 + I^-$$

*(Equation 5.1)*

$I_2$ can exist in aqueous solution as $I^-$ or as HOI, with the latter species being most relevant to antibacterial applications; and of particular interest to the results of this chapter.[229] Unfortunately, the inherent properties of $I_2$ mean that it is very unstable when in aqueous solution. The development of iodophors such as PVP-I that store unbound $I_2$ within their matrices have facilitated their extended use within wound healing and chronic wounds.[226]

Like $I_2$, $H_2O_2$ is also an oxidising agent with antimicrobial properties. As discussed previously in Chapter 4, the mechanism of action of $H_2O_2$ is through oxidative stress and lipid peroxidation.[231] In clinical practice, a solution of 3% of $H_2O_2$ is used against Gram-positive bacteria, making it an established method of treatment of wounds.[232] Relevant to this work, Chapter 4 has shown that the CAP jet is also an active source of $H_2O_2$ and other oxidative species with a production of 1.91 mM after 5 minutes plasma irradiation of DIW. As discussed in Chapter 3, CAP-treated solution such as PAW have anti-microbial potential, which can be attributed to RONS.

## 5.2.1 Hydrogels

Hydrogels are defined as three-dimensional networks of molecules that can swell and retain water without dissolving.[233] Their ability to retain water without dissolving means that they have been heavily utilised within the field of biomedicine, tissue engineering[234] and wearable electronics due to their its similar physical qualities to that of human tissue. Within the three-dimensional network, cross-linkages are formed which cause the hydrogel to solidify and facilitate the incorporation of drugs which may be hydrophilic.[233] These cross-linkages can either be permanent through chemical cross-linkage or non-permanent through physical cross-linking. Within permanent cross-linkages, hydrogen bonds are replaced with stronger covalent bonds, whereas in physical cross-linkage the

crossing of hydrogen bonds along with electrostatic forces are enough to withstand dissolution in water.[235]

As discussed in Chapter 3, PAW exhibits a greater bactericidal effect than the equivalent concentration of $H_2O_2$. Therefore, in this chapter, the potential interaction of $H_2O_2$ from CAP jet and PVP-I was investigated using a combination of UV-Vis, pH and hydrogels as a qualitative assay. The mixture of PVP-I and $H_2O_2$ has been reported in a few studies to date. Where the mixture had been investigated, it showed synergism in combination against *P. aeruginosa* and *S. aureus* and in clinical practice reduced the rate of infection following spinal surgery.[236, 237] Here, we propose to study of the PVP-I-$H_2O_2$ mixture thorough plasma activation.

## 5.3  Materials and Methods

### 5.3.1  Plasma Source

Section 4.3 outlines a schematic and details of the Ar-driven CAP jet used in this Chapter. Operating parameters of the CAP jet are $V_{p-p} = 6.96$ kV at 23.53 kHz at a constant 1 SLPM Ar.

### 5.3.2  Activation of PVP-I by CAP

A stock solution of 10% (w/v) PVP-I was prepared by mixing 20 g of PVP-I (CAS number: 25655-41-8, Sigma-Aldrich Corporation) in 200 ml of DIW using a magnetic bead stirrer at 500 rpm. 350 µl of PVP-I (0.04% (v/v), 0.1% (v/v), 0.5% (v/v) was then dispensed into a well of 96-well plate (CLS3599, Corning Inc.) and exposed to CAP jet for 1, 2, 3, 4, and 5 minutes at a fixed distance of 10 mm between the end of the quartz tube and top of the well. The plasma was in direct contact with the PVP-I throughout plasma-activation.

#### 5.3.2.1 Measurement of $H_2O_2$

The concentration of $H_2O_2$ delivered by the CAP jet in PVP-I was calculated by using commercially available kit: ODP (CAS number: 95-54-5, Sigma-Aldrich Corporation) and HRP (CAS number: 9003-99-0, Sigma-Aldrich Corporation). This process involved preparation of a calibration curve with known concentrations of $H_2O_2$ (detailed explanation in Chapter 4, Section 4.3.2.1). The line of best fit obtained from the calibration curve was used to estimate the residual $H_2O_2$ in plasma activated PVP-I.

$H_2O_2$ delivered by the CAP jet in PVP-I solution reacts with $I_3^-$ to form HOI. As $I_3^-$ reacts with $H_2O_2$ the OPD/HRP in this case underestimate the true concentration of $H_2O_2$ and will instead measure 'residual' $H_2O_2$ remaining after the aforementioned reaction. To calculate the total $H_2O_2$ produced in plasma-activated PVP-I Equation 5.2, was used, wherein $H_2O_2$ concentration in PAW was determined from Section 4.4.4. PAW as prepared as per Section 4.3.2 with 2 minutes plasma-treatment time.

$$\text{Total } H_2O_2 \text{ in PVP-I} = H_2O_2 \text{ concentration in PAW} - \text{Residual } H_2O_2 \text{ in PVP-I} \qquad \textit{(Equation 5.2)}$$

### 5.3.3  Qualitative Analysis

A commonly used method to visualize the effect of plasma treatment is to use potassium iodide (KI)-starch gels.[238] The principle is based on the oxidation of KI by plasma generated RONS to form a complex with starch that lead to the formation of purple colour.

Two types of indicator hydrogels were prepared:

(a) 0.5% (w/v) starch (CAS number: 9005-25-8, Sigma-Aldrich Corporation) in 1% agarose gel which was prepared by mixing 0.5 g of starch and 1 g of agarose in 100 mL of DIW and heating in microwave until they were dissolved.

(b) 0.5% (w/v) starch and 0.3% KI (CAS number: 7861-11-0, Sigma-Aldrich Corporation) in 1% agarose gel prepared by mixing 0.5 g of starch, 1g of agarose and 0.3g of KI in 100 mL of DIW and heating until completely dissolved.

Solution (a) and (b) were poured in separate 60 mm petri-dishes (CLS3260, Corning Inc.) to a thickness of 5 mm (5.65 mL) and left to set at room temperature.

Once set, 20 µl of DIW, PAW, PVP-I (0.04% (v/v), 0.5% (v/v)) or plasma-treated PVP-I (0.04%, 0.5%) solution was added atop of the gel. The agarose gels were then incubated at room temperature before photos taken after 90 minutes.

### 5.3.4  UV-Vis
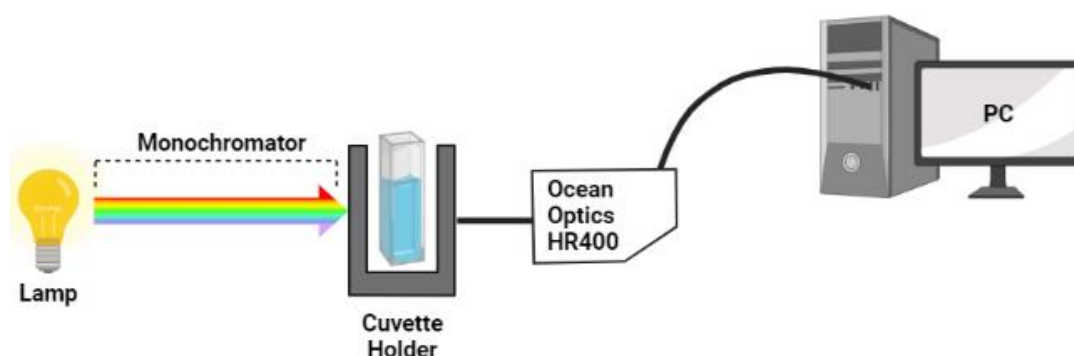


*Figure 5.2: Schematic for UV-Vis absorption spectrometry.*

UV-Vis spectra of the plasma activated solutions were measured by using a Deuterium-Halogen Lamp (Ocean Optics Inc.) and HR4000 spectrometer (Ocean Optics Inc.). The schematic for

measurement is as shown in Figure 5.2. A cuvette (Z637157, Sigma-Aldrich Corporation) was filled with 3 mL of DIW before adding 20 µL of test solutions (plasma treated/untreated) was added into it.

Equation 5.3 represents the absorbance of a sample where $I(\lambda)$ and $I'(\lambda)$ represent the intensities of the UV light before and after adding test solutions in DIW respectively. The Beer-Lambert's law was utilised to calculate the concentration of species in a solution from its absorbance: absorbance is equal to concentration ($c$) in mol dm$^{-3}$, multiplied by the optical path length or the dimensions of the cuvette ($l$), and the molar extinction coefficient of the solution ($\varepsilon$) mol dm$^{-3}$ cm$^{-1}$, Equation 5.4.

$$Absorbance = -log_{10}\left(\frac{I'(\lambda)}{I(\lambda)}\right)$$

*(Equation 5.3)*

$$Absorbance = cl\varepsilon$$

*(Equation 5.4)*

## 5.3.5  pH Determination

pH of plasma-activated PVP-I was measured using pH indicator paper (catalogue number: 110962, Merek Millipore). The change in colour of the indicator paper was matched with the provided scale (Section 5.7, Figure 5.7) and corresponding values were plotted (Section 5.7, Figure 5.5-6).

## 5.3.6  Data Analysis

Microsoft Excel was used for data handling and quantitative analysis of $H_2O_2$ concentration. OriginPro 2020b (Academic) was used to perform the one-way ANOVA, Tukey Test and Levene's Test to determine statistical significance. A *P*-value of <0.05 was used as statistically significant for all cases. A mixture of OriginPro 2020b (Academic) and MATLAB R 2017a was used to plot the graphs in this chapter. Experiments were performed in triplicate with the mean and standard deviations plotted. Unless stated, and error bars on respective graphs represent standard deviations unless stated otherwise.

## 5.4 Results and Discussion

### 5.4.1 Measurement of H2O2 in plasma-activated PVP-I

The $I_2$ species present in PVP-I are known to react with $H_2O_2$ leading to the formation of HOI through several reaction pathways (Equation 5.1-4):

$$I^- + H_2O_2 \rightarrow [I^-H_2O_2]^- \rightarrow HOI + OH^- \qquad \text{(Equation 5.5)}$$

$$I^- + H_2O_2 \rightarrow [I^-H_2O_2]^- \rightarrow 2OH^- + I^+ \qquad \text{(Equation 5.6)}$$

$$I^+ + OH^- \rightarrow HOI \qquad \text{(Equation 5.7)}$$

$$I^- + {}^1O_2 \rightarrow [I^-O_2]^- + H_2O \rightarrow HO_2 + HOI \qquad \text{(Equation 5.8)}$$
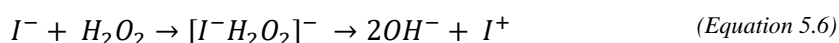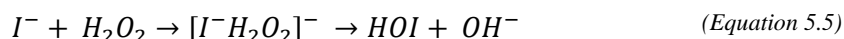
In other words, $H_2O_2$ (from the CAP jet) is consumed by PVP-I and the concentration of $H_2O_2$ in plasma activated PVP-I decreases. This phenomenon was observed in 0.1% (w/v) PVP-I solutions, as shown in Figure 5.3. The concentration of consumed $H_2O_2$ was determined using Equation 5.1 (Section 5.3.2.1).

As shown in Figure 5.3, in 0.1% PVP-I, the concentration of consumed $H_2O_2$ at all plasma exposure times (1-5 minutes) is ≈0.30 mM. There is no statistically significant difference between consumed $H_2O_2$ concentration at treatment times of 2-5 minutes compared to 1 minute. However, when compared to 1 minute of plasma treatment, the residual $H_2O_2$ concentrations after 3-5 minutes plasma treatment was significantly different. No significant difference was observed between amount of residual H2O2 formed after 1 minute and 2 minutes plasma treatment time.

The average residual $H_2O_2$ increases with plasma exposure time (5 > 4 > 3> 2>1 min), instead of decreasing. This could be due to scarcity of iodine species in PVP-I, due to a low concentration (0.1%), for the $H_2O_2$ to react with. It can, therefore, be speculated that 1.63 mM is the maximum concentration of $H_2O_2$ that a 0.1% PVP-I concentration can consume to form HOI.
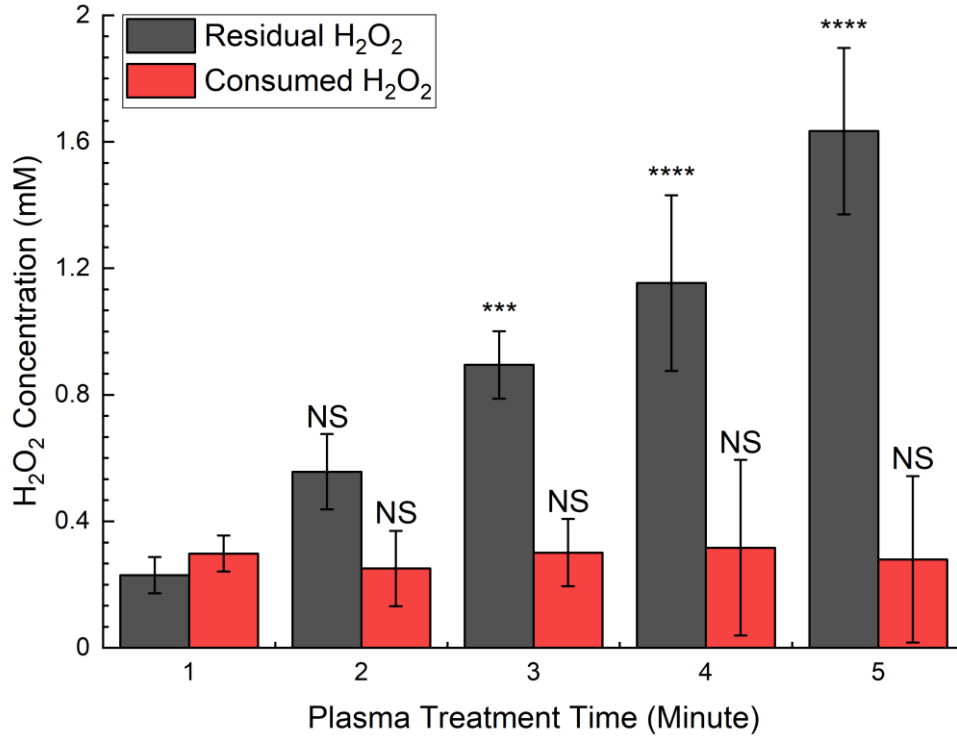
*Figure 5.3: Residual and consumed $H_2O_2$ concentrations for plasma-activated 0.1% PVP-I (w/v) calculated using ODP/HRP assay. Comparison of means between 1-minute plasma-treatment time and all other times (i.e. 1 versus 3) performed by Tukey Test: $p<0.001$ (***), $p<0.0001$ (****), not statistically significant (NS). Error bars represent standard deviations. Experient carried out in triplicate (n=3). Operating parameters: $V_{p-p} = 6.96$ kV at 23.5 kHz, Ar gas flow rate = 1 SLPM.*

## 5.4.2 Evidence of depletion of $I_3^-$ reservoir
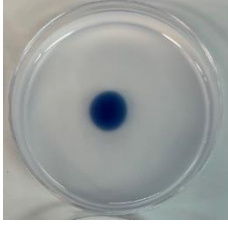
To further understand the characteristics of plasma activated PVP-I solutions, a qualitative assay based on KI-starch and agarose was utilised. The reaction mechanisms for this assay are shown below. Equations 5.8 to 5.10 show that the addition of an oxidising agent such as $H_2O_2$ to $I^-$ produces $I_2$ which further reacts with $I^-$ to create $I_3^-$.

$$2I^- + oxidising\ agent \rightarrow I_2 \qquad \textit{(Equation 5.9)}$$

$$I^- + I_2 \rightarrow I_3^- \qquad \textit{(Equation 5.10)}$$

$$I^{3-} + starch \rightarrow purple\ colour \qquad \textit{(Equation 5.11)}$$
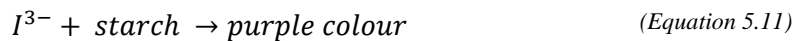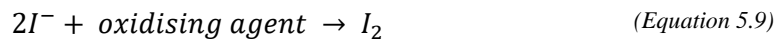
As the PVP-I solution already contained iodine species, qualitative analysis was performed on starch-agarose gels both with and without KI to avoid the over-estimation of effects induced by iodine species.

Firstly, different concentrations of PVP-I (0.04% and 0.5%, untreated/treated) were tested on agarose-starch gel (without KI). As shown in Table 5.1, none of the conditions except 0.5% PVP-I (untreated) resulted in the formation of the starch complex, observed as purple saturation in the gel. With 0% PVP-I (both untreated and plasma treated), no colour changes were observed, as expected, because the iodine species were absent. Similarly, at 0.04% PVP-I, the concentration of iodine species may be too low and that might have resulted in the colour change of the starch gel. For 0.5% PVP-I, colour change is observed with untreated PVP-I. This could be due to the presence of a sufficient quantity of available $I_3^-$ to react with starch. Interestingly, no colour is formed in case of plasma treated PVP-I. This could be attributed to the conversion of all the iodine species, including $I_3^-$, to HOI in presence of plasma delivered $H_2O_2$, resulting in no observed purple saturation in the gel.

Table 5.1: Photographs of starch-agarose hydrogel with (plasma treatment) and without (control) plasma treated solutions of 0%, 0.04% and 0.5% PVP-I. Operating parameters: $V_{p-p}$ = 6.96 kV at 23.5 kHz, Ar gas flow rate = 1 SLPM.

| Gel composition | PVP-I Concentration | Control (untreated) | Plasma Treatment |
|---|---|---|---|
| 0.5% w/v starch + 1% w/v agarose | 0% |  |  |
| | 0.04% |  |  |
| | 0.5% |  |  |

The second step involved qualitative analysis of plasma-treated of the same PVP-I concentrations as above, but using a KI-agarose-starch gel (Table 5.2) this time. In Table 5.1, no colour change was
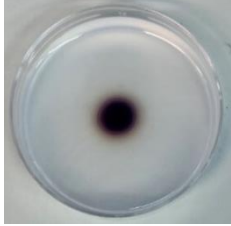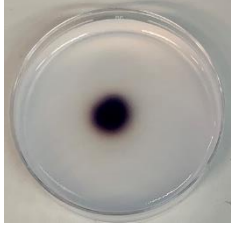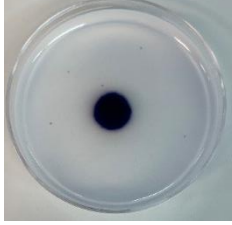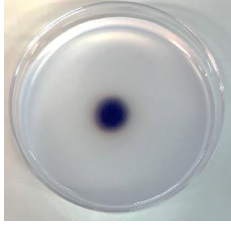
observed in any of the plasma treated PVP-I solutions due to the absence of a reporter system such as KI which can directly react with $H_2O_2$ to form the same purple starch-complex as shown in (Equation 5.8-10). Therefore, the addition of KI to this system allows us to assess the 'direct' effects arising from plasma-generated $H_2O_2$.

As shown in Table 5.2, at 0% PVP-I concentration (untreated), no starch complex was visualised in the gel due to the absence of oxidising species. The addition of PAW (plasma treated), acts as an oxidising species, resulting in the formation of the purple starch-complex from to the reaction between $H_2O_2$ and KI-starch.

At 0.04% PVP-I, no colour change was observed in untreated PVP-I as there are insufficient $I_3^-$ species to produce a visible colour. The colour change associated in plasma treated solution, with or without PVP-I, can be attributed to the presence of $H_2O_2$ as opposed to the presence of iodine species. This assumption is further strengthened by Figure 5.3 wherein in the case of plasma-activated 0.1% (v/v) PVP-I, only ≈0.3 mM of $H_2O_2$ is consumed out of the 1.63 mM surplus $H_2O_2$ at 5 minutes.

Finally, at 0.5% (v/v) PVP-I, both untreated and treated PVP-I solutions induce purple colour formation. This implies that there is enough $I_3^-$ delivered in starch-KI-agarose gel to produce the purple starch complex. But in plasma treated 0.5% PVP-I, the colour generated is not as strong as the untreated solution. This could be due to reaction of iodine species with plasma-generated $H_2O_2$ to form HOI.

*Table 5.2: Photographs of starch-KI-agarose hydrogel with untreated (control) and treated (plasma treated) solutions of 0%, 0.04% and 0.5% PVP-I.  Operating parameters: $V_{p-p}$ = 6.96 kV at 23.5 kHz, Ar gas flow rate = 1 SLPM.*

| Gel composition | PVP-I Concentration | Control (untreated) | Plasma Treatment |
|---|---|---|---|
| 0.3%  w/v KI + 0.5% w/v Starch + 1%  w/v Agarose | 0.00% | | |
| | 0.04% | | |
| | 0.50% | | |

## 5.4.3  UV-Vis Spectra

The UV-Vis spectra of the plasma activated PVP-I solutions were carried out to further support our observations for residual $H_2O_2$ measurements and the colour change observations in agarose gels in section 5.4.2. Figure 5.4 shows the UV-Vis spectra of 0%, 0.04% and 0.5% (v/v) PVP-I solution (in DIW): untreated (Figure 5.4A) and plasma-treated (Figure 5.4B).

At 0.5 % PVP-I concentration (Figure 5.4A), four absorption peaks: 225 nm, 288 nm, 350 nm, and a small peak at 460 nm can be observed. The peak at 225 nm is associated with $I^-$ while 288 nm and 350 nm peaks are associated with $I_3^-$ and $I_2$ at 460 nm.[239, 240] The intensity of these peaks were smaller at 0.04% (v/v) PVP-I than 0.5% (v/v) PVP-and no peaks were observed at 0% PVP-I.

The UV-Vis spectra following 2 minutes of plasma treatment are shown in Figures 5.4B. Like untreated, the same four absorption peaks occur. Comparing untreated PVP-I (Figure 5.4A) with treated (Figure 5.4B) indicates that the peak at 226 nm for PVP-I has similar absorbance as the corresponding peak in untreated PVP-I. However, the peaks at 288 nm, 350 nm, and 460 nm attributable to the iodine species, have decreased absorbance than the corresponding peaks in untreated PVP-I. The decrease in absorption may be attributable to plasma-jet-derived $H_2O_2$ reacting

with these iodine species in PVP-I and forming HOI. These results are in agreement to those observed with residual $H_2O_2$ concentrations (Section 5.4.1) and qualitative analysis experiments (Section 5.4.2).
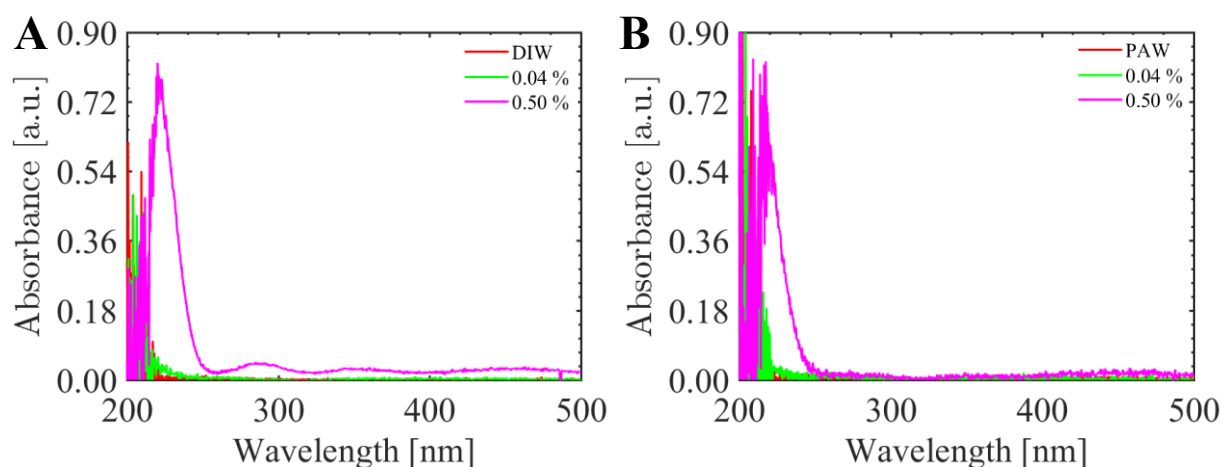


*Figure 5.4: UV-Vis of different concentrations of PVP-I (v/v) (A) before plasma treatment (B) after plasma treatment. Operating parameters: $V_{p-p}$ = 6.96 kV at 23.5 kHz, Ar gas flow rate = 1 SLPM.*

## 5.4.4  pH measurements

Figure 5.5 shows the changes in pH of plasma treated PVP-I (at 0.04 and 0.5%). At 0.04% (v/v) the pH of the solution decreases with increase in plasma treatment time between 1 to 5 minutes. One explanation for this is, as shown in Figure 5.3, the constant consumed $H_2O_2$ of ≈0.3 mM means that as plasma treatment time increases, as does residual $H_2O_2$ which becomes the dominant species responsible for the pH of the solution. At the higher concentration of 0.5% (v/v) PVP-I itself is inherently more acidic due to the $H^+$ found within its structure (Figure 5.1) hence the pH of 0.5% untreated PVP-I (0 minute) is lower than 0.04% (v/v). But, after 4 minutes of plasma treatment, both concentrations result in the same pH of 4.5 and as treatment time increases to 5 minutes, the trend is reversed such that pH at 0.50% is higher than 0.04% PVP-I. Figure 5.4 also shows that following CAP of 0.5% (v/v) PVP-I, for 1, 2, and 3 minutes the pH remains constant. This could be due to ongoing consumption of all the iodine species to form HOI and not all of the $H_2O_2$ and $H^+$ from the PVP-I structure has been consumed. However, an increase in pH is observed as plasma treatment increased to 4 and 5 minutes, suggesting that all of the $H_2O_2$ produced by the CAP jet has reacted with the $I^-$ resulting in HOI production, and there is proportionally more HOI than $H_2O_2$ which is a weaker acid than $H_2O_2$ resulting in a less-acidic pH. The results in Figure 5.5 compliment the results reported in Figure 5.3

76

.
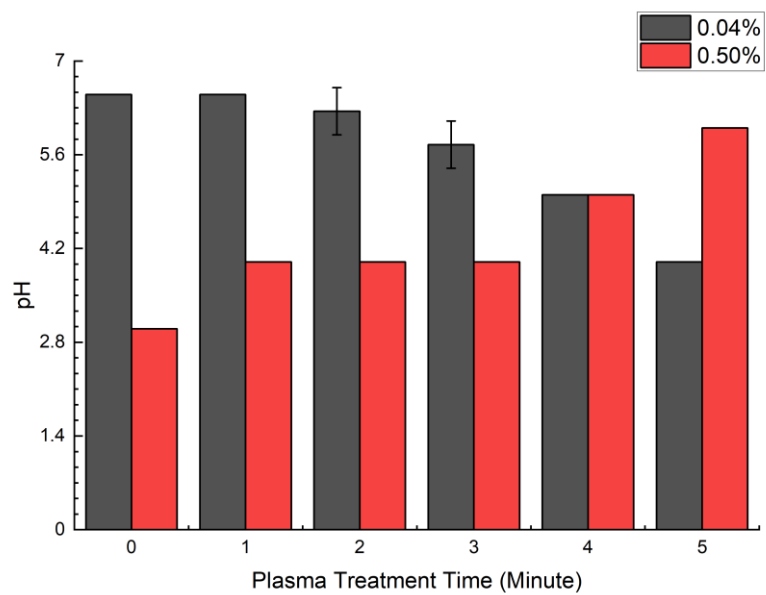
*Figure 5.5: pH of plasma activated PVP-I at two concentrations 0.04% (v/v) and 0.5% (v/v) at plasma treatment time of 1-5 minutes. Error bars represent standard deviations. Experiment carried out in duplicate (n=2).*

## 5.5  Conclusions

Overall, the background of the iodophor PVP-I has been explored and these results support its potential crucial role in antimicrobial repurposing. As aforementioned, only a few studies have investigated the effect of a $H_2O_2$-PVP-I mixture on wound healing. Here, production of this mixture is through the plasma-activation of PVP-I using CAP irradiation. Within a $H_2O_2$-PVP-I mixture, Equations 5.4-7 illustrate the production of HOI. Important to infection resolution is the $I_2$ from the $I_3^-$ equilibrium in PVP-I (Equation 5.1) as well as the production of HOI, which act as the bactericidal agents.

The experiments of this chapter have aimed to provide evidence of the formation of the highly unstable HOI. The results obtained in the agarose-starch reporter system and UV-Vis spectra demonstrate the consumption of $I^-$ and $I_3^-$ species, confirming the hypothesis that the $H_2O_2$-PVP-I mixture is forming HOI. Section 5.4.2 showed qualitative evidence using two different agarose-starch reporter systems. It was important to determine the presence of the starch-complex formation without KI in the agarose gel. The addition of KI provided an endogenous supply of $I^-$ for 0% PVP-I, and as $H_2O_2$, is an oxidising agent, the purple complex was seen. The addition of KI also confirmed with the results in Figure 5.3 and the supported the initial claim that iodine species were being consumed, as illustrated by the attenuation in Table 5.2. Interestingly, at a lower concentration of PVP-I (0.1% w/v) the consumption of $H_2O_2$ for the production of HOI was constant and with no statistical difference across the plasma treatment times for consumed $H_2O_2$. The pH characterisation between the two concentrations of PVP-I provide evidence that the more acidic $H_2O_2$ is being consumed for the less acidic HOI, as seen by the increase in pH with increasing plasma treatment times.

To best of my knowledge, this is the first work that has been done to try and characterise plasma-activated PVP-I, and concept of residual $H_2O_2$. The qualitative starch-agarose assays were developed to measure the total concentration of $H_2O_2$ delivered in plasma activated PVP-I. It is important for the application into the real-world to have more definite estimation of concentrations of $H_2O_2$ in order to monitor the dosage delivered to the DFUs. Further work to detect HOI directly would be prudent to achieve this. This study of PVP-I in Chapter 5 has allowed for a better understanding of the characteristics of plasma-activated PVP-I, including the hypothesised formation of HOI, which will be incorporated into the PAHT within Chapter 6, and subsequently released upon plasma irradiation of the gel onto bacteria.

# 6 Chapter 6 : Development of a Plasma-Activated Hydrogel Therapy

## 6.1 Aim

The overall aim of this chapter is to develop a plasma-activated hydrogel therapy (PAHT) for wound decontamination. Previous chapters have characterised the plasma source as well as investigate the properties of PVP-I. Chapter 6 will summate this and incorporate PVP-I into a PAHT for the application against DFU bacteria as determined through the systematic review in Chapter 2. This will complete the overall aim of this thesis of developing a PAHT for the specific application in DFUs.

The first portion covers a background on hydrogels, commonly used microbiology terms such as MIC, MBEC, and antibacterial assays utilised to determine the efficacy of PAHT. In order to achieve this, firstly, a plasma-activated polyvinyl alcohol (PVA) hydrogel dressing will be established, followed with assessing the delivery of RONS including $H_2O_2$ through the hydrogel. The latter portion of the chapter involved studying the anti-bacterial activity of the established PAHT (i.e. PVA) in planktonic cultures of *S. aureus* and *P. aeruginosa* and immature/mature biofilms of *P. aeruginosa*.

In previous chapters, the anti-microbial potential of various plasma-activated solutions such as PAW and an established antiseptic PVP-I was discussed. The results from previous chapters support the PAHT development a PVA-hydrogel dressing will be developed loaded with PVP-I to be released upon plasma jet-activation into the wound. In a clinical setting, the PAHT will involve placing a PVP-I- loaded PVA dressing on top of the DFU wound. The dressing will, then, be exposed to CAP treatment for a fixed duration. The action of plasma mediates the delivery of the reaction products (RONS and PVP-I) from the hydrogel dressing into the wound.

## 6.2 Background

### 6.2.1 Hydrogels

Hydrogels are defined as hydrophilic polymeric networks that are able to swell to many times their original size, as well as shrink for controlled drug elution.[241] Investigating the structure of a hydrogel at a nanometre level, the structure is such that cross-linkages surround water molecules within the matrix. The mesh structure of the hydrogel at this level will dictate what drug can be deposited into the hydrogel due to the size of spaces in the surrounding mesh as well as the properties of the drug, for example hydrophobicity.[242]

There are a variety of hydrogels available such as agarose, PVA, and carboxymethylcellulose, and depending on which hydrogel is selected, their size, structure, and function is different.[242] For example, the pore size of PVA is much smaller than that of agarose, with 10 µm and 550 µM respectively.[243, 244] In the development of PAHT, PVA has been chosen as the hydrogel polymer of choice. PVA is a widely used synthetic polymer ($C_2H_4O$) for drug delivery systems due to its three main properties: (i) low cell adhesion; (ii) high surface stability; (iii) and its ability to chelate. PVA is also non-toxic, water-soluble, non-carcinogenic, is able to biodegrade in human tissues or fluids, and has a high tensile strength making it ideal for use as a dressing in PAHT.[245]

The current problems facing that the traditional drug administration such as β-lactam antibiotics, particularly in treatment of DFUs, is the inability for sustained high circulating doses due to short half-lives of drugs. Antibiotics such as β-lactams and macrolides (as discussed in Chapter 2) are both time-dependent and concentration-dependent antibiotics meaning that they are only bactericidal when the circulating concentration reaches above MIC for that drug against a specific bacterium.[246] The need for frequent administration of the drug causes reduced patient compliance due to their adverse side effect profiles.[247] To address these issues, alternative drug delivery systems such as hydrogels have been developed in the hope to produce more beneficial outcomes for a given drug when incorporated. Current uses for hydrogels include their biomedical use in nanoparticles,[248] use as protective films, use as a coating, and as a drug delivery system.[241]

Hydrogels are also biocompatible compounds, due to their high-water content and similar physiochemical structure, meaning that they have been successfully implemented in a variety of anatomical sites such as the peritoneum (located within the abdomen).[242] Hydrogels have also been implemented as an alternative therapy for chronic wounds. Current "gold standard" therapies for large chronic wounds include partial- or full-thickness skin flaps, and although recommended, are not without problems such as flap donor site shortage or the psychological sequelae of having a skin flap.[249] Important for DFUs, hydrogels have a unique property compared to other dressings or

synthetic skin substitutes, whereby they can conform to its location and mimic the environment. If a drug could be incorporated into the hydrogel matrix, the drug will have complete contact as it elutes onto the surface of the wound and thus providing the ultimate drug-targeting solution.[242] Balakrishnan, B *et al.* studied the effect of an *in situ* forming hydrogel consisting of oxidised alginate and gelatine. They reported that after 2 weeks of use with the hydrogel on a full-thickness wound murine model that the wound had fully healed without any observed side effects. Also important for wound healing, they report that the hydrogel had swollen to 90% of its weight with fluid from the wound, and thus preventing the formation of any wound exudate that would hamper wound healing.[250]

$O_2$ is an especially important molecule for the success of wound healing due to an increase in requirement during the wound healing process.[251] It has been reported that wounds in hyperoxic environments show greater angiogenesis than respective hypoxic environments.[252] One of the major pathways that it is implicated in during wound healing is through the generation of ATP in the mitochondria from oxidative phosphorylation.[253] Previous agarose tissue models have shown that CAP treatment will increase the oxygenation of the local area.[206] This finding is important for the application of PAHT to DFUs which are inherently hypoxic due to peripheral vascular disease (Section 1.2.1.2). The ischaemia in DFUs has been shown to impair wound healing.[28] As such, the increase in oxygen thorough an agarose tissue model would oppose this and accelerate wound healing and vessel growth.[251]

As shown in Chapter 4, the Ar-driven CAP jet ignited under standard operating parameters produces •OH, a potentially harmful species inducing DNA damage within cells. The results from Gaur, N *et al.* using a commercially available hydrogel dressing and a simple gelatine hydrogel show the potential application for a PAHT, not only to deliver $H_2O_2$ to the wound, but also to mop up any •OH that is produced through plasma irradiation. Direct plasma irradiation has been shown to be potentially cytotoxic and contain genotoxic elements. The application of PAHT has been shown to be a reservoir for these species and preventing their penetration into cells and prevent the adverse consequences of CAP.[254-256] We hypothesise that a PAHT treatment regime would also produce none or limited side-effects such that the side-effect profile of PAHT would be less than that of a traditional antibiotic therapy.

One of the main choices of drugs used in wound healing are antibiotics such as β-lactams and macrolides to prevent infection. Antibiotics have inherently poor drug targeting abilities and short drug circulating times, often less than 12 h.[247] PAHT provides a solution to this problem through facilitating an exact dose of active antimicrobial, be it incorporated into the dressing or RONS delivered by plasma, as well as ensuring ease of drug targeting through direct contact to the uninfected or infected wound site, as shown in Figure 6.1.
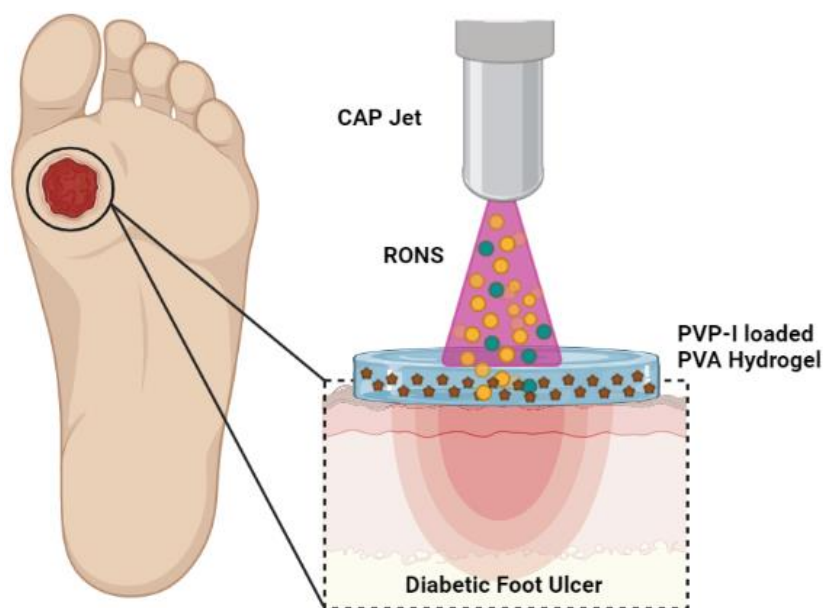
*Figure 6.1: Proposed schematic for the use of PAHT atop of a DFU. (Created by D Beith in BioRender.com).*

Unfortunately, hydrogels in biomedical applications are not without problems. Depending on the hydrogel polymer selected, they may have a low tensile strength, and may be damaged in transit, resulting in the loss or reduction of dose of the incorporated drug. Further disadvantages of hydrogels is due to their hydrophobicity, drugs that are also hydrophobic, and an estimated 40% of available drugs have poor water solubility, are not able to be combined and thus limit the potential application of a hydrogel therapy and PAHT.[241, 257, 258] It is such that during the development of the PAHT in this project, hydrogel parameters such as concentration of hydrogel polymer, number of cross-linkages, and thickness to create a robust product were considered.

## 6.2.2 Bacteria

As indicated through the systematic review of bacteria detected in DFUs using two different diagnostic methods (Chapter 2), the most abundant bacteria found in DFUs were *S. aureus* followed by *P. aeruginosa*. It is for this reason that this chapter will focus on the use of PAHT treatment against both species. Table 6.1 provides a concise overview of the bacterial assays used.

| Bacterial Assay | Description | Reference |
|---|---|---|
| MIC | MIC is defined as the lowest concentration of an antimicrobial that prevents planktonic microbial growth following incubation | 259 |
| Checkerboard Synergy | Use of MIC techniques to measure the cumulative effect of two drugs in tandem against a bacterium. The hypothesised eradication would occur at sub-MIC concentrations of each compared to each antibacterial in isolation. | 260 |
| Kirby-Bauer | A disk diffusion method to determine efficacy of an antimicrobial against a bacterium through production of a zone of inhibition | 261 |

One of the assays used against *S. aureus* is a checkerboard assay. It is able to determine the efficacy of the antimicrobial combination effect through producing a Fractional Inhibitory Concentration (FIC) Index. FIC Indexes are used to determine if the combination of antimicrobials was beneficial for the eradication of said bacterium. Equation 6.1 shows how it is calculated. A FIC Index of less than 0.5 indicates synergism, ≥0.5-4 is an additive response and above 4 is antagonistic.

$$\frac{FIC}{Index} = \frac{MIC\ H_2O_2\ Combination}{MIC\ H_2O_2\ Only} + \frac{MIC\ PVP - I\ Combination}{MIC\ PVP - I\ Only} = FIC_a + FIC_b \qquad \text{(Equation 6.1)}$$

## 6.3 Materials and Methods

### 6.3.1 Plasma Source

Section 4.3 outlines the operating parameters of the CAP jet used throughout this work. The CAP jet was ignited at a $V_{p\text{-}p}$ of 6.96 kV at a frequency of 23.53 kHz. The jet was operated at a gas flow rate of 1 SLPM.

### 6.3.2 Optimisation of the PAHT

#### 6.3.2.1 PVA hydrogel

A 5% (w/v) PVA gel ($M_w$ 146,000-186,000, CAS number: 9002-89-5, Sigma-Aldrich Corporation) was prepared by adding 20 g of PVA into 200 ml of DIW and stirring it using a magnetic bead stirrer at 800 rpm and 95°C until dissolved. After achieving a homogenous solution of PVA, the mixture was allowed to cool at room temperature. The following thicknesses (1) 2mm, (3) 4mm, (4) 8mm were cast in 60 mm culture dishes (CLS430166, Corning Inc.) and placed in a -10°C freezer overnight. The PVA hydrogels were subject to a total of 3 freeze-thaw cycles and remained frozen until allowed to thaw completely at room temperature before any CAP jet experiment.

#### 6.3.2.2 PAHT treatment regimen

A 10 mm dimeter disc of 5% PVA hydrogels following 3 freeze-thaw cycles was placed on top of a well in a 96-well microtiter plate (CLS3599, Corning Inc.) containing 350 µL DIW. Plasma treatment was carried out as per Figure 6.2 which was done using raster mode, for 5 minutes. Plasma-irradiated PVA hydrogels were then left on top of the well and incubated for 150 minutes at room temperature before RONS quantification.
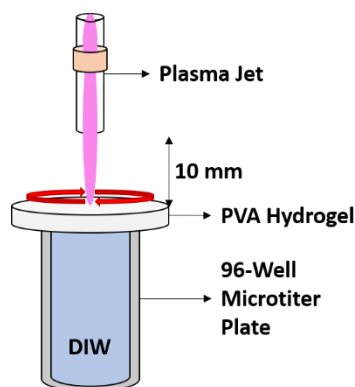
*Figure 6.2: Schematic for quantitative quantification of the effect of PVA screen thickness on RONS delivery.*

### 6.3.2.3 Gas flow and RONS transport

The effect of gas flow on RONS movement through the PVA screen was also investigated (Figure 6.3). 10 mm diameter discs of 5% PVA were plasma irradiated on top of a 96-well microtiter plate (CLS3599, Corning Inc.) containing 350 µL of DIW for 5 minutes in a raster (Figure 6.3A). The plasma was subsequently turned off and 1 SLPM of Ar gas was applied to the top of the PVA hydrogel in a raster for a further 15 minutes (Figure 6.3B). The PVA hydrogel was left on top of the well and incubated at room temperature for 150 minutes before RONS quantification of the liquid below the PVA hydrogel.
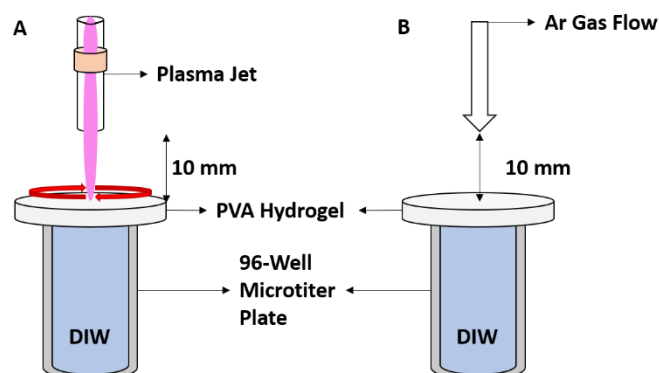


*Figure 6.3: Schematic for the quantitative analysis of the role of gas flow on the delivery of RONS through PVA screens of different thicknesses. d = 10 mm.*

## 6.3.2.4     H$_2$O$_2$ Quantification

A broad range RONS reporter – KI was used to measure the plasma-delivery of RONS from PVA into DIW. Colourless KI upon reaction with RONS undergoes oxidation to form a purple-coloured product. After 150 minutes of incubation, 50 μL of plasma treated DIW was resuspended in 150 μL of 10 µM w/v KI (CAS number: 7681-11-0, Sigma-Aldrich Corporation) in a 96-well microtiter plate (CLS3599, Corning Inc.). This was followed with an incubation of 15 minutes at room temperature. Absorbance was recorded at 350 nm wavelength with Synergy LX, BioTek plate reader.

Section 4.3.2.1 provides the method for the determination of H$_2$O$_2$ concentration using the commercially available ODP/HRP kit. Absorbance was recorded at 450 nm wavelength (Synergy LX, BioTek plate reader) before normalising the results by removing the background (DIW). Once normalised, the absorbance values were divided by the gradient of the H$_2$O$_2$ calibration curve (Figure 4.3) to produce the H$_2$O$_2$ concentration.

## 6.3.2.5     Qualitative RONS analysis

Figure 6.4 illustrates the schematic for qualitative RONS quantification through the PVA hydrogel of varying thicknesses using a KI-starch-agarose hydrogel indicator. Section 5.3.3 describes the protocol for making 0.3% (w/v) KI 0.5% (w/v) starch-1% (w/v) agarose hydrogels to as a qualitative indicator for RONS delivery. Hydrogels were cast in 60 mm plastic culture dishes (CLS430166, Corning Inc.) to a hydrogel thickness of 5 mm (5.65 mL) and stored at 4°C until used. PVA hydrogels of varying thicknesses were placed on top of identically sized agarose indicator gels before plasma irradiation for 5 minutes, moving the plasma continuously in a raster for the duration of the irradiation. Samples were then incubated at room temperature for 150 minutes before observing a colour change.
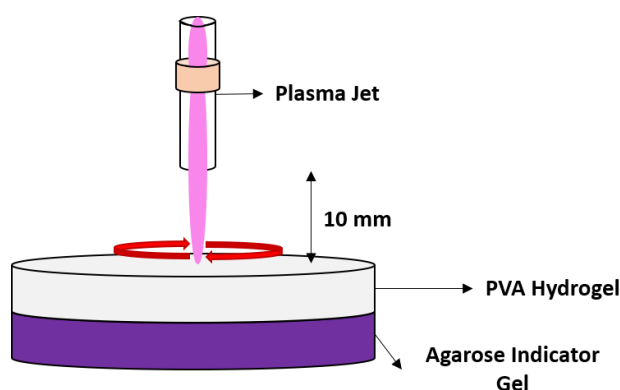


*Figure 6.4: Schematic for qualitative RONS analysis.*

The effect of gas flow was also determined qualitatively using the KI-Starch-Agarose indicator gel as an indicator of RONS transport and the formation of the purple complex is outlined in Equation 5.9-5.11. PVA screens were cast 2 mm, 4 mm, and 8 mm thicknesses in 60 mm plastic culture dishes before undergoing 3 freeze-thaw cycles at -10°C in a conventional freezer. They were then placed atop of an identically sized set 0.3% w/v KI 0.5% w/v Starch 1% w/v Agarose bottom gel. The agarose bottom gels were then plasma irradiated through the PVA screen for 5 minutes moving the plasma in a raster fashion for the duration of the irradiation before turning off the plasma and subjecting the gels to 15 minutes of 1 SLPM Ar continuously moved in a raster. Samples were then incubated at room temperature for 150 minutes before observing any colour change.
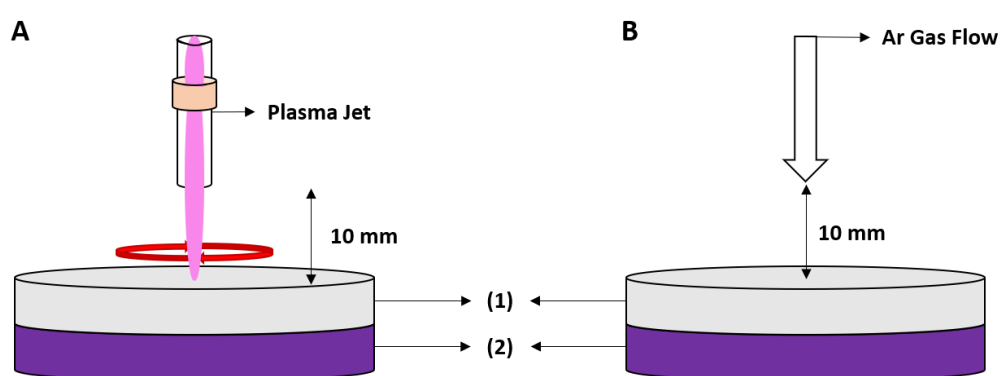


*Figure 6.5: Schematic for the qualitative analysis of the effect of gas flow on RONS transport through a variety of PVA screen thicknesses. (1) 5% PVA screen at thicknesses 2 mm, 4 mm, 8 mm; (2) 0.3% w/v KI 0.5% w/v Starch 1% w/v Agarose top gel.*

## 6.3.3  Bacteria culture

*S. aureus* (H560) and *P. aeruginosa* (PAO1), previously stored at -80°C, were grown for 18 h at 37°C on tryptic soy agar (TSA) (22091, Sigma-Aldrich Corporation) plate and Luria Bertani agar (LBA) (22700025, Fischer Scientific UK Ltd.) plate, respectively from the Jenkins Research Group at the University of Bath*. The following day, single colonies of H560 and PAO1 were transferred into 10 mL of trypticase soy broth (TSB) (Z699209, Sigma-Aldrich Corporation) and Luria Bertani (LB) broth (10855001, Fischer Scientific UK Ltd.), respectively. These were allowed to grow in a shaking incubator for another 18 h at 37°C at 200 rpm. The product was an overnight (ON) culture of H560 and PAO1 at a population density of $10^9$ CFU per mL.

For subcultures, the ON 10 mL cultures were centrifuged (Eppendorf, 5810R) at 4000 rpm for 10 minutes. The supernatant was discarded and 10 mL of phosphate buffer solution (PBS) (Fischer Scientific UK Ltd.) was added to the bacterial pellet before resuspension. 10 µL of this resuspended bacterial solution was dispensed in a separate falcon tube containing 10 mL of PBS, such that the final bacterial suspension had a population density of $10^5$ CFU per mL.

*All bacterial work done in this chapter was performed by Dominic Beith, in collaboration with Professor Toby Jenkins at the University of Bath, under the supervision of Dr Bethany Patenall.

## 6.3.4  96-well microtiter plate biofilms

ON cultures were sub-cultured as described in Section 6.2.5. 10 µL of the H560 and PAO1 suspension was resuspended in TSB with 1% (v/v) D (+) glucose and LB with 50% v/v D (+) glucose, respectively. These sub-cultured bacterial suspensions had a population density of $10^5$ CFU per mL. 200 µL of each of these bacterial suspensions was then added to a well of a 96-well microtiter plate. Wells without bacteria i.e. with 200 µL of TSB with 1% (v/v) D (+) glucose or LB with 50% v/v D (+) glucose were negative controls. All plates were incubated at 37°C for 18 h to allow biofilm formation on the inside of the microwell surface.

## 6.3.5  Minimum inhibitory concentration

The MIC was determined for H560 against a mixture of $H_2O_2$ and PVP-I. Figure 6.2 displays the labelled layout of a 96-well plate used for the determination of MIC for H560.

First, 100 µL of TSB was added to the blue microwells in a 96-wells plate; herein, I will describe the 96-well plate as column number followed by row letter, for example 1 A is the first column and first row. 200 µL of stock solutions of 8.9 M $H_2O_2$ (Sigma-Aldrich Corporation) or 10% (w/v) PVP-I was added to 2 B-D. Serial dilution was performed by transferring 100 µL of the solution from 2 B-D to 10 B-D before continuing the dilution from 10 B-D into 2 E-G and so on until 10 E-G. It was such that 10 E-G had a final concentration of 3.40E-2 mM $H_2O_2$ or 3.81E-5 % (w/v) PVP-I.

To these dilutions, 100 µL of H560 subculture was then added to each of the blue wells for a final volume in each microwell of 300 µL. 200 µL of TSB (without bacteria) and H560 subculture only,

were utilised as a negative (red coloured wells in Figure 6.6) and positive (green coloured wells in Figure 6.6) controls, respectively.

The FLUROstar plate reader was used to measure absorbance (Optical Density) at a wavelength of 600 nm. Optical Density measurements were performed immediately before (at 0 h) and after an incubation (at 37°C) of 18 h. The value of absorbance was used as an indicator of bacterial growth. MIC was determined between the minimum concentration to that inhibited H560 growth and the following column which would be the maximum concentration that uninterrupted the growth of H560 (Appendix 6.6.1).

|   | 1 | 2 | 3 | 4 | 5 | 6 | 7 | 8 | 9 | 10 | 11 | 12 |
|---|---|---|---|---|---|---|---|---|---|----|----|----|
| A |   |   |   |   |   |   |   |   |   |    |    |    |
| B |   |   |   |   |   |   |   |   |   | *  | -  |    |
| C |   |   |   |   |   |   |   |   |   | *  | -  |    |
| D |   |   |   |   |   |   |   |   |   | *  | -  |    |
| E |   | * |   |   |   |   |   |   |   |    | +  |    |
| F |   | * |   |   |   |   |   |   |   |    | +  |    |
| G |   | * |   |   |   |   |   |   |   |    | +  |    |
| H |   |   |   |   |   |   |   |   |   |    |    |    |

*Figure 6.6: Schematic of 96-well microtiter plate for determination of H560 MIC. Blue wells indicate combination of serially diluted $H_2O_2$/ PVP-I, H560 subculture, and TSB. Red wells act as a negative control containing only TSB. Green wells equal the positive control containing only H560 subculture. Yellow arrows indicate direction of serial dilution. \* indicate transposition of serial dilution from 10 B-D to 2 E-G.*

## 6.3.6  Checkerboard synergy assay

Figure 6.7 illustrates a schematic of the 96-well plate for the checkerboard synergy assay. In a 96-well microtiter plate, 100 µL of TSB was added to each well of 2-12 A-G. 100 µL of 200 mM (v/v) $H_2O_2$ was added to the wells of rows 1 A-G, and serial dilution across the abscissa was performed by transferring 50 µL of 200 mM (v/v) $H_2O_2$ from 1 A-G to 2 A-G, and so forth finishing with 11 A-G. 50 µL of 10% (w/v) PVP-I was added to the wells of 1-10 A. Serial dilution was performed by transferring 50 µL from the well in row A down the ordinate of the plate up to Row G. Completion of both serial dilutions is illustrated in Figure 6.3 as yellow wells. The MIC for $H_2O_2$ against H560 (blue wells) was then determined by adding 50 µL of 200 mM (v/v) $H_2O_2$ to 1 H and serially diluting across abscissa of the plate until 11 H. For PVP-I MIC determination against H560 (orange wells), 50 µL of

10% (w/v) PVP-I was added to 11 A and serially diluted down the column finishing at 11 H. The brown well in Figure 6.3 indicates a mixture of PVP-I and $H_2O_2$ in the MIC determination study.

H560 subcultures were prepared as per Section 6.2.5 and 100 µL was dispensed to all the wells, except in column 12. 100 µL TSB in wells B-D and 100 µL of H560 in the wells E-G contained 100 µL H560 subculture, of column 12, were used as negative (red) and positive (green) controls.

The FLUROstar plate reader was used to measure absorbance at a wavelength of 600 nm. Optical Density measurements were performed immediately before (at 0 h) and after an incubation (at 37°C) of 18 h. The value of absorbance was used as an indicator of bacterial growth. Appendix 6.6.3 shows raw absorbance recording at 600 nm following incubation.

| | | | | | | $H_2O_2$ Concentration (mM) | | | | | | |
|---|---|---|---|---|---|---|---|---|---|---|---|---|
| | | 50 | 25 | 12.5 | 6.25 | 3.13 | 1.56 | 0.78 | 0.39 | 0.19 | 0.01 | PVP-I MIC |
| PVP-I Concentration (% (v/v)) | 2.50 | | | | | | | | | | | |
| | 1.25 | | | | | | | | | | | |
| | 0.63 | | | | | | | | | | | |
| | 0.31 | | | | | | | | | | | |
| | 0.16 | | | | | | | | | | | |
| | 0.08 | | | | | | | | | | | |
| | 0.04 | | | | | | | | | | | |
| | $H_2O_2$ MIC | | | | | | | | | | | |

*Figure 6.7: Schematic of 96-well microtiter plate for Checkerboard Synergy Assay of H560 with $H_2O_2$ and PVP-I. Yellow wells indicate a mixture of serially diluted PVP-I (ordinate) and $H_2O_2$ (abscissa). Blue wells indicate MIC $H_2O_2$ and orange indicates MIC PVP-I. 11 H (brown) represents a mixture of PVP-I and $H_2O_2$ in the MIC determination study.*

## 6.3.7  PVP-I loaded PVA hydrogels

For the creation of PVA-PVP-I hydrogel, 10% (w/v) PVA ($M_w$ 146,000-186,000, CAS number: 9002-89-5, Sigma-Aldrich Corporation) was created as per Section 6.2.2. to create a homogenous solution and allowed to cool to room temperature. A 10% PVP-I (w/v) (CAS number: 25655-41-8, Sigma-Aldrich Corporation) was made up in DIW and mixed in a 1:1 ratio with the cooled 10% (w/v) PVA with constant stirring at 800 rpm for 15 minutes.

PVA-PVP-I hydrogels were then cast in 60 mm culture dishes (CLS430166, Corning Inc.) to a thickness of 5 mm and placed in a -10 °C freezer. The PVA-PVP-I hydrogels underwent 3 freeze-thaw cycles before CAP jet experiments.

## 6.3.8  Kirby-Baur Assay

100 µL of H560 or PAO1 bacterial subculture was inoculated onto the surface of a Mueller-Hinton (MH) agar (70191, Sigma-Aldrich Corporation) using a cell spreader. The plates were left to air-dry at room temperature for 15 minutes before placing a PVP-I PVA hydrogel disc of 10 mm in diameter, in the middle (Figure 6.8A). Plates were incubated overnight at 37°C. Following incubation, the diameter of the zone of inhibition was measured using a ruler in mm across the widest point as shown in Figure 6.8B. Experiments were performed in triplicate with mean zone of inhibition and standard deviations were calculated.
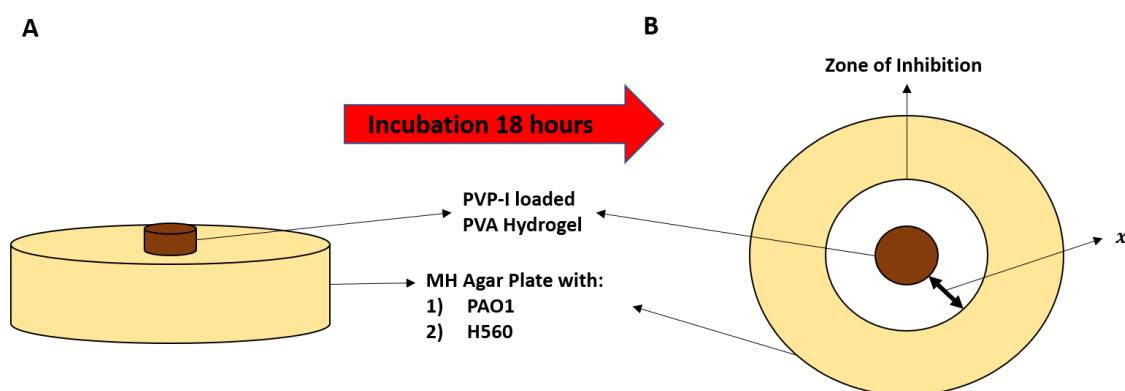


*Figure 6.8: Schematic for Kirby Bauer Assay with PVP-I PVA hydrogels. x represents the recorded distance for zone of inhibition from the edge of the PVP-I loaded PVA hydrogel to the edge of the zone in millimetres.*

## 6.3.8.1    Effect of PVP-I concentration

Three different concentrations of PVP-I (w/v) (0.1%, 1%, 10%) were studied. For each concentration a PVP-I hydrogel solution was mixed in a 1:1 dilution with 5% (w/v) PVA solution and later subjected to 3 freeze-thaw cycles. PVP-I loaded screens were then punched out into discs of diameter 10 mm before washing with PBS to remove any residual surface PVP-I. PVP-I loaded PVA hydrogels were placed in the centre of the inoculated plate (H560/PAO1) before plasma irradiation for 3 minutes (raster mode) was carried out under the operating parameters described in 6.3.1, Figure 6.9. Plates were then incubated at 37°C for 18 h and the zone of inhibition for each plate was measured after 18 h (Appendix 8.5).
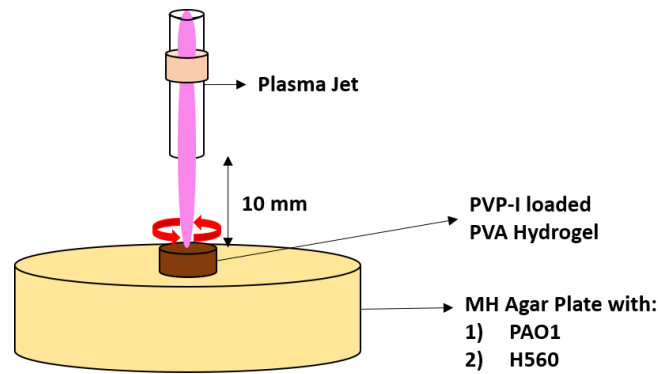
*Figure 6.9: Schematic for the Kirby-Bauer Assay with varied PVP-I concentrations loaded into a PVA screen against PAO1 and H560. Mueller-Hinton (MH); d = 10 mm.*

## 6.3.8.2    Effect of gas flow against PAO1

The effect of gas-flow was studied independent to CAP irradiation this time. PVP-I loaded-PVA hydrogels at the following concentrations 0.1%, 1% and 10% (w/v) were cast to a thickness of 4 mm and subject to 3 freeze-thaw cycles. 10 mm diameter discs were punched out and washed in PBS before placing the centre of the PAO1 inoculated MH agar plates. Figure 6.10 shows the schematic for the gas-flow condition in this experiment. Ar gas flow at 1 SLPM was moved in a raster across the surface of the PVA screen for 3 minutes before incubation for 18 h at 37°C.
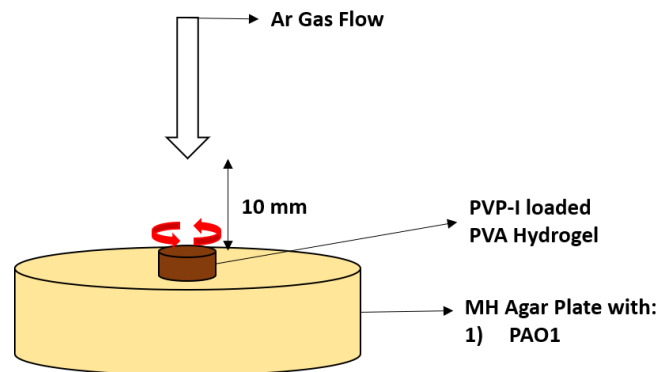


*Figure 6.10: Schematic for Kirby-Bauer Assay for the determination of the effect of gas flow on PAO1 zone of inhibition. Mueller-Hinton (MH); d = 10 mm.*

### *6.3.9* **Wound Biofilm Model** *In vitro*

In the centre of a brain-heart infusion agar (BHIA) (70138, Sigma Aldrich Corporation), 25 mm diameter Whatman®nuclepore™ track-etched membrane discs (WM) (WHA110659, Sigma-Aldrich Corporation) were placed shiny-side up. The plates were then placed in a laminar air flow hood and sterilised for 10 minutes using the in-built UV-C lamp.

Artificial wound fluid (AWF) was prepared by mixing foetal bovine serum and peptide solution, both sourced from Sigma-Aldrich Corporation, in a ratio of 1:1. 20 µL of AWF was added on top of WM in the sterilised plate and left to air-dry at room temperature for 15 minutes. This was followed by adding 30 µL of PAO1 subculture on the WM before incubation at 37°C for 8 h and 24 h, resulting in an *immature* and *mature* biofilm model, respectively. These *in vitro* biofilm models would be used for PAHT testing.

## 6.3.9.1 **Bacterial viability assay in wound biofilm model**

The Miles and Misra technique was utilised to quantify viable bacteria following PAHT treatment.[262] In this method, CFUs are used to estimate viable bacterial count whereby one viable bacterium is equivalent to one colony. The PAO1 bacterial cultures following incubation were resuspended in 10 mL of PBS. 100 µL of the resuspended solutions was diluted in 900 µL PBS to prepare 1 mL of bacterial suspensions. This was subsequently further serially diluted to create solutions with population densities between $10^{-1}$ and $10^{-8}$.

An LBA plate was divided into 8 sections for each bacterial dilution and 10 µL of the bacterial solution (of each dilution) was aliquoted into each respective section (Figure 6.5). Each section consisted of three spots (aliquots) totalling 30 µL in each section. Agar plates were then incubated at 37°C for 18 h. Following incubation, the number of colonies per spot were counted with the naked eye for each dilution factor, where possible to generate the CFU per mL for each PAHT variable tested. Three biological repeats were performed for each bacterial density, and standard deviations of CFU per mL calculated.
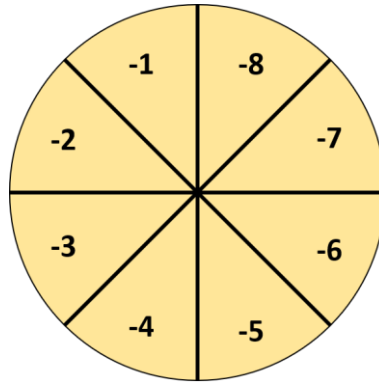
*Figure 6.11: Schematic for dilution aliquoting for the Miles and Misra method.*

## 6.3.9.2　PVP-I loaded PVA hydrogels on *In vitro* biofilms

An *In vitro* wound biofilm model was created using the methodology described in Section 6.2.9 and 10% (w/v) PVP-I loaded PVA hydrogels were made as per Section 6.2.7 to a thickness of 4 mm in plastic culture dishes and subject to 3 freeze-thaw cycles. The PVP-I-loaded-PVA hydrogel was atop of the WM containing an 8 h PAO1 biofilm. The loaded hydrogels were then subject to 3 minutes plasma irradiation in a raster under the standard operating parameters (Section 6.2.1) before static incubation for 24 h. The Miles and Misra method described in above was utilised for the quantification of CFU reduction following incubation.
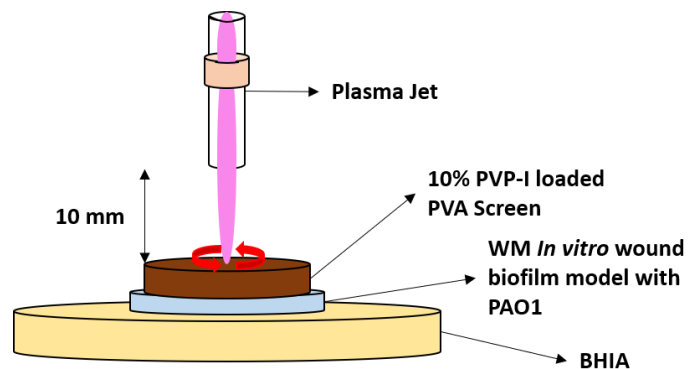


*Figure 6.12: Schematic for Wound Biofilm Model In vitro with PAO1.*

### 6.3.10 Data Analysis

Microsoft Excel was used for data handling and quantitative analysis of $H_2O_2$ concentration. OriginPro 2020b (Academic) was used to perform the one-way ANOVA, Tukey Test and Levene's Test, and Two-Sample t-Test to determine statistical significance. A $P$-value of $<0.05$ was used as statistically significant for all cases. A mixture of OriginPro 2020b (Academic) and MATLAB R 2017a was used to plot the graphs in this chapter. The mean of three replicates were used in all experiments and plotted, and error bars on respective graphs represent standard deviations unless stated otherwise.

# 6.4  Results and Discussion

## 6.4.1  Optimisation of the PAHT

### 6.4.1.1    $H_2O_2$ Quantification

In order to optimise PAHT, thicknesses of PVA were varied on top of a 96-well plate containing DIW in order to determine the most effective option for RONS delivery, and thus bacterial eradication. RONS delivery was measured with 2 assays, KI oxidation at 350 nm, denoting overall RONS delivery through the PAHT, and the ODP/HRP assay for determination of the $H_2O_2$ concentration. Figure 6.13 shows the results of both KI oxidation and $H_2O_2$ concentrations found beneath the PVA hydrogel for varying PVA hydrogel thicknesses. Using a Two-Sample t-Test between 0 mm (direct CAP) and 2 mm, both KI oxidation and $H_2O_2$ concentrations are statistically significantly lower, $p < 0.0001$ and $p = 0.004$ respectively. In this setup, the results suggest that the PVA hydrogel acts as a reservoir for RONS species with some apparent retention of longer-lived species such as $H_2O_2$. The process by which the reactive species move through the screen is hypothesised to be a slow molecular transport process.[178] For all PVA hydrogel thicknesses, there is a statistically significant decrease in both the absorbance recorded at 350 nm and $H_2O_2$ concentration with increasing hydrogel thickness between 2 mm and 8 mm. For the PAHT regimen, the thinnest screen thickness is the most optimal for $H_2O_2$ delivery. At $H_2O_2$ concentrations of less than 50 mM, it has been shown in a murine model of wound healing that $H_2O_2$ facilitates angiogenesis and improves wound closure.[263, 264]
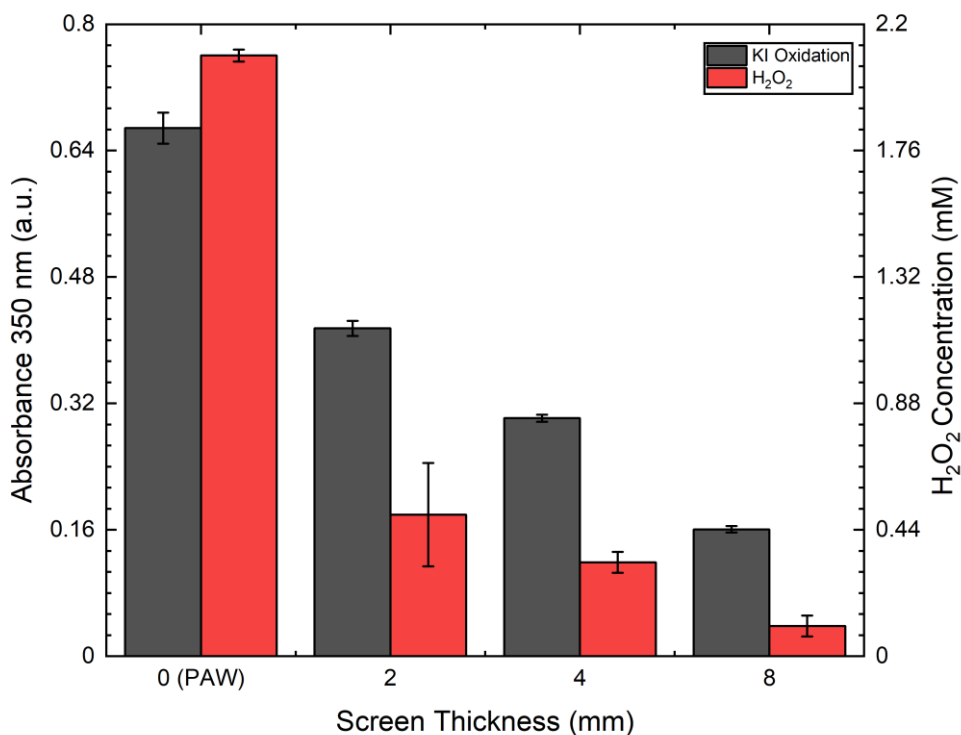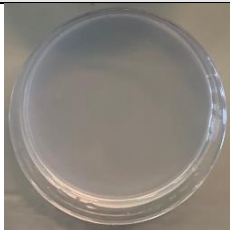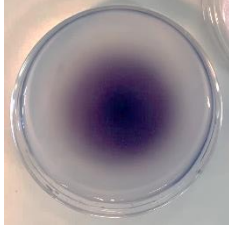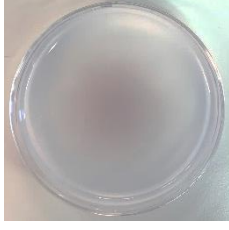
*Figure 6.13: H₂O₂ concentrations and KI Oxidation beneath PVA screens of varying thicknesses. H₂O₂ concentration determined using ODP/HRP assay and KI Oxidation determined by absorbance at 350 nm. Error bars represent standard deviations. Experiments carried out in triplicate (n=3).*

$$2I^- + oxidising\ agent\ \rightarrow\ I_2 \qquad \text{(Equation 6.2)}$$

$$I^- + I_2\ \rightarrow I^{3-} \qquad \text{(Equation 6.3)}$$

$$I^{3-} + starch \rightarrow purple\ colour \qquad \text{(Equation 6.4)}$$
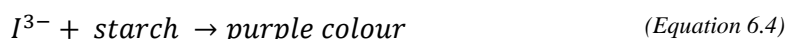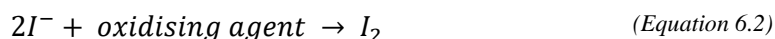
The chemical equations for the reaction occurring between RONS and the agarose indicator gel are shown in Equations 6.2 to 6.4. KI contained within the agarose indicator gel is the source of $I^-$. Plasma irradiation of the PVA screen produces $H_2O_2$, a key oxidising agent, and so forming $I_2$ (Equation 6.2). Equation 6.3 shows that the newly formed $I_2$ further reacts with the free $I^-$ within the agarose indicator gel to form $I_3^-$. Finally, $I_3^-$ reacts with the starch for form the purple saturation seen in Table 6.2, Equation 6.4. The results in Table 6.2 show that in the absence of an oxidising agent i.e. untreated PVA hydrogel, no colour change is observed in the agarose indicator gel hydrogel. This is because there is no endogenous oxidising agent contained within the PVA hydrogel to create $I_2$. Following plasma irradiation of the PVA hydrogel, Table 6.2 shows that for all PVA screen thicknesses, some

degree of purple saturation can be observed with the naked eye. In keeping with the results above, the results in Table 6.2 show the attenuation of the purple saturation with increasing PVA screen thickness, further supporting the claim that the screen acts as a RONS reservoir and that $H_2O_2$ concentration beneath the hydrogel diminishes with increasing PVA hydrogel thickness.

*Table 6.2: Qualitative analysis of a 0.3% KI 0.5% starch 1% agarose hydrogel through different PVA screen thicknesses with plasma-activation.*

| PVA Screen Thickness | Untreated | Plasma Treated |
|---|---|---|
| 2 mm |  |  |
| 4 mm |  |  |
| 8 mm |  |  |

## 6.4.1.2 Gas flow and RONS transport

The results from Figure 6.13 illustrate how the PVA hydrogel is acting as a reservoir for RONS species through the decrease in $H_2O_2$ and KI oxidation under the hydrogel. RONS are hypothesised to move through the PVA hydrogel via a slow molecular transport process and as such gas flow post-plasma irradiation was investigated in order to determine if an external pressure could affect this process.[178] The effect of gas flow post-plasma irradiation on $H_2O_2$ concentrations beneath the PVA hydrogel were plotted against the $H_2O_2$ concentrations seen in Figure 6.13 without gas flow in Figure 6.14. The results in Figure 6.14 show that the added effect of gas flow post-plasma irradiation does not produce a statistically significant difference in $H_2O_2$ concentration across all PVA screen thicknesses.
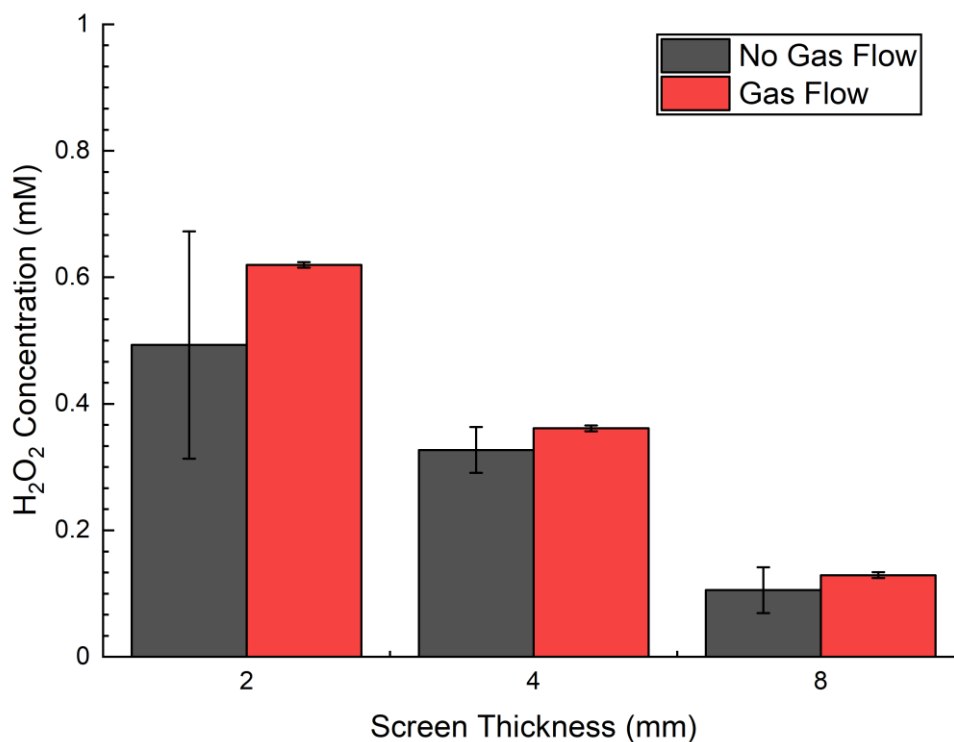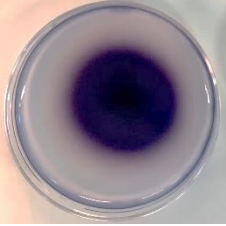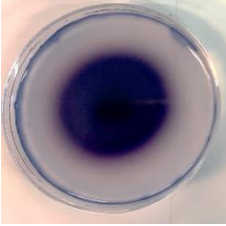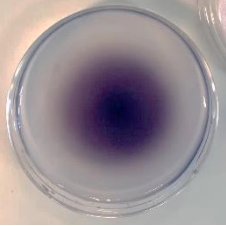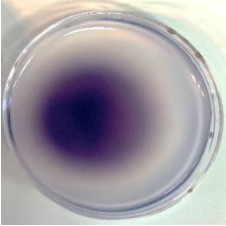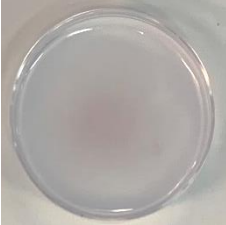
*Figure 6.14 Quantitative effect of gas-flow on RONS transport through a variety of PVA screen thicknesses on $H_2O_2$ concentration calculated using ODP/HRP assay. Error bars represent standard deviations. Experiments performed in triplicate (n = 3).*

Results of the colour change are displayed in Table 6.3. Colour changes seen in Table 6.3 are caused by Equations 6.2 to 6.4. The control in this experiment was plasma irradiation without any additional gas flow. The addition of Ar gas flow for 15 minutes shows no enhancement of the purple complex saturation in the KI-starch-agarose hydrogels which is in keeping with the quantitative results showing no statistically significant decrease between gas flow and no-gas flow between any of the screen thicknesses.

Although not investigated in this work, the transport of RONS through a hydrogel is time dependent. In a study conducted by Oh, J *et al.*[265] it was reported that when compared to the direct treatment of DIW, RONS production through a hydrogel showed that there was an initial lag-phase of 12 minutes, proved through UV-VIS absorbance between 190 nm and 400 nm. The mechanisms by which longer-lived reactive species form between direct plasma treatment and through PAHT was also proposed to be by two different mechanisms. The production of RONS through direct treatment of DIW is thought to be due to direct solvation of RONS into the DIW and is subsequently a fast reaction. It is hypothesised when a hydrogel is placed above DIW, RONS first dissolve in the water and then there is slow molecular transport moves that the RONS into the DIW. Additionally, new RONS may be formed within the hydrogel due to secondary reactions between the existing RONS.

*Table 6.3: Qualitative analysis of the effect of gas flow on the oxidation of a 0.3% KI 0.5% starch 1% agarose hydrogel through different thickness plasma-treated PVA screens.*

| PVA Hydrogel Thickness | Without Gas Flow | With Gas Flow |
|---|---|---|
| 2 mm |  |  |
| 4 mm |  |  |
| 8 mm |  |  |

## 6.4.2  Applications of H₂O₂ and PVP-I to Bacteria

Due to the coronavirus pandemic and subsequent restrictions, only H560 MIC results were able to be carried out by D Beith. As such, results for PAO1 MIC were performed by Dr B Patenall, University of Bath.[266] Two antimicrobials were tested in this project: $H_2O_2$ and PVP-I against H560 and PAO1. Methodology for the determination of MIC of PVP-I and $H_2O_2$ is detailed in Section 6.2.5. Results of the MIC of $H_2O_2$ and PVP-I are shown in Table 6.4 with the Optical Density at 600 nm for each respective antibacterial against H560 displayed in Appendix 8.3.

The results for H560 and PAO1 show that the MIC of both $H_2O_2$ and PVP-I occur at the same concentrations for each strain: 0.44-0.87 mM for $H_2O_2$ and 0.31-0.63% (w/v) PVP-I. Unfortunately, the both PAO1 and H560 MIC $H_2O_2$ values are only achievable with direct plasma irradiation of a substrate using the plasma parameters described in 6.2.1. For example, after 1-minute direct plasma irradiation, 0.53 mM $H_2O_2$ is produced, meaning that the $H_2O_2$ component of CAP should be capable of killing planktonic PAO1.

*Table 6.4: Minimum Inhibitory Concentrations for PAO1 and H560 against H₂O₂ and PVP-I. PAO1 results are reproduced from Dr B Patenall at the University of Bath.[266]*

| Bacterial Strain | H₂O₂ MIC (mM) | PVP-I MIC % (w/v) |
|---|---|---|
| H560 | 4.35-8.69 | 0.31-0.63 |
| PAO1 | 0.44-0.87 | 0.31-0.63 |

## 6.4.2.1    Checkerboard Synergy Assay

The combination of antimicrobials can potentially have additive or synergistic effects for their performance against bacteria, especially towards those bacteria with multi-drug resistances. The combination of PVP-I and $H_2O_2$ has been reported to produce either a synergistic or additive effect in combination, depending on the bacteria. A checkerboard assay was used to determine the combination effect of $H_2O_2$ and PVP-I against H560; the methodology is as detailed in Section 6.2.6.

The results from three biological repeats are shown in Figure 6.15. Concentrations from 2.5% (v/v) and serially diluted to 0.04 % (v/v) PVP-I and $H_2O_2$ from 50 mM and serially diluted to 0.01 mM were tested against H560. MIC values for $H_2O_2$ against H560 were found on the checkerboard synergy assay between 6.25 – 12.5 mM (v/v) and PVP-I between 0.16-0.31% (v/v). FIC indexes were

calculated for H560 using Equation 1 with values ranging between 0.500 and 0.9992. This indicates that the combination of PVP-I and $H_2O_2$ against planktonic H560 is an additive result rather than synergistic. Apart from an additional well found in Figure 6.15 C (gold), all biological replicates showed the same FIC values. The lowest FIC Index was 0.5000 and represented the strongest additive effect of PVP-I and $H_2O_2$ whereby both PVP-I and $H_2O_2$ concentrations in combination were a quarter of the concentration of their MIC when acting alone.

The results in Figure 6.15 A-C show promise for the application of the CAP jet in combination with PVP-I against H560 and other planktonic bacteria. $H_2O_2$ is a major RONS component of the CAP jet and under the operating parameters in Section 6.3.1. $H_2O_2$ concentrations required when in combination with PVP-I largely falls within the same range as when in insolation (3.13-6.25 mM). Results from the optimised PVA hydrogel show that a screen thickness between 2-4 mm is suitable for transporting this concentration of $H_2O_2$ to the target. Further optimisation of plasma parameters could be yielded from another checkerboard synergy assay. In the previous experiment, we used a standard $H_2O_2$ solution rather than $H_2O_2$ generated through the CAP jet and as such this should be repeated to determine the effect of PAW and PVP-I. Differences in results would confirm if other RONS species aside from $H_2O_2$ were responsible for bacterial death.

**A**

| | | 50 | 25 | 12.5 | 6.25 | 3.13 | 1.56 | 0.78 | 0.39 | 0.19 | 0.01 | PVP-I MIC |
|---|---|---|---|---|---|---|---|---|---|---|---|---|
| | | | | | | **H₂O₂ Concentration (mM)** | | | | | | |
| **PVP-I Concentration (% (v/v))** | 2.5 | | | | | | | | | | | |
| | 1.25 | | | | | | | | | | | |
| | 0.63 | | | | | | | | | | | |
| | 0.31 | | | | | | | | | | | MIC |
| | 0.16 | | | | 0.9992 | 0.7496 | 0.6240 | | | | | |
| | 0.08 | | | | 0.7496 | | | | | | | |
| | 0.04 | | | | 0.6248 | | | | | | | |
| | H₂O₂ MIC | | | MIC | | | | | | | | |

**B**

| | | 50 | 25 | 12.5 | 6.25 | 3.13 | 1.56 | 0.78 | 0.39 | 0.19 | 0.01 | PVP-I MIC |
|---|---|---|---|---|---|---|---|---|---|---|---|---|
| | | | | | | **H₂O₂ Concentration (mM)** | | | | | | |
| **PVP-I Concentration (% (v/v))** | 2.5 | | | | | | | | | | | |
| | 1.25 | | | | | | | | | | | |
| | 0.63 | | | | | | | | | | | |
| | 0.31 | | | | | | | | | | | MIC |
| | 0.16 | | | | 0.9992 | 0.7496 | 0.6240 | | | | | |
| | 0.08 | | | | 0.7496 | | | | | | | |
| | 0.04 | | | | 0.6248 | | | | | | | |
| | H₂O₂ MIC | | | MIC | | | | | | | | |

**C**

| | | 50 | 25 | 12.5 | 6.25 | 3.13 | 1.56 | 0.78 | 0.39 | 0.19 | 0.01 | PVP-I MIC |
|---|---|---|---|---|---|---|---|---|---|---|---|---|
| | | | | | | **H₂O₂ Concentration (mM)** | | | | | | |
| **PVP-I Concentration (% (v/v))** | 2.5 | | | | | | | | | | | |
| | 1.25 | | | | | | | | | | | |
| | 0.63 | | | | | | | | | | | |
| | 0.31 | | | | | | | | | | | MIC |
| | 0.16 | | | | 0.9992 | 0.7496 | 0.6240 | | | | | |
| | 0.08 | | | | 0.7496 | 0.5000 | | | | | | |
| | 0.04 | | | | 0.6248 | | | | | | | |
| | H₂O₂ MIC | | | MIC | | | | | | | | |

*Figure 6.15: Checkerboard Synergy Assay against planktonic H560 with a combination of H₂O₂ and PVP-I showing FIC indexes (blue). Additional FIC value not seen in A and B highlighted in C in gold. Three biological replicates are represented A-C.*

### 6.4.3  Applications of PAHT to DFU Bacteria

### 6.4.3.1    Kirby-Bauer Assay

The 5% PVA screen has been optimised for screen thickness for maximum RONS delivery and the effect of gas-flow on slow molecular transport of RONS through the PVA screen has been determined. The results concluded that at every PVA screen thickness, gas flow had no statistically significant effect and that a thinner PVA screen was better for $H_2O_2$ concentration beneath the screen. Based upon a consideration of mechanical properties versus thickness of the hydrogel, it was found that a 4 mm 5% PVA screens was best suited for plasma irradiation and therefore used for Kirby-Bauer Assays against both H560 and PAO1 bacterial strains.

### 6.4.3.1.1 Effect of Povidone-Iodine Concentration

In order to produce the most affective PAHT for bacterial eradication in DFUs, varying concentrations of PVP-I were loaded into the PVA hydrogel against H560 and PAO1. This experiment would kickstart achieving aim (iii), loading the PAHT with PVP-I and testing against H560 and PAO1. The concentration with the highest zone of inhibition would be taken forward and applied against the *In-vitro* wound biofilm model. Three concentrations of PVP-I at 10-fold concentration intervals (0.1%, 1% and 10%) were incorporated into the 4 mm PVA hydrogel, PVP-I-PAHT before application against H560 and PAO1. Plasma-irradiated PVP-I-PAHT were compared against their non-irradiated counterparts, as well as an unloaded 4 mm 5% PVA hydrogel.

Three biological repeats were performed with the mean and standard deviations given below in Figure 6.16. For both H560 (Figure 6.16A) and PAO1 (Figure 6.16B), the 10% PVP-I loaded PVA screen had the greatest inhibitory effect. Interestingly, between untreated 10% PVP-I and with CAP, H560 showed a statistically significant difference in the zone of inhibition of $P < 0.0001$ and PAO1 of $P < 0.001$. For most of the other PVP-I concentrations loaded into the PVA screen, no significant difference was found, and interestingly at 1% with H560 it was found that CAP had a negative effect on the zone of inhibition compared with just the loaded screen, $P < 0.05$.

It was also observed that the addition of CAP at each PVP-I concentration in Figure 6.16B produced greater zone of inhibitions, and thus a greater bactericidal response, when compared against 6.16A. CAP exhibits different efficacies against gram-positive and gram-negative bacteria, and between bacterial species with varying cell wall thicknesses. CAP has been shown to be more effective against gram-negative bacteria, such as PAO1 in Figure 6.16B, due to the absence of a cell wall and better

penetration of RONS in gram-negative bacteria.[267] As such, this is one explanation for why an there is an absent effect following plasma-irradiation in Figure 6.16A, which is tested against a gram-positive bacteria (H560).

Unexpectedly, a zone of inhibition against H560 in Figure 6.16A was seen with just PVA alone and an absence of inhibition was noted when CAP was added. This result goes against the literature which reports that PVA has no antibacterial properties, and also that the addition of RONS from CAP treatment did not produce a bactericidal response.[268] Although this no significant difference was observed between PVA and PVA with CAP on further analysis with a Tukey Test, $P = 0.42$, this experiment should be repeated in order to confirm the below results are not erroneous.
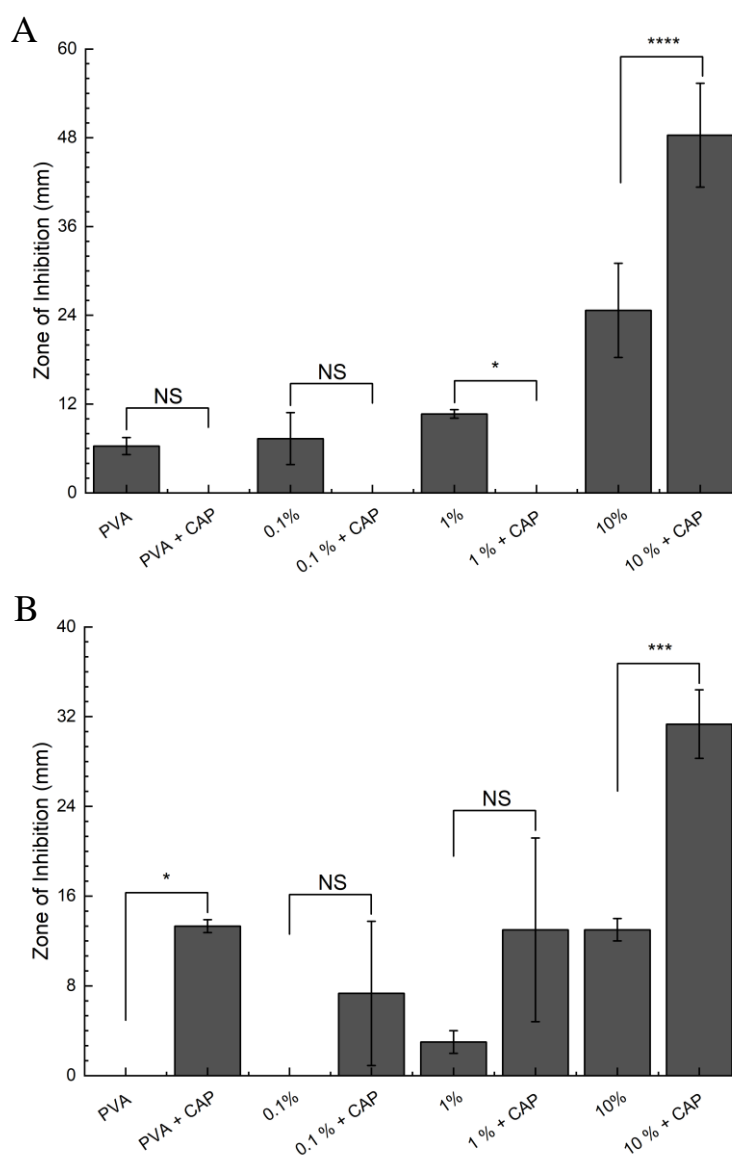


*Figure 6.16: Zone of Inhibition following Kirby-Bauer Assay with varied PVP-I concentrations loaded into a PVA Screen against (A) H560 and (B) PAO1. Comparison of means between CAP and untreated variable for each PVP-I percentage performed by ANOVA-One Way and Tukey Test: p<0.05 (*), p<0.001 (***), p<0.0001 (****), not statistically significant (NS). Errors bars represent standard deviations. Experiments carried out in triplicate (n=3).*

$$I^- + H_2O_2 \rightarrow [I^-H_2O_2]^- \rightarrow HOI + OH^-$$ *(Equation 6.5)*

$$I^- + H_2O_2 \rightarrow [I^-H_2O_2]^- \rightarrow 2OH^- + I^+$$ *(Equation 6.6)*

$$I^+ + OH^- \rightarrow HOI$$ *(Equation 6.7)*

$$I^- + {}^1O_2 \rightarrow [I^-O_2]^- + H_2O \rightarrow HO_2 + HOI$$ *(Equation 6.8)*
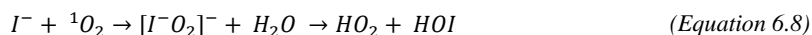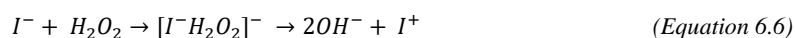
As discussed in Chapter 5, the results from both agarose hydrogel systems and UV-VIS spectra illustrated the consumption of iodine species $I^-$ and $I_3^-$ following plasma irradiation. It was hypothesised that the consumption of these species leads to the formation of the antimicrobial compound HOI. Equations 6.5-8 show the 4 likely reactions that occur within the PVP-I loaded PVA screen following plasma irradiation. Oxidation of $I^-$ as shown in Equation 6.5 produces HOI which is a known disinfectant. When compared to $I_2$, HOI has nearly twice the oxidising power suggesting greater disinfection power.

$$I_2 + H_2O \rightleftharpoons HOI + H^+ + I^-$$ *(Equation 6.9)*
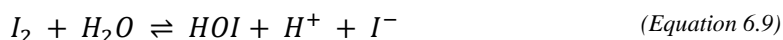
Along with the formation of HOI through combination with RONS, another mechanism for the formation of HOI is through the hydrolysis of $I_2$ as shown in Equation 6.9. This reaction is pH dependent and as such that is reported that the optimum condition for HOI formation is at pH 7-7.5 whereby 52% of species exist as $I_2$ and the rest HOI. Above pH 8, it has been shown that HOI will decompose into iodate, $OI^-$, and $H^+$.[269] The results from this Kirby-Bauer assay show an increase in the bactericidal properties of PVP-I at 10% (w/v) PVP-I loaded PVA hydrogel when plasma irradiated. Results in Chapter 5 combined with this assay support the theory that plasma-activated PVP-I promotes the formation of the more bactericidal compound HOI.

## 6.4.3.1.2 Effect of Gas-Flow on Varied Povidone-Iodine Concentrations against PAO1

The mean zone of inhibitions for each variable were plotted (Figure 6.17) and the standard deviations representative of the experiment performed in triplicate. The results demonstrate again that 10% (w/v) PVP-I with CAP irradiation shows the highest potential for PAO1 inhibition. With regards to gas flow, it was shown that there was no statistically significant difference between the zone of inhibition for control and gas flow, concluding that the effect of gas flow has no effect on the slow molecular transport within hydrogels. Interestingly, this dataset against PAO1 shows that there was no statistically significant difference between 0.1% (w/v) PVP-I and 1% (w/v) PVP-I following CAP treatment and in 2 out of the 3 PVP-I conditions, additional gas flow caused a decrease in the zone of inhibition.
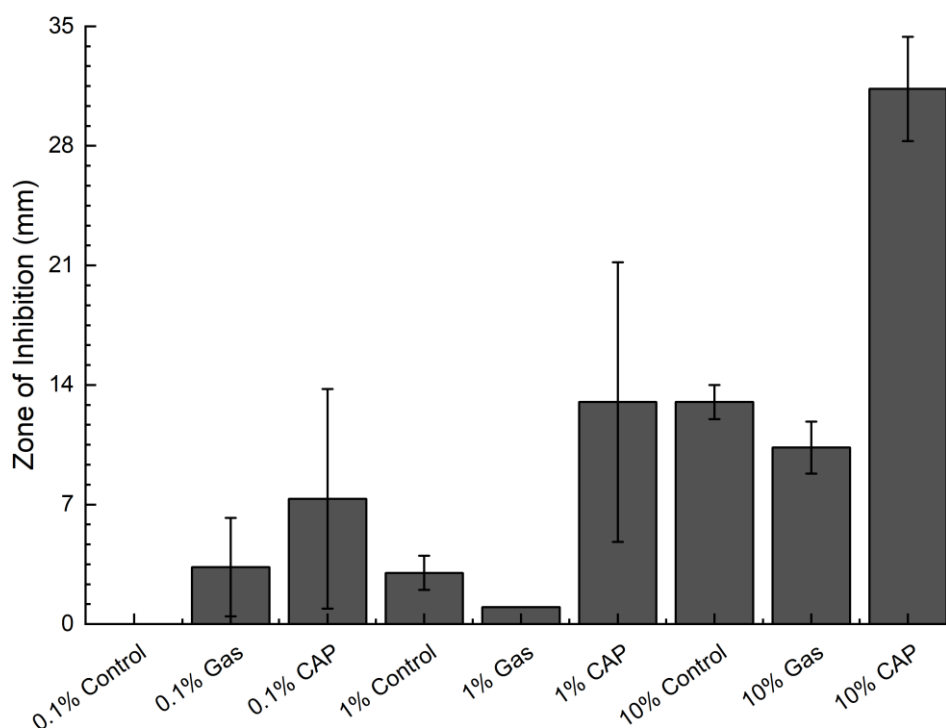


*Figure 6.17: Determination of the effect of gas-flow on varied PVP-I concentration loaded PVA screens against PAO1 using a Kirby-Bauer Assay. Experiment performed in triplicate (n = 3) with means and standard deviations plotted. Data for Control and CAP at each concentration is taken from PVA and PVA + CAP groups respectively in Figure 6.16B.*

## 6.4.3.2    Effect of PVP-I/plasma-PVP-I on an 8 h biofilms

Kirby-Bauer Assays have been utilised in Section 6.4.3.1.1 and 6.4.3.1.2 in order to optimise the PVP-I loading into a 4 mm PVA hydrogel against H560 and PAO1.  Evaluating the results from these experiments, it was found that 10% PVP-I loaded into a 4 mm 5% PVA screen was best suited for maximum bacterial eradiation of both species. The following parameters were therefore applied against our 8 h PAO1 *In vitro* wound biofilm model to better simulate the potential against DFUs.

The results in Figure 6.18 show that direct CAP i.e. no PVA screen above polycarbonate membrane and CAP PVP-I –PAHT screen are the most effective at CFU reduction against an immature 8 h PAO1 biofilm. However, using the Miles and Misra technique for CFU determination, we are unable to ascertain any superiority in CFU reduction between the Direct CAP and CAP PVP-I –PAHT screen as they have both have no growth. There was no statistically significant difference in the biofilm CFU between an unloaded screen (PVA) and a CAP-treated unloaded-screen (CAP-PVA).

This report has determined, through characterisation of the jet and under the operating parameters used throughout this thesis, that the maximum concentration of $H_2O_2$ produced following 3 minutes of direct irradiation at 10 mm distance is 1.20 mM. Patenall, B reports the minimum biofilm eradication concentration of $H_2O_2$ against PAO1 to be 1110-2230 mM. My above findings of 1.20 mM following 3 minutes direct irradiation indicate that the current CAP parameters produce 1000 times less $H_2O_2$ than what is needed to eradicate a PAO1 biofilm.[266] Furthermore, when a 4 mm hydrogel is placed atop of the target, this concentration is reduced dramatically. The additive effect of PVP-I and $H_2O_2$ as confirmed through the checkerboard synergy assay (Section 6.3.6), combined with the theorised production of HOI is the proposed explanation behind the effectiveness of CFU reduction following CAP jet treatment in the presence of ≈1000 times less $H_2O_2$ concentration.
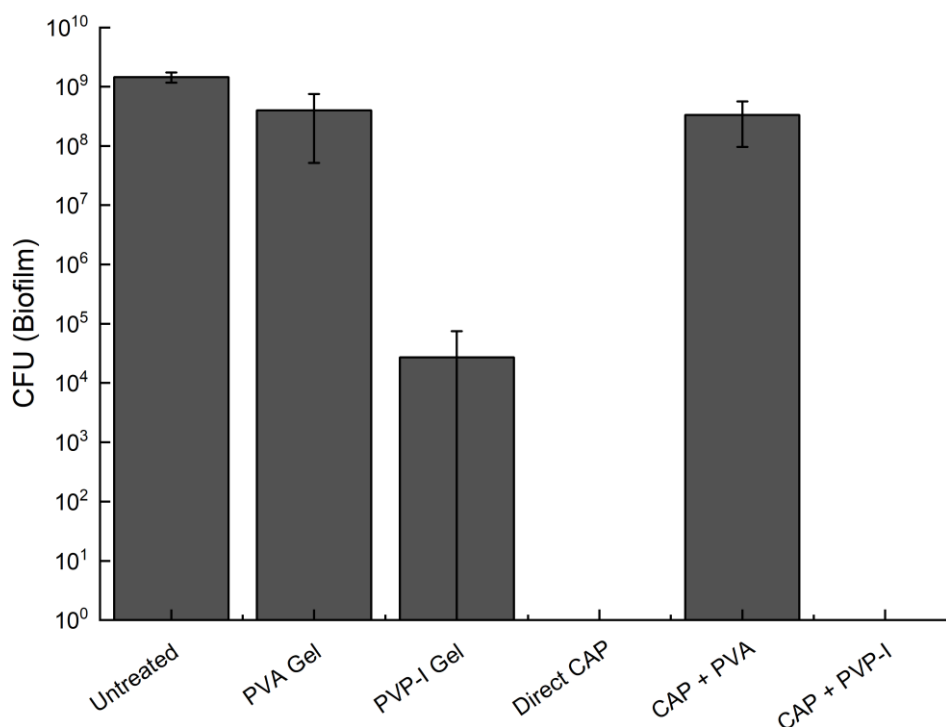
*Figure 6.18: Effect of CAP-treated PVP-I-PVA screens against an In vitro 8 h PAO1 wound biofilm model. Colony Forming Unit (CFU). Error bars represent standard deviations. Experiments performed in triplicate (n = 3).*

## 6.4.3.3    Effect on Post-Plasma Incubation Time on CFU Reduction

More substantial biofilms were grown for the following experiments using 24 h incubated PAO1 biofilms grown using the *in vitro* wound biofilm model (Section 6.3.9). The experimental design was the same as detailed in Figure 6.18 however, CFU determination was carried out 1-h post-plasma irradiation and at 24 h post-treatment incubation. The following CAP treated variables were compared against their respective untreated versions, direct CAP, 5% (w/v) PVA screen, and 10% (w/v) PVP-I – PAHT. The hypothesis tested here was that against substantial biofilms, $\approx 10^{10}$ CFU/biofilm, that the CAP jet provides only a short-term antimicrobial effect.

The results in Figure 6.19 show that there was a statistically significant ($P < 0.001$) decrease in CFU/biofilm following CAP treatment of the PVP-I –PAHT screen. This again suggests that that the additive behaviour of PVP-I and $H_2O_2$ are capable of a $10^1$ reduction in CFU/biofilm and compared to the original biofilm, a $10^2$ reduction in CFU/biofilm. Unlike with an 8 h immature PAO1 biofilm, Figure 6.19 shows that Direct CAP provides the largest reduction in CFU/biofilm with a $10^3$ reduction at 1 h and after 24 h a $10^2$ reduction. For all other variables after 24 h, there was no statistically significant difference between no plasma and plasma-irradiation of the PVA screen. The results from the mature biofilm post 24 h incubation micro-organisms show almost full recovery from both direct

CAP and from CAP treatment of PVP-I –PAHT screen. It is reported that the efficacy of CAP decreases with biofilm maturity. Proposed reasons for the decreased efficacy include the increased production of EPS in well-established biofilms compared to their immature counterparts, and a change in the expressed genotype through QS with increasing biofilm.[270, 271]

It was also noted that although decreased efficacy was shown, in all CAP treated groups, there was incomplete "healing" of biofilm back to the original CFU count. One of the mechanisms behind the bactericidal action of CAP is an increase in bacterial cell wall permeability, achieved through thermal, chemical and electromechanical mechanisms.[202] It has also been reported that CAP irradiation against established biofilm causes a complete breakdown in the bacterial cell wall, and as such this coupled with the increased permeability could explain why full regrowth of PAO1 at 24 h incubation was not observed.[272]
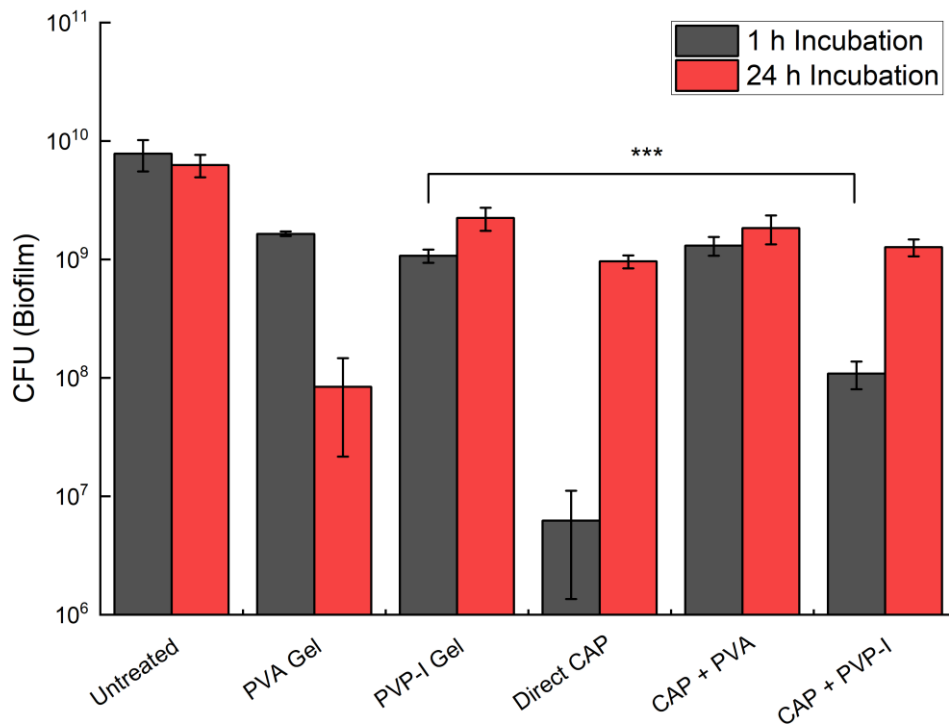


*Figure 6.19: Effect of 1 h and 24 h incubation post CAP treatment on the colony forming unit (CFU) in a biofilm model. Comparison of means performed using Tukey Test: p < 0.001 (***). Error bars represent standard deviations. Experiment performed in triplicate (n = 3).*

## 6.5  Conclusions

This chapter describes optimisation, bacterial efficacy and latterly the combined effect of an antimicrobial loaded into a PVA screen for the treatment of DFU biofilms. The work shows that PVA screen thickness has a large effect on the RONS transport to the target via slow molecular transport, and it has also showed that external forces such as maintained Ar gas flow at 1 SLPM does not affect this process. A balance between PVA screen stability and $H_2O_2$ delivery meant that 4 mm screen thickness was decided upon. Further quantification of PVP-I and plasma-derived $H_2O_2$ showed that in combination, an additive response against H560. Importantly, it showed that the required $H_2O_2$ for dissolution of planktonic H560 in combination with PVP-I was capable through a 4 mm PVA screen.

Through Kirby-Bauer Assays and *In vitro* wound biofilm models, I have characterised the PAO1 response to a therapeutic hydrogel, created using a 1:1 dilution of 10% (w/v) PVP-I and 5% PVA. The Kirby-Bauer Assays were used to determine the optimum concentrations of PVP-I against planktonic PAO1 and H560, and later applied to the WM *in vitro* wound biofilm models. Against *immature* biofilms (8 h) a complete reduction in CFU/biofilm was seen with both direct CAP and CAP PVP-I – PAHT hydrogel indicating similar efficacy against a biofilm of $10^9$ CFU. The results from this demonstrate that it could be a promising treatment for post-debridement DFUs whereby the CFU count will be much lower than that of an established chronic wound. Results from the 24 h biofilm at varying post-incubation times show an immediate antibacterial effect of the CAP jet using the PVP-I-PVA screen and as such may enable better response to antibiotics if co-delivered.

# 7   Chapter 7 : Conclusions and Future Work

DFUs pose an underappreciated financial and social burden with the management for DFUs costing the NHS £650 million per year and leading to 1 amputation every 30 seconds globally.[224, 273] The most frequent cause of hospitalisation and amputations for individuals with DFUs is infection and patients at hospitals are exposed to dangerous bacteria with multi-drug resistances.[26, 274] One of the major challenges faced by patients is their long-term exposure to and systemic use of broad-spectrum antibiotics and this contributes to the ever-growing risk of AMR. The potential future burden of AMR is such that it could be attributable to more deaths than cancer by 2050. AMR therefore poses a dangerous threat to DFIs through their chronicity, the poor drug targeting abilities of antibiotics in tissue, and frequent long antibiotic administration required for infection resolution.[275]

Currently, there is still no effective treatment other than antibiotics that prevents amputations in those with deep-seated infection. This has provoked research into alternative novel or repurposed therapies for DFUs which would prevent further contribution towards AMR.[43] One avenue of interest in this work is the field of plasma medicine which utilises CAP jets in healthcare applications such as cancer treatment, sterilisation, dentistry and chronic wounds.[276-278] CAP, or plasma, is an ionised gas which consists RONS such as NO, $NO_2^-$, $O_2^-$, $H_2O_2$ and $O_3$, UV component, electric field, etc. The antibacterial nature of CAP can be attributed to the following: (i) cell-wall permeabilisation; (ii) penetration of reactive species into the bacterium; and (iii) reactions within the bacterium leading to DNA damage. However, to-date the exact mechanisms of action if CAP in tissues have not been fully determined. Importantly for a new potential treatment in DFUs, CAP has also to be shown to not contribute to AMR development due to its widespread mechanism of action.[202, 279]

The clinical landscape within plasma medicine is limited, with only three RCTs conducted so far on DFUs and show statistically significant reductions in wound size but are restricted to low grade ulcers only.[43, 46, 47] As such, this work is a step in the direction of exploring the use of CAP jets as a potential treatment for DFUs.

The particular focus of this work was to develop a PAHT, which is a hydrogel loaded with antimicrobials such as PVP-I. In order to achieve this, three key aims needed to be investigated: (i) investigating the bacteriology of DFUs; (ii) characterisation of the CAP jet and plasma-activated solutions; and (iii) optimisation the PAHT treatment parameters for optimal RONS delivery.

The first aim was achieved in Chapter 2 through the completion of a systematic review. The systematic review compared traditional culture techniques versus broad-range 16S rRNA gene PCR for the identification of the most predominant bacteria within DFUs. Outcomes from the systematic review found that from both detection modalities, *Staphylococcal spp.* and *Pseudomonas spp.* were

most common within DFUs and this was in line with similar reviews.[280-282] Important for subsequent CAP treatment, studies have shown attenuation of the effect of CAP against Gram-positive bacteria, *Staphylococcal spp.* when compared to Gram-negative bacteria, *Pseudomonas spp.* due to the presence of the cell wall.[283] It was also found that patient country of origin played a factor in bacterial predominance and this was in line with what is reported within the literature, whereby *Pseudomonas spp.* are more likely to be found in temperature climates compared to Gram-positive bacteria.[284, 285] It was therefore decided that when applying future PAHT treatments to bacteria, that any *in vitro* wound biofilm models or planktonic assays should be carried out with both bacteria.

The CAP jet was established and characterised in Chapter 4 through investigating the physical (electrical and optical) and chemical characteristics of CAP. Electrical analysis was used to finalise the parameters which were optimum for the treatment of thermally sensitive tissues/hydrogels and low power consuming. These were $V_{p-p}$= 6.96 kV and 23.5 kHz with a power of 2.61E+3 W between t = 0 and t = 42.5 µS. Analysis also showed that there were two primary current peaks that can be observed at 2.11 µS and 3.96 µS caused by excited species which were subsequently visualised through OES. OES spectra confirmed the production of highlighted reactive ROS such as •OH, which have key role in DNA damage and diffuse into the target (solvent) to form other types of ROS such as $H_2O_2$. $N_2$SPS species were also detected in gas-phase which lead to production of $NO_2^-$. Significant to chronic wounds, the longer-lived species $H_2O_2$ was quantified using OPD/HRP colourimetric dye. $H_2O_2$ is a clinically important species and is key in bacterial eradication, as detailed in Chapter 3. Important for its potential use as a medical device, the temperature of the jet was recorded at 313K, confirming its safety for use against sensitive materials. $H_2O_2$ was shown to increase with increasing plasma treatment time whilst interestingly the concentration of $NO_2^-$ was not proportional to plasma treatment time. The use of $H_2O_2$ as an antiseptic is well established and 3% $H_2O_2$ is widely used in order to clean wounds. It is thought that due to the long-lived nature of this species, it can act as a signalling molecule and assist in wound healing.[232] It has been reported that concentrations of $H_2O_2$ below 10 µM stimulate cellular proliferation through redox-sensitive signalling mechanisms whilst causing cellular death, and importantly bacterial death at concentrations above 0.1 mM.[286] Our plasma jet following 5 minutes produces ≈20 times the latter concentrations, and as such future research needs to explore the application of the CAP jet against relevant cells such as keratinocytes or HaCaT cells as to avoid damage to healthy tissue when this technique is applied in the clinical environment.

Whilst investigating the characteristics of the CAP jet, the chemical properties of plasma-activated PVP-I were characterised in Chapter 5. In the age where AMR is a huge problem and the rate of new antibiotic development has slowed, a new method has arisen whereby drugs are repurposed.[287] PVP-I is an established antimicrobial agent, with widespread use in surgery and wound healing.[228] Only a few studies[236, 237] have investigated the effect of a $H_2O_2$-PVP-I mixture on wound healing or on bacterial eradication in this work. To the best of my knowledge, no one to date has studied and

characterised the effect of plasma activation of PVP-I.  Herein, we provide a novel method for production of this mixture through the plasma-activation of PVP-I using direct treatment with the CAP jet.

The experiments of Chapter 5 have aimed study the mechanisms and chemistry underlying plasma-activated PVPI. $H_2O_2$ from CAP and PVP-may interact and produce the hypothesised formation of HOI. This claim was supported by the findings through UV-Vis spectra whereby the consumption of $I^-$ and $I^{3-}$ species following plasma-activation, indirectly provides evidence for the formation of HOI. Plasma-activation is shown to deplete the $I^{3-}$ reservoir within the PVP-I molecule.at a given concentration of PVP-I, and consumption of $H_2O_2$ was constant and with no statistical difference across the plasma treatment times shown with ODP/HRP. Qualitative analysis using a starch-agarose assay further highlighted the attenuation of iodine species following plasma treatment, as well as highlighting the role of $H_2O_2$ as a potential oxidising formation in the presence of iodine.

The work in this thesis, particularly in Chapter 5, has shown that the delivery of plasma-activated PVP-I is much more complex than previously hypothesised. One of the particular challenges to characterising PVP-I was the formation of what is believed to be HOI. HOI is an incredibly unstable substance, with varying degrees of stability with different pH environments. We have shown pH of plasma-treated PVP-I to be drastically influenced with increasing plasma treatment time due to the production of $H_2O_2$, and higher concentrations of PVP-I becoming less acidic with increasing time.

The hydrolysis of $I_2$ is known to be pH dependent: increasing pH between 5 and 8 and causing a shift from $I_2$ into HOI and $OI^-$ where maximum percentage is reached at pH 8. Our data shows an increase in pH to ≈6.5 following 5 minutes plasma treatment time whereby $I_2$ and HOI equilibrium is at a midpoint.[269] pH analysis has therefore shown that increasing plasma-treatment time is of benefit for increasing the production of HOI. The antimicrobial ability of a substance can be determined through its oxidising potential and has been shown that HOI has ≈2 fold the oxidising potential of $I_2$.[288] Interesting, depending on the susceptibility of the bacteria depends on whether HOI or $I_2$ is more effective: against vegetative bacteria, HOI is more effective, whereas against more resistant bacterial spores, $I_2$ is predominant.[289] The greater oxidising potential of HOI and shift in equilibrium with increasing pH means that the effect of plasma-irradiation would enhance bacterial killing through the hypothesised increase in HOI.

The finally aim was achieved in Chapter 6. In order to finish the development of the PAHT, the effect of RONS transport through PVA was investigated. Completion of this would allow the best suited parameters to be applied a PAHT containing PVP-I which would be released upon irradiation onto planktonic H560, PAO1, and PAO1 *In vitro* wound biofilms. Thickness of PAHT were first investigated ranging between 2 mm and 8 mm. Quantitative and qualitative experiments showed that increasing hydrogel thickness negatively affected RONS transport to beneath the hydrogel. It is

hypothesised within the literature[265] that the mechanism behind RONS transport through a hydrogel is by slow molecular transport. As such, the effect of gas flow was studied in order to determine if these transport mechanisms were influenced by external pressures such as continuous gas flow post plasma irradiation. Preliminary data in this thesis showed that gas-flow post-plasma irradiation provided no change in the RONS transport at a given thickness. Potential future experiments to better understand the flow of RONS through PAHT could aim to determine factors that influence slow molecular transport such as using a stimuli responsive polymer collapsing of a hydrogel. Optimisation of the hydrogel should also be investigated in the future with the addition of rheology data in order to accurately determine the thinnest possible stable PVA hydrogel following plasma-irradiation.

Once PVA parameters had been determined, bacterial work was conducted at the University of Bath under the supervision of Dr B Patenall. The first assay used for further PAHT optimisation was the Kirby-Bauer Assays. The effect of plasma-activated PVA hydrogels and PVP-I-PAHT was studied against planktonic H560 and PAO1 on MH agar. Literature searching for the current use of PVP-I within commercial dressings found that the most common concentration used was 10%. We therefore tested three concentrations of PVP-I-PAHT, at 10-fold dilutions of each other against PAO1 and H560 planktonic cultures. The results of this showed a statistically significant result with 10% PVP-I with CAP providing the highest zone of inhibition against both planktonic PAO1 and H560. The role of gas flow as an independent factor to plasma irradiation was investigated against planktonic PAO1 and performed significantly worse than CAP. The following parameters were therefore taken forward for application against PAO1 *in vitro* wound biofilms models: 4mm thickness 10% PVP-I loaded PVA hydrogel.

Against an immature PAO1 biofilm of $10^9$ CFU, both direct CAP and plasma-activated PVP-I-PAHT result in complete eradication of the biofilm following plasma treatment. The result of this shows promise for both PAHT without drug loading and the potential applications of plasma-activated PVP-I-PAHT. As both direct CAP and through PVA (i.e. PVP-I – PAHT) yielded the same result, it is unclear to ascertain superiority of moiety from a $10^9$ biofilm. But, in terms of superiority for clinical applications, PAHT is advantageous as direct CAP is potentially cytotoxic and genotoxic, whereas PAHT has been shown to be a reservoir for these species and preventing their penetration into the cells.[254-256]

Direct CAP and PAHT were then applied to more established PAO1 biofilms at $10^{10}$ CFU. Direct CAP provided the largest reduction in CFU/biofilm with a regrowth of $10^1$ following 24 h incubation. At 1 h incubation, plasma irradiated PVP-I-PVA hydrogel shows a $\approx 10^2$ reduction (P<0.001) however after 24 h, regrowth is such that there is no statistical significance between non-irradiated and plasma-irradiated PAHT.

Unfortunately, due to the SARS-CoV-2 pandemic, not all of the bacterial work at the University of Bath could be carried out. Future work should aim to characterise the effects of PVP-I-PVA hydrogels against H560 through the *In vitro* wound biofilm. Although not in the scope of this project, looking forward at the real-world applicability of PAHT, it should be later tested against multispecies biofilms for a more accurate representation of DFU wounds.

Overall, the results in this work have shown a potential of PAHT to for infection eradication in DFUs. The technology of PAHT is adaptable to a wide range of antimicrobial drugs such as PVP-I. In a real-life scenario, PAHT would involve placing the hydrogel dressing (loaded with antimicrobial drugs) on top of the wound and activated with the CAP jet. The action of CAP would not only drive the antimicrobials from the hydrogel deep into the wound but also plasma-generated RONS, thus enhancing the anti-microbial efficiency. PAHT atop of a wound is a localised mode of treatment wherein the concentration of drug can be controlled by CAP exposure time, thus proving superior than systemic prolonged antibiotic therapy treatments. PAHT can also enhance the oxygen tension in the wound thus overcoming the problem of anaerobic bacteria found within DFUs, which remains the biggest challenge in wound healing.[206] Future work should aim to repurpose different antimicrobials for incorporation into PAHT, or consider plasma-activating antibiotics mentioned in the NICE Guideline 19[9] for DFUs such as Gentamicin, potentially overcoming the reduction in the efficacy of CAP against Gram-positive bacteria.[60]

## 7.1 References

1. American Diabetes A. Diagnosis and classification of diabetes mellitus. Diabetes care. 2010;33 Suppl 1(Suppl 1):S62-S9.
2. Kharroubi AT, Darwish HM. Diabetes mellitus: The epidemic of the century. World J Diabetes. 2015;6(6):850-67.
3. American Diabetes A. 2. Classification and Diagnosis of Diabetes: Standards of Medical Care in Diabetes—2021. Diabetes Care. 2021;44(Supplement 1):S15-S33.
4. Sinwar PD. The diabetic foot management – Recent advance. International Journal of Surgery. 2015;15:27-30.
5. England. PH. Diabetes Prevalence Model2016 24 June 2021. Available from: https://assets.publishing.service.gov.uk/government/uploads/system/uploads/attachment_data/file/612306/Diabetesprevalencemodelbriefing.pdf.
6. Whicher CA, O'Neill S, Holt RIG. Diabetes in the UK: 2019. Diabetic Medicine. 2020;37(2):242-7.
7. UK D. Tackling the crisis: Transforming diabetes care for a better future2019 24 June 2021. Available from: https://www.diabetes.org.uk/resources-s3/2019-04/Diabetes%20UK%20Tackling%20the%20Crisis.pdf.
8. Hex N, Bartlett C, Wright D, Taylor M, Varley D. Estimating the current and future costs of Type 1 and Type 2 diabetes in the UK, including direct health costs and indirect societal and productivity costs. Diabet Med. 2012;29(7):855-62.
9. National Institute for Health and Care Excellence (NICE). Diabetic foot problems: prevention and management. National Institute for Health and Care Excellence: Clinical Guidelines. 2019.
10. International Diabetes Federation. Diabetes Atlas. 9th ed2019.
11. Ntuk UE, Gill JM, Mackay DF, Sattar N, Pell JP. Ethnic-specific obesity cutoffs for diabetes risk: cross-sectional study of 490,288 UK biobank participants. Diabetes Care. 2014;37(9):2500-7.
12. Grunfeld C. Diabetic foot ulcers: etiology, treatment, and prevention. Advances in internal medicine. 1992;37:103-32.
13. Volmer-Thole M, Lobmann R. Neuropathy and Diabetic Foot Syndrome. Int J Mol Sci. 2016;17(6).
14. Zimmermann A, Reeps C, Härtl F, Ockert S, Eckstein H. The diabetic foot. Der Chirurg; Zeitschrift fur Alle Gebiete der Operativen Medizen. 2009;80(5):430-6.
15. Noor S, Zubair M, Ahmad J. Diabetic foot ulcer--A review on pathophysiology, classification and microbial etiology. Diabetes Metab Syndr. 2015;9(3):192-9.
16. Pecoraro RE, Reiber GE, Burgess EM. Pathways to diabetic limb amputation: basis for prevention. Diabetes care. 1990;13(5):513-21.
17. Amin N, Doupis J. Diabetic foot disease: From the evaluation of the "foot at risk" to the novel diabetic ulcer treatment modalities. World J Diabetes. 2016;7(7):153-64.
18. Pendsey SP. Understanding diabetic foot. Int J Diabetes Dev Ctries. 2010;30(2):75-9.
19. Alexiadou K, Doupis J. Management of diabetic foot ulcers. Diabetes Ther. 2012;3(1):4-.
20. Hammi C, Yeung B. Neuropathy. Treasure Island (FL): StatPearls Publishing; 2021.
21. Clayton W, Elasy TA. A review of the pathophysiology, classification, and treatment of foot ulcers in diabetic patients. Clinical diabetes. 2009;27(2):52-8.
22. Gabbay KH. The sorbitol pathway and the complications of diabetes. N Engl J Med. 1973;288(16):831-6.
23. Boulton A, Ward J. Diabetic neuropathies and pain. Clinics in endocrinology and metabolism. 1986;15(4):917-31.
24. Bandyk DF. The diabetic foot: Pathophysiology, evaluation, and treatment. Seminars in Vascular Surgery. 2018;31(2):43-8.
25. Bowering CK. Diabetic foot ulcers. Pathophysiology, assessment, and therapy. Can Fam Physician. 2001;47:1007-16.

26.     Pitocco D, Spanu T, Di Leo M, Vitiello R, Rizzi A, Tartaglione L, et al. Diabetic foot infections: a comprehensive overview. Eur Rev Med Pharmacol Sci. 2019;23(2 Suppl):26-37.
27.     Young MJ, Breddy JL, Veves A, Boulton AJ. The prediction of diabetic neuropathic foot ulceration using vibration perception thresholds. A prospective study. Diabetes Care. 1994;17(6):557-60.
28.     Noor S, Ahmad J, Parwez I, Ozair M. Culture-Based Screening of Aerobic Microbiome in Diabetic Foot Subjects and Developing Non-healing Ulcers. Front Microbiol. 2016;7:1792.
29.     Jouhar L, Jaafar RF, Nasreddine R, Itani O, Haddad F, Rizk N, et al. Microbiological profile and antimicrobial resistance among diabetic foot infections in Lebanon. Int Wound J. 2020.
30.     Lipsky BA, Berendt AR, Deery HG, Embil JM, Joseph WS, Karchmer AW, et al. Diagnosis and treatment of diabetic foot infections. Plast Reconstr Surg. 2006;117(7 Suppl):212s-38s.
31.     Malhotra R, Chan CS-Y, Nather A. Osteomyelitis in the diabetic foot. Diabet Foot Ankle. 2014;5:10.3402/dfa.v5.24445.
32.     Monteiro-Soares M, Boyko EJ, Jeffcoate W, Mills JL, Russell D, Morbach S, et al. Diabetic foot ulcer classifications: A critical review. Diabetes/Metabolism Research and Reviews. 2020;36(S1):e3272.
33.     Wagner FW, Jr. The dysvascular foot: a system for diagnosis and treatment. Foot Ankle. 1981;2(2):64-122.
34.     Lavery LA, Armstrong DG, Harkless LB. Classification of diabetic foot wounds. J Foot Ankle Surg. 1996;35(6):528-31.
35.     Oyibo SO, Jude EB, Tarawneh I, Nguyen HC, Harkless LB, Boulton AJM. A Comparison of Two Diabetic Foot Ulcer Classification Systems. Diabetes Care. 2001;24(1):84.
36.     Everett E, Mathioudakis N. Update on management of diabetic foot ulcers. Ann N Y Acad Sci. 2018;1411(1):153-65.
37.     Armstrong DG, Boulton AJM, Bus SA. Diabetic Foot Ulcers and Their Recurrence. N Engl J Med. 2017;376(24):2367-75.
38.     Treves F. TREATMENT OF PERFORATING ULCER OF THE FOOT. The Lancet. 1884;124(3196):949-51.
39.     Naves CC. The Diabetic Foot: A Historical Overview and Gaps in Current Treatment. Adv Wound Care (New Rochelle). 2016;5(5):191-7.
40.     Turns M. Prevention and management of diabetic foot ulcers. British Journal of Community Nursing. 2015;20(Sup3):S30-S7.
41.     Bowling FL, Jude EB, Boulton AJ. MRSA and diabetic foot wounds: contaminating or infecting organisms? Curr Diab Rep. 2009;9(6):440-4.
42.     Senneville E, Robineau O. Treatment options for diabetic foot osteomyelitis. Expert Opin Pharmacother. 2017;18(8):759-65.
43.     Mirpour S, Fathollah S, Mansouri P, Larijani B, Ghoranneviss M, Mohajeri Tehrani M, et al. Cold atmospheric plasma as an effective method to treat diabetic foot ulcers: A randomized clinical trial. Sci Rep. 2020;10(1):10440.
44.     von Woedtke T, Jünger M, Kocher T, Kramer A, Lademann J, Lindequist U, et al., editors. Plasma medicine - therapeutic application of physical plasmas. World Congress on Medical Physics and Biomedical Engineering, September 7 - 12, 2009, Munich, Germany; 2010 2010//; Berlin, Heidelberg: Springer Berlin Heidelberg.
45.     Tominami K, Kanetaka H, Sasaki S, Mokudai T, Kaneko T, Niwano Y. Cold atmospheric plasma enhances osteoblast differentiation. PloS one. 2017;12(7):e0180507-e.
46.     Amini MR, Sheikh Hosseini M, Fatollah S, Mirpour S, Ghoranneviss M, Larijani B, et al. Beneficial effects of cold atmospheric plasma on inflammatory phase of diabetic foot ulcers; a randomized clinical trial. Journal of Diabetes & Metabolic Disorders. 2020;19(2):895-905.
47.     Stratmann B, Costea TC, Nolte C, Hiller J, Schmidt J, Reindel J, et al. Effect of Cold Atmospheric Plasma Therapy vs Standard Therapy Placebo on Wound Healing in Patients With Diabetic Foot Ulcers: A Randomized Clinical Trial. JAMA Netw Open. 2020;3(7):e2010411.
48.     Cheng K-Y, Lin Z-H, Cheng Y-P, Chiu H-Y, Yeh N-L, Wu T-K, et al. Wound Healing in Streptozotocin-Induced Diabetic Rats Using Atmospheric-Pressure Argon Plasma Jet. Scientific Reports. 2018;8(1):12214.

49.     Calhoun C WH, Hall GA. Antibiotics. 2021 29th July 2021. In: StatPearls [Internet]. Treasure Island (FL): StatPearls Publishing. Available from: https://www.ncbi.nlm.nih.gov/books/NBK535443/.

50.     Hutchings MI, Truman AW, Wilkinson B. Antibiotics: past, present and future. Current Opinion in Microbiology. 2019;51:72-80.

51.     Lobanovska M, Pilla G. Penicillin's Discovery and Antibiotic Resistance: Lessons for the Future? The Yale journal of biology and medicine. 2017;90(1):135-45.

52.     Fleming A. On the antibacterial action of cultures of a penicillium, with special reference to their use in the isolation of B. influenzae. British journal of experimental pathology. 1929;10(3):226.

53.     Džidić S, Šušković J, Kos B. Antibiotic resistance mechanisms in bacteria: biochemical and genetic aspects. Food Technology & Biotechnology. 2008;46(1).

54.     Kohanski MA, Dwyer DJ, Collins JJ. How antibiotics kill bacteria: from targets to networks. Nat Rev Microbiol. 2010;8(6):423-35.

55.     Yoneyama H, Katsumata R. Antibiotic Resistance in Bacteria and Its Future for Novel Antibiotic Development. Bioscience, Biotechnology, and Biochemistry. 2006;70(5):1060-75.

56.     Kapoor G, Saigal S, Elongavan A. Action and resistance mechanisms of antibiotics: A guide for clinicians. Journal of anaesthesiology, clinical pharmacology. 2017;33(3):300-5.

57.     Chellat MF, Raguž L, Riedl R. Targeting Antibiotic Resistance. Angew Chem Int Ed Engl. 2016;55(23):6600-26.

58.     Ventola CL. The antibiotic resistance crisis: part 1: causes and threats. P T. 2015;40(4):277-83.

59.     Bozdogan B, Appelbaum PC. Oxazolidinones: activity, mode of action, and mechanism of resistance. International Journal of Antimicrobial Agents. 2004;23(2):113-9.

60.     Kotra LP, Haddad J, Mobashery S. Aminoglycosides: perspectives on mechanisms of action and resistance and strategies to counter resistance. Antimicrob Agents Chemother. 2000;44(12):3249-56.

61.     Chopra I, Roberts M. Tetracycline antibiotics: mode of action, applications, molecular biology, and epidemiology of bacterial resistance. Microbiol Mol Biol Rev. 2001;65(2):232-60.

62.     World Health Organisation. Antimicrobial resistance 2020 [Available from: https://www.who.int/en/news-room/fact-sheets/detail/antimicrobial-resistance.

63.     Brinkac L, Voorhies A, Gomez A, Nelson KE. The Threat of Antimicrobial Resistance on the Human Microbiome. Microbial ecology. 2017;74(4):1001-8.

64.     O'Neill J. Tackling Drug-Resistant Infections Globally: Final Report and Recommendations2016 15 October 2020. Available from: https://amr-review.org/sites/default/files/160525_Final%20paper_with%20cover.pdf.

65.     Wright GD. The antibiotic resistome: the nexus of chemical and genetic diversity. Nat Rev Microbiol. 2007;5(3):175-86.

66.     Landers TF, Cohen B, Wittum TE, Larson EL. A review of antibiotic use in food animals: perspective, policy, and potential. Public Health Rep. 2012;127(1):4-22.

67.     Huijbers PMC, Blaak H, de Jong MCM, Graat EAM, Vandenbroucke-Grauls CMJE, de Roda Husman AM. Role of the Environment in the Transmission of Antimicrobial Resistance to Humans: A Review. Environmental Science & Technology. 2015;49(20):11993-2004.

68.     Rammelkamp CH, Maxon T. Resistance of Staphylococcus aureus to the Action of Penicillin. Proceedings of the Society for Experimental Biology and Medicine. 1942;51(3):386-9.

69.     Reygaert WC. An overview of the antimicrobial resistance mechanisms of bacteria. AIMS Microbiol. 2018;4(3):482-501.

70.     Munita JM, Arias CA. Mechanisms of Antibiotic Resistance. Microbiology spectrum. 2016;4(2):10.1128/microbiolspec.VMBF-0016-2015.

71.     Katayama Y, Ito T, Hiramatsu K. A new class of genetic element, staphylococcus cassette chromosome mec, encodes methicillin resistance in Staphylococcus aureus. Antimicrob Agents Chemother. 2000;44(6):1549-55.

72.     Pouget C, Dunyach-Remy C, Pantel A, Schuldiner S, Sotto A, Lavigne J-P. Biofilms in Diabetic Foot Ulcers: Significance and Clinical Relevance. Microorganisms. 2020;8(10):1580.

73.	Percival SL, Malone M, Mayer D, Salisbury AM, Schultz G. Role of anaerobes in polymicrobial communities and biofilms complicating diabetic foot ulcers. Int Wound J. 2018;15(5):776-82.

74.	Becker P, Hufnagle W, Peters G, Herrmann M. Detection of differential gene expression in biofilm-forming versus planktonic populations of Staphylococcus aureus using micro-representational-difference analysis. Appl Environ Microbiol. 2001;67(7):2958-65.

75.	Lee B, Schjerling CK, Kirkby N, Hoffmann N, Borup R, Molin S, et al. Mucoid Pseudomonas aeruginosa isolates maintain the biofilm formation capacity and the gene expression profiles during the chronic lung infection of CF patients. Apmis. 2011;119(4-5):263-74.

76.	Alav I, Sutton JM, Rahman KM. Role of bacterial efflux pumps in biofilm formation. J Antimicrob Chemother. 2018;73(8):2003-20.

77.	Mah T-FC, O'Toole GA. Mechanisms of biofilm resistance to antimicrobial agents. Trends in Microbiology. 2001;9(1):34-9.

78.	Perim MC, Borges Jda C, Celeste SR, Orsolin Ede F, Mendes RR, Mendes GO, et al. Aerobic bacterial profile and antibiotic resistance in patients with diabetic foot infections. Rev Soc Bras Med Trop. 2015;48(5):546-54.

79.	Chaudhry WN, Badar R, Jamal M, Jeong J, Zafar J, Andleeb S. Clinico-microbiological study and antibiotic resistance profile of mecA and ESBL gene prevalence in patients with diabetic foot infections. Exp Ther Med. 2016;11(3):1031-8.

80.	Kareliya H, Bichile L, Bal A, Varaiya A, Bhalekar P. Fungal Infection in Diabetic Foot A Clinicomicrobiological Study. Acta Scientific Microbiology. 2019;2(7):49-55.

81.	Salton MRJ, Kim KS. Medical Microbiology. 4th ed. Baron S, editor: Galveston (TX): University of Texas Medical Branch at Galveston; 1996.

82.	Bartholomew JW, Mittwer T. The Gram stain. Bacteriol Rev. 1952;16(1):1-29.

83.	Silhavy TJ, Kahne D, Walker S. The bacterial cell envelope. Cold Spring Harb Perspect Biol. 2010;2(5):a000414-a.

84.	Beveridge TJ, Graham LL. Surface layers of bacteria. Microbiol Rev. 1991;55(4):684-705.

85.	Haslett AS. The chemical significance of the Gram test for bacteria. Aust J Sci. 1947;9(6):211.

86.	Haesler E, Ousey K. Evolution of the wound infection continuum. Wounds International. 2018;9(4):6-10.

87.	Davis E, editor Don't deny the chance to heal. 2nd Joint Meeting of the Wound Healing Society and the European Tissue Repair Society, Boston, Mass; 1996.

88.	Farhan N, Jeffery S. Diagnosing Burn Wounds Infection: The Practice Gap &amp; Advances with MolecuLight Bacterial Imaging. Diagnostics. 2021;11(2):268.

89.	Donlan RM. Biofilms: microbial life on surfaces. Emerg Infect Dis. 2002;8(9):881-90.

90.	James GA, Swogger E, Wolcott R, Pulcini E, Secor P, Sestrich J, et al. Biofilms in chronic wounds. Wound Repair Regen. 2008;16(1):37-44.

91.	Malone M, Bjarnsholt T, McBain AJ, James GA, Stoodley P, Leaper D, et al. The prevalence of biofilms in chronic wounds: a systematic review and meta-analysis of published data. J Wound Care. 2017;26(1):20-5.

92.	Stoodley P, Sauer K, Davies DG, Costerton JW. Biofilms as Complex Differentiated Communities. Annual Review of Microbiology. 2002;56(1):187-209.

93.	Bjarnsholt T. The role of bacterial biofilms in chronic infections. APMIS Suppl. 2013(136):1-51.

94.	Solano C, Echeverz M, Lasa I. Biofilm dispersion and quorum sensing. Curr Opin Microbiol. 2014;18:96-104.

95.	Otto M. Staphylococcal infections: mechanisms of biofilm maturation and detachment as critical determinants of pathogenicity. Annual review of medicine. 2013;64:175-88.

96.	Dowd SE, Wolcott RD, Sun Y, McKeehan T, Smith E, Rhoads D. Polymicrobial nature of chronic diabetic foot ulcer biofilm infections determined using bacterial tag encoded FLX amplicon pyrosequencing (bTEFAP). PLoS One. 2008;3(10):e3326.

97.	Wolcott R, Costerton JW, Raoult D, Cutler SJ. The polymicrobial nature of biofilm infection. Clinical Microbiology and Infection. 2013;19(2):107-12.

98.     Fazli M, Bjarnsholt T, Kirketerp-Møller K, Jørgensen B, Andersen AS, Krogfelt KA, et al. Nonrandom distribution of Pseudomonas aeruginosa and Staphylococcus aureus in chronic wounds. J Clin Microbiol. 2009;47(12):4084-9.

99.     Mottola C, Mendes JJ, Cristino JM, Cavaco-Silva P, Tavares L, Oliveira M. Polymicrobial biofilms by diabetic foot clinical isolates. Folia Microbiol (Praha). 2016;61(1):35-43.

100.    Cramton SE, Gerke C, Schnell NF, Nichols WW, Götz F. The intercellular adhesion (ica) locus is present in Staphylococcus aureus and is required for biofilm formation. Infect Immun. 1999;67(10):5427-33.

101.    Donlan R. Biofilms: Microbial Life on Surfaces. Emerging infectious diseases. 2002;8:881-90.

102.    Fournier B, Klier A, Rapoport G. The two-component system ArlS-ArlR is a regulator of virulence gene expression in Staphylococcus aureus. Mol Microbiol. 2001;41(1):247-61.

103.    Bahador N, Shoja S, Faridi F, Dozandeh-Mobarrez B, Qeshmi FI, Javadpour S, et al. Molecular detection of virulence factors and biofilm formation in Pseudomonas aeruginosa obtained from different clinical specimens in Bandar Abbas. Iran J Microbiol. 2019;11(1):25-30.

104.    Banu A, Noorul Hassan MM, Rajkumar J, Srinivasa S. Spectrum of bacteria associated with diabetic foot ulcer and biofilm formation: A prospective study. Australas Med J. 2015;8(9):280-5.

105.    Tolker-Nielsen T. Pseudomonas aeruginosa biofilm infections: from molecular biofilm biology to new treatment possibilities. APMIS Suppl. 2014(138):1-51.

106.    Thi MTT, Wibowo D, Rehm BHA. Pseudomonas aeruginosa Biofilms. Int J Mol Sci. 2020;21(22).

107.    Lin J, Cheng J. Quorum Sensing in <italic>Pseudomonas aeruginosa</italic> and Its Relationship to Biofilm Development.  Introduction to Biofilm Engineering. ACS Symposium Series. 1323: American Chemical Society; 2019. p. 1-16.

108.    Maurice NM, Bedi B, Sadikot RT. Pseudomonas aeruginosa Biofilms: Host Response and Clinical Implications in Lung Infections. Am J Respir Cell Mol Biol. 2018;58(4):428-39.

109.    Wei Q, Ma LZ. Biofilm matrix and its regulation in Pseudomonas aeruginosa. Int J Mol Sci. 2013;14(10):20983-1005.

110.    Giuliano C, Patel CR, Kale-Pradhan PB. A Guide to Bacterial Culture Identification And Results Interpretation. P T. 2019;44(4):192-200.

111.    Laupland KB, Valiquette L. The changing culture of the microbiology laboratory. Can J Infect Dis Med Microbiol. 2013;24(3):125-8.

112.    Lagier J-C, Edouard S, Pagnier I, Mediannikov O, Drancourt M, Raoult D. Current and past strategies for bacterial culture in clinical microbiology. Clin Microbiol Rev. 2015;28(1):208-36.

113.    Houpikian P, Raoult D. Traditional and molecular techniques for the study of emerging bacterial diseases: one laboratory's perspective. Emerging infectious diseases. 2002;8(2):122-31.

114.    Manaka A, Tokue Y, Murakami M. Comparison of 16S ribosomal RNA gene sequence analysis and conventional culture in the environmental survey of a hospital. J Pharm Health Care Sci. 2017;3:8-.

115.    Relman DA, Schmidt TM, MacDermott RP, Falkow S. Identification of the uncultured bacillus of Whipple's disease. N Engl J Med. 1992;327(5):293-301.

116.    Rampini SK, Bloemberg GV, Keller PM, Büchler AC, Dollenmaier G, Speck RF, et al. Broad-range 16S rRNA gene polymerase chain reaction for diagnosis of culture-negative bacterial infections. Clin Infect Dis. 2011;53(12):1245-51.

117.    Patel A, Harris KA, Fitzgerald F. What is broad-range 16S rDNA PCR? Archives of Disease in Childhood-Education and Practice. 2017;102(5):261-4.

118.    Akhi MT, Ghotaslou R, Asgharzadeh M, Varshochi M, Pirzadeh T, Memar MY, et al. Bacterial etiology and antibiotic susceptibility pattern of diabetic foot infections in Tabriz, Iran. Gms Hygiene and Infection Control. 2015;10.

119.    Al Ayed MY, Ababneh M, Robert AA, Alzaid A, Ahmed RA, Salman A, et al. Common Pathogens and Antibiotic Sensitivity Profiles of Infected Diabetic Foot Ulcers in Saudi Arabia. International Journal of Lower Extremity Wounds. 2018;17(3):161-8.

120.    Al Benwan K, Al Mulla A, Rotimi VO. A study of the microbiology of diabetic foot infections in a teaching hospital in Kuwait. J Infect Public Health. 2012;5(1):1-8.

121.    Aysert Yıldız P, Özdil T, Dizbay M, Güzel Tunçcan Ö, Hızel K. Peripheral arterial disease increases the risk of multidrug-resistant bacteria and amputation in diabetic foot infections. Turk J Med Sci. 2018;48(4):845-50.

122.    Birra V, Hanumanthu AK, Budati S, Murty SN, Hanumanthu R, Tulasi S. A STUDY OF AEROBIC BACTERIAL PROFILE AND ANTIBIOTIC RESISTANCE IN PATIENTS WITH DIABETIC AND NON-DIABETIC WOUND INFECTIONS. Journal of Evolution of Medical and Dental Sciences-Jemds. 2016;5(98):7180-4.

123.    Carro GV, Saurral R, Saguez FS, Witman EL. Diabetic Foot Infections: Bacterial Isolates From the Centers and Hospitals of Latin American Countries. International Journal of Lower Extremity Wounds. 2020.

124.    Gadepalli R, Dhawan B, Sreenivas V, Kapil A, Ammini AC, Chaudhry R. A clinico-microbiological study of diabetic foot ulcers in an Indian tertiary care hospital. Diabetes Care. 2006;29(8):1727-32.

125.    Islam S, Cawich SO, Budhooram S, Harnarayan P, Mahabir V, Ramsewak S, et al. Microbial profile of diabetic foot infections in Trinidad and Tobago. Prim Care Diabetes. 2013;7(4):303-8.

126.    Jaju K, Pichare A, Davane M, Nagoba B. Profile and Antibiotic Susceptibility of Bacterial Pathogens Associated With Diabetic Foot Ulcers From a Rural Area. Wounds. 2019;31(6):158-62.

127.    Kow RY, Low CL, Ruben JK, Zaharul Azri WMZ, Mor Japar Khan ESK. Microbiology of diabetic foot infections in three district hospital in Malaysia and comparison with South East Asian Countries. Med J Malaysia. 2019;74(5):394-9.

128.    Kunjappan SP, Saju IM. AEROBIC BACTERIAL PROFILE OF DIABETIC ULCER IN A TERTIARY CARE CENTRE. Journal of Evolution of Medical and Dental Sciences-Jemds. 2017;6(68):4859-62.

129.    Li X, Qi X, Yuan G, Ju S, Yu Z, Deng W, et al. Microbiological profile and clinical characteristics of diabetic foot infection in northern China: a retrospective multicentre survey in the Beijing area. J Med Microbiol. 2018;67(2):160-8.

130.    Macdonald KE, Jordan CY, Crichton E, Barnes JE, Harkin GE, Hall LML, et al. A retrospective analysis of the microbiology of diabetic foot infections at a Scottish tertiary hospital. BMC Infect Dis. 2020;20(1):218.

131.    Machado C, Teixeira S, Fonseca L, Abreu M, Carvalho A, Pereira MT, et al. Evolutionary trends in bacteria isolated from moderate and severe diabetic foot infections in a Portuguese tertiary center. Diabetes & Metabolic Syndrome-Clinical Research & Reviews. 2020;14(3):205-9.

132.    Mendes JJ, Marques-Costa A, Vilela C, Neves J, Candeias N, Cavaco-Silva P, et al. Clinical and bacteriological survey of diabetic foot infections in Lisbon. Diabetes Res Clin Pract. 2012;95(1):153-61.

133.    Neves JM, Duarte B, Pinto M, Formiga A, Neves J. Diabetic Foot Infection: Causative Pathogens and Empiric Antibiotherapy Considerations-The Experience of a Tertiary Center. Int J Low Extrem Wounds. 2019;18(2):122-8.

134.    Perim MC, Borges JD, Celeste SRC, Orsolin ED, Mendes RR, Mendes GO, et al. Aerobic bacterial profile and antibiotic resistance in patients with diabetic foot infections. Revista Da Sociedade Brasileira De Medicina Tropical. 2015;48(5):546-54.

135.    Ramakant P, Verma AK, Misra R, Prasad KN, Chand G, Mishra A, et al. Changing microbiological profile of pathogenic bacteria in diabetic foot infections: time for a rethink on which empirical therapy to choose? Diabetologia. 2011;54(1):58-64.

136.    Shankar EM, Mohan V, Premalatha G, Srinivasan RS, Usha AR. Bacterial etiology of diabetic foot infections in South India. Eur J Intern Med. 2005;16(8):567-70.

137.    Appapalam ST, Muniyan A, Mohan KV, Panchamoorthy R. A Study on Isolation, Characterization, and Exploration of Multiantibiotic-Resistant Bacteria in the Wound Site of Diabetic Foot Ulcer Patients. International Journal of Lower Extremity Wounds. 2019.

138.    Turhan V, Mutluoglu M, Acar A, Hatipoğlu M, Önem Y, Uzun G, et al. Increasing incidence of Gram-negative organisms in bacterial agents isolated from diabetic foot ulcers. J Infect Dev Ctries. 2013;7(10):707-12.

139.    Wu M, Pan H, Leng W, Lei X, Chen L, Liang Z. Distribution of Microbes and Drug Susceptibility in Patients with Diabetic Foot Infections in Southwest China. J Diabetes Res. 2018;2018:9817308.

140.    Zubair M, Malik A, Ahmad J. Clinico-microbiological study and antimicrobial drug resistance profile of diabetic foot infections in North India. Foot (Edinb). 2011;21(1):6-14.

141.    Akhi MT, Ghotaslou R, Asgharzadeh M, Varshochi M, Pirzadeh T, Memar MY, et al. Bacterial etiology and antibiotic susceptibility pattern of diabetic foot infections in Tabriz, Iran. GMS Hyg Infect Control. 2015;10:Doc02.

142.    Akyshbayeva K, Ramazanova B, Bissekenova A, Nakisbekov N, Smagul A, Sarniyaziova C, et al. MICROBIOTA OF PURULENT NECROTIC LESIONS IN PATIENTS WITH DIABETIC FOOT SYNDROME. Ad Alta-Journal of Interdisciplinary Research. 2018;8(1):139-44.

143.    Gardner SE, Hillis SL, Heilmann K, Segre JA, Grice EA. The neuropathic diabetic foot ulcer microbiome is associated with clinical factors. Diabetes. 2013;62(3):923-30.

144.    Hu P, Zou MC, Cao Y, Pan YL, Luo XR, Jiang Y, et al. [Pathogen analysis in patients with diabetic foot osteomyelitis using 16S rRNA high-throughput sequencing]. Nan Fang Yi Ke Da Xue Xue Bao. 2017;37(11):1448-55.

145.    Malone M, Johani K, Jensen SO, Gosbell IB, Dickson HG, Hu H, et al. Next Generation DNA Sequencing of Tissues from Infected Diabetic Foot Ulcers. EBioMedicine. 2017;21:142-9.

146.    Min KR, Galvis A, Baquerizo Nole KL, Sinha R, Clarke J, Kirsner RS, et al. Association between baseline abundance of Peptoniphilus, a Gram-positive anaerobic coccus, and wound healing outcomes of DFUs. PLoS One. 2020;15(1):e0227006.

147.    Sloan TJ, Turton JC, Tyson J, Musgrove A, Fleming VM, Lister MM, et al. Examining diabetic heel ulcers through an ecological lens: microbial community dynamics associated with healing and infection. J Med Microbiol. 2019;68(2):230-40.

148.    Smith K, Collier A, Townsend EM, O'Donnell LE, Bal AM, Butcher J, et al. One step closer to understanding the role of bacteria in diabetic foot ulcers: characterising the microbiome of ulcers. BMC Microbiol. 2016;16:54.

149.    van Asten SA, La Fontaine J, Peters EJ, Bhavan K, Kim PJ, Lavery LA. The microbiome of diabetic foot osteomyelitis. Eur J Clin Microbiol Infect Dis. 2016;35(2):293-8.

150.    Zou M, Cai Y, Hu P, Cao Y, Luo X, Fan X, et al. Analysis of the Composition and Functions of the Microbiome in Diabetic Foot Osteomyelitis Based on 16S rRNA and Metagenome Sequencing Technology. Diabetes. 2020;69(11):2423-39.

151.    Wolcott RD, Hanson JD, Rees EJ, Koenig LD, Phillips CD, Wolcott RA, et al. Analysis of the chronic wound microbiota of 2,963 patients by 16S rDNA pyrosequencing. Wound Repair Regen. 2016;24(1):163-74.

152.    Lladó Fernández S, Větrovský T, Baldrian P. The concept of operational taxonomic units revisited: genomes of bacteria that are regarded as closely related are often highly dissimilar. Folia Microbiol (Praha). 2019;64(1):19-23.

153.    Grice EA, Kong HH, Renaud G, Young AC, Bouffard GG, Blakesley RW, et al. A diversity profile of the human skin microbiota. Genome Res. 2008;18(7):1043-50.

154.    Aggarwal D, Kanitkar T, Narouz M, Azadian BS, Moore LSP, Mughal N. Clinical utility and cost-effectiveness of bacterial 16S rRNA and targeted PCR based diagnostic testing in a UK microbiology laboratory network. Scientific Reports. 2020;10(1):7965.

155.    Kong HH, Segre JA. Skin microbiome: looking back to move forward. Journal of Investigative Dermatology. 2012;132(3):933-9.

156.    Skvarc M, Stubljar D, Rogina P, Kaasch AJ. Non-culture-based methods to diagnose bloodstream infection: Does it work? Eur J Microbiol Immunol (Bp). 2013;3(2):97-104.

157.    Jneid J, Lavigne JP, La Scola B, Cassir N. The diabetic foot microbiota: A review. Human Microbiome Journal. 2017;5-6:1-6.

158.    Citron DM, Goldstein EJC, Merriam CV, Lipsky BA, Abramson MA. Bacteriology of moderate-to-severe diabetic foot infections and in vitro activity of antimicrobial agents. Journal of clinical microbiology. 2007;45(9):2819-28.

159.    Li R, Tun HM, Jahan M, Zhang Z, Kumar A, Dilantha Fernando WG, et al. Comparison of DNA-, PMA-, and RNA-based 16S rRNA Illumina sequencing for detection of live bacteria in water. Scientific Reports. 2017;7(1):5752.

160.    Chakravorty S, Sarkar S, Gachhui R. Identification of new conserved and variable regions in the 16S rRNA gene of acetic acid bacteria and acetobacteraceae family. Molecular Biology. 2015;49(5):668-77.

161.	Fuks G, Elgart M, Amir A, Zeisel A, Turnbaugh PJ, Soen Y, et al. Combining 16S rRNA gene variable regions enables high-resolution microbial community profiling. Microbiome. 2018;6(1):17.

162.	Schloss PD, Handelsman J. Introducing DOTUR, a computer program for defining operational taxonomic units and estimating species richness. Applied and environmental microbiology. 2005;71(3):1501-6.

163.	Johnson JS, Spakowicz DJ, Hong B-Y, Petersen LM, Demkowicz P, Chen L, et al. Evaluation of 16S rRNA gene sequencing for species and strain-level microbiome analysis. Nature Communications. 2019;10(1):5029.

164.	Abdulrazak A, Bitar ZI, Al-Shamali AA, Mobasher LA. Bacteriological study of diabetic foot infections. J Diabetes Complications. 2005;19(3):138-41.

165.	Vali Y, Leeflang MMG, Bossuyt PMM. Application of weighting methods for presenting risk-of-bias assessments in systematic reviews of diagnostic test accuracy studies. Systematic Reviews. 2021;10(1):191.

166.	Lee CH, Cook S, Lee JS, Han B. Comparison of Two Meta-Analysis Methods: Inverse-Variance-Weighted Average and Weighted Sum of Z-Scores. Genomics Inform. 2016;14(4):173-80.

167.	Langmuir I. Oscillations in Ionized Gases. Proc Natl Acad Sci U S A. 1928;14(8):627-37.

168.	Brany D, Dvorská D, Halašová E, Škovierová H. Cold Atmospheric Plasma: A Powerful Tool for Modern Medicine. Int J Mol Sci. 2020;21(8):2932.

169.	López M, Calvo T, Prieto M, Múgica-Vidal R, Muro-Fraguas I, Alba-Elías F, et al. A Review on Non-thermal Atmospheric Plasma for Food Preservation: Mode of Action, Determinants of Effectiveness, and Applications. Frontiers in Microbiology. 2019;10(622).

170.	Hoffmann C, Berganza C, Zhang J. Cold Atmospheric Plasma: methods of production and application in dentistry and oncology. Med Gas Res. 2013;3(1):21-.

171.	Lu X, Naidis G, Laroussi M, Reuter S, Graves D, Ostrikov K. Reactive species in non-equilibrium atmospheric-pressure plasmas: Generation, transport, and biological effects. Physics Reports. 2016;630:1-84.

172.	Bárdos L, Baránková H. Plasma processes at atmospheric and low pressures. Vacuum. 2008;83(3):522-7.

173.	Domonkos M, Tichá P, Trejbal J, Demo P. Applications of Cold Atmospheric Pressure Plasma Technology in Medicine, Agriculture and Food Industry. Applied Sciences. 2021;11(11):4809.

174.	Jungbauer G, Moser D, Müller S, Pfister W, Sculean A, Eick S. The Antimicrobial Effect of Cold Atmospheric Plasma against Dental Pathogens-A Systematic Review of In-Vitro Studies. Antibiotics (Basel). 2021;10(2):211.

175.	Laroussi M. Plasma medicine: a brief introduction. Plasma. 2018;1(1):47-60.

176.	Laroussi M. Sterilization of contaminated matter with an atmospheric pressure plasma. IEEE Transactions on Plasma Science. 1996;24(3):1188-91.

177.	Gherardi M, Tonini R, Colombo V. Plasma in Dentistry: Brief History and Current Status. Trends Biotechnol. 2018;36(6):583-5.

178.	Gaur N, Kurita H, Oh J-S, Miyachika S, Ito M, Mizuno A, et al. On cold atmospheric-pressure plasma jet induced DNA damage in cells. Journal of Physics D: Applied Physics. 2020;54(3):035203.

179.	Laroussi M. Cold plasma in medicine and healthcare: The new frontier in low temperature plasma applications. Frontiers in Physics. 2020;8:74.

180.	Smolková B, Frtús A, Uzhytchak M, Lunova M, Kubinová Š, Dejneka A, et al. Critical Analysis of Non-Thermal Plasma-Driven Modulation of Immune Cells from Clinical Perspective. Int J Mol Sci. 2020;21(17):6226.

181.	Gay-Mimbrera J, García MC, Isla-Tejera B, Rodero-Serrano A, García-Nieto AV, Ruano J. Clinical and Biological Principles of Cold Atmospheric Plasma Application in Skin Cancer. Adv Ther. 2016;33(6):894-909.

182.	Siemens W. Ueber die elektrostatische Induction und die Verzögerung des Stroms in Flaschendrähten. Annalen der Physik. 1857;178(9):66-122.

183.	Kogelschatz U. Dielectric-Barrier Discharges: Their History, Discharge Physics, and Industrial Applications. Plasma Chemistry and Plasma Processing. 2003;23(1):1-46.

184.	Von Woedtke T, Schmidt A, Bekeschus S, Wende K, Weltmann K-D. Plasma Medicine: A Field of Applied Redox Biology. In Vivo. 2019;33(4):1011-26.
185.	Von Woedtke T, Reuter S, Masur K, Weltmann K-D. Plasmas for medicine. Physics Reports. 2013;530(4):291-320.
186.	Conrads H, Schmidt M. Plasma generation and plasma sources. Plasma Sources Science and Technology. 2000;9(4):441.
187.	Bekeschus S, Schmidt A, Weltmann K-D, von Woedtke T. The plasma jet kINPen – A powerful tool for wound healing. Clinical Plasma Medicine. 2016;4(1):19-28.
188.	Shimizu T, Steffes B, Pompl R, Jamitzky F, Bunk W, Ramrath K, et al. Characterization of microwave plasma torch for decontamination. Plasma Processes and Polymers. 2008;5(6):577-82.
189.	Arndt S, Schmidt A, Karrer S, von Woedtke T. Comparing two different plasma devices kINPen and Adtec SteriPlas regarding their molecular and cellular effects on wound healing. Clinical Plasma Medicine. 2018;9:24-33.
190.	Görlach A, Bertram K, Hudecova S, Krizanova O. Calcium and ROS: A mutual interplay. Redox Biol. 2015;6:260-71.
191.	Moncada S, Erusalimsky JD. Does nitric oxide modulate mitochondrial energy generation and apoptosis? Nat Rev Mol Cell Biol. 2002;3(3):214-20.
192.	Semmler ML, Bekeschus S, Schäfer M, Bernhardt T, Fischer T, Witzke K, et al. Molecular Mechanisms of the Efficacy of Cold Atmospheric Pressure Plasma (CAP) in Cancer Treatment. Cancers (Basel). 2020;12(2):269.
193.	Kim SJ, Chung TH. Cold atmospheric plasma jet-generated RONS and their selective effects on normal and carcinoma cells. Scientific Reports. 2016;6(1):20332.
194.	Gonzalez ACdO, Costa TF, Andrade ZdA, Medrado ARAP. Wound healing - A literature review. An Bras Dermatol. 2016;91(5):614-20.
195.	Dunnill C, Patton T, Brennan J, Barrett J, Dryden M, Cooke J, et al. Reactive oxygen species (ROS) and wound healing: the functional role of ROS and emerging ROS-modulating technologies for augmentation of the healing process. International wound journal. 2017;14(1):89-96.
196.	Schäfer M, Werner S. Oxidative stress in normal and impaired wound repair. Pharmacol Res. 2008;58(2):165-71.
197.	Bylund J, Björnsdottir H, Sundqvist M, Karlsson A, Dahlgren C. Measurement of respiratory burst products, released or retained, during activation of professional phagocytes. Methods Mol Biol. 2014;1124:321-38.
198.	McIntosh C. Impaired Wound Healing in the Diabetic Foot. Wounds Essentials. 2017.
199.	McIntosh C, Ivory JD, Gethin G. Managing wound exudate in diabetic foot ulcers. Diabetic Foot Journal. 2019;22(1).
200.	Isbary G, Zimmermann JL, Shimizu T, Li YF, Morfill GE, Thomas HM, et al. Non-thermal plasma—More than five years of clinical experience. Clinical Plasma Medicine. 2013;1(1):19-23.
201.	Fathollah S, Mirpour S, Mansouri P, Dehpour AR, Ghoranneviss M, Rahimi N, et al. Investigation on the effects of the atmospheric pressure plasma on wound healing in diabetic rats. Scientific reports. 2016;6(1):1-9.
202.	Zimmermann J, Shimizu T, Schmidt H, Li Y, Morfill G, Isbary G. Test for bacterial resistance build-up against plasma treatment. New Journal of Physics. 2012;14(7):073037.
203.	Arndt S, Unger P, Wacker E, Shimizu T, Heinlin J, Li Y-F, et al. Cold atmospheric plasma (CAP) changes gene expression of key molecules of the wound healing machinery and improves wound healing in vitro and in vivo. PloS one. 2013;8(11):e79325-e.
204.	Isbary G, Morfill G, Schmidt HU, Georgi M, Ramrath K, Heinlin J, et al. A first prospective randomized controlled trial to decrease bacterial load using cold atmospheric argon plasma on chronic wounds in patients. British Journal of Dermatology. 2010;163(1):78-82.
205.	Hong S-H, Szili EJ, Fenech M, Gaur N, Short RD. Genotoxicity and cytotoxicity of the plasma jet-treated medium on lymphoblastoid WIL2-NS cell line using the cytokinesis block micronucleus cytome assay. Scientific Reports. 2017;7(1):3854.
206.	Szili EJ, Oh J-S, Fukuhara H, Bhatia R, Gaur N, Nguyen CK, et al. Modelling the helium plasma jet delivery of reactive species into a 3D cancer tumour. Plasma Sources Science and Technology. 2017;27(1):014001.

207.    Weidinger A, Kozlov AV. Biological Activities of Reactive Oxygen and Nitrogen Species: Oxidative Stress versus Signal Transduction. Biomolecules. 2015;5(2):472-84.

208.    Schulz E, Wenzel P, Münzel T, Daiber A. Mitochondrial redox signaling: Interaction of mitochondrial reactive oxygen species with other sources of oxidative stress. Antioxid Redox Signal. 2014;20(2):308-24.

209.    Bashan N, Kovsan J, Kachko I, Ovadia H, Rudich A. Positive and negative regulation of insulin signaling by reactive oxygen and nitrogen species. Physiol Rev. 2009;89(1):27-71.

210.    Khlyustova A, Labay C, Machala Z, Ginebra M-P, Canal C. Important parameters in plasma jets for the production of RONS in liquids for plasma medicine: A brief review. Frontiers of Chemical Science and Engineering. 2019;13(2):238-52.

211.    Ghimire B, Szili E, Patenall B, Lamichhane P, Gaur N, Robson A, et al. Enhancement of hydrogen peroxide production from an atmospheric pressure argon plasma jet and implications to the antibacterial activity of plasma activated water. Plasma Sources Science and Technology. 2021.

212.    Kolpaková A, Kudrna P, Tichý M, editors. Study of plasma system by OES (optical emission spectroscopy). Proc of 20th Annual Conference of Doctoral Students; 2011.

213.    Bryan NS, Grisham MB. Methods to detect nitric oxide and its metabolites in biological samples. Free Radic Biol Med. 2007;43(5):645-57.

214.    Laroussi M, Lu X, Kolobov V, Arslanbekov R. Power consideration in the pulsed dielectric barrier discharge at atmospheric pressure. Journal of Applied Physics. 2004;96(5):3028-30.

215.    Pipa AV, Brandenburg R. The equivalent circuit approach for the electrical diagnostics of dielectric barrier discharges: The classical theory and recent developments. Atoms. 2019;7(1):14.

216.    Kim YH, Hong YJ, Baik KY, Kwon GC, Choi JJ, Cho GS, et al. Measurement of reactive hydroxyl radical species inside the biosolutions during non-thermal atmospheric pressure plasma jet bombardment onto the solution. Plasma Chemistry and Plasma Processing. 2014;34(3):457-72.

217.    Thiyagarajan M, Sarani A, Nicula C. Optical emission spectroscopic diagnostics of a non-thermal atmospheric pressure helium-oxygen plasma jet for biomedical applications. Journal of Applied Physics. 2013;113(23):233302.

218.    Fornera S, Walde P. Spectrophotometric quantification of horseradish peroxidase with o-phenylenediamine. Analytical Biochemistry. 2010;407(2):293-5.

219.    Julák J, Hujacová A, Scholtz V, Khun J, Holada K. Contribution to the Chemistry of Plasma-Activated Water. Plasma Physics Reports. 2018;44:125.

220.    Kleinbongard P, Rassaf T, Dejam A, Kerber S, Kelm M. Griess method for nitrite measurement of aqueous and protein-containing samples. Methods Enzymol. 2002;359:158-68.

221.    Mai-Prochnow A, Zhou R, Zhang T, Ostrikov K, Mugunthan S, Rice SA, et al. Interactions of plasma-activated water with biofilms: inactivation, dispersal effects and mechanisms of action. npj Biofilms and Microbiomes. 2021;7(1):11.

222.    Zhou R, Zhou R, Prasad K, Fang Z, Speight R, Bazaka K, et al. Cold atmospheric plasma activated water as a prospective disinfectant: the crucial role of peroxynitrite. Green Chemistry. 2018;20(23):5276-84.

223.    Liu DX, Liu ZC, Chen C, Yang AJ, Li D, Rong MZ, et al. Aqueous reactive species induced by a surface air discharge: Heterogeneous mass transfer and liquid chemistry pathways. Sci Rep. 2016;6:23737.

224.    Gwak HC, Han SH, Lee J, Park S, Sung KS, Kim HJ, et al. Efficacy of a povidone-iodine foam dressing (Betafoam) on diabetic foot ulcer. Int Wound J. 2020;17(1):91-9.

225.    Miró-Canturri A, Ayerbe-Algaba R, Smani Y. Drug Repurposing for the Treatment of Bacterial and Fungal Infections. Frontiers in Microbiology. 2019;10(41).

226.    Gottardi W, Block S. Disinfection, sterilization and preservation. Lea & Febiger: Philadelphia. 1991:152-65.

227.    Vermeulen H, Westerbos SJ, Ubbink DT. Benefit and harm of iodine in wound care: a systematic review. Journal of Hospital Infection. 2010;76(3):191-9.

228.    Bigliardi PL, Alsagoff SAL, El-Kafrawi HY, Pyon J-K, Wa CTC, Villa MA. Povidone iodine in wound healing: A review of current concepts and practices. International Journal of Surgery. 2017;44:260-8.

229.    Eggers M. Infectious Disease Management and Control with Povidone Iodine. Infectious Diseases and Therapy. 2019;8(4):581-93.

230.     McDonnell G, Russell AD. Antiseptics and disinfectants: activity, action, and resistance. Clin Microbiol Rev. 1999;12(1):147-79.
231.     McDonnell G. The Use of Hydrogen Peroxide for Disinfection and Sterilization Applications. PATAI'S Chemistry of Functional Groups. p. 1-34.
232.     Zhu G, Wang Q, Lu S, Niu Y. Hydrogen Peroxide: A Potential Wound Therapeutic Target? Med Princ Pract. 2017;26(4):301-8.
233.     Zhang Z, Li T, Liu Y, Shang F, Chen B, Hu Y, et al. Supramolecular hydrogel of poly (vinyl alcohol)/chitosan: A dual cross-link design. Advances in Polymer Technology. 2018;37(6):2186-94.
234.     Lee KY, Mooney DJ. Hydrogels for tissue engineering. Chem Rev. 2001;101(7):1869-79.
235.     Parhi R. Cross-Linked Hydrogel for Pharmaceutical Applications: A Review. Adv Pharm Bull. 2017;7(4):515-30.
236.     Zubko EI, Zubko MK. Co-operative inhibitory effects of hydrogen peroxide and iodine against bacterial and yeast species. BMC Research Notes. 2013;6(1):272.
237.     Ulivieri S, Toninelli S, Petrini C, Giorgio A, Oliveri G. Prevention of post-operative infections in spine surgery by wound irrigation with a solution of povidone-iodine and hydrogen peroxide. Arch Orthop Trauma Surg. 2011;131(9):1203-6.
238.     Mitsugi F, Wago M, Sakamoto R, Nishida K, Kawasaki T. Influence of Retrogradation on KI–Starch Visualization of Reactive Oxygen Species Emitted by Plasma Jets. IEEE Transactions on Plasma Science. 2021;49(7):2141-7.
239.     Kida D, Gładysz O, Szulc M, Zborowski J, Junka A, Janeczek M, et al. Development and evaluation of a polyvinylalcohol-cellulose derivative-based film with povidone-iodine predicted for wound treatment. Polymers. 2020;12(6):1271.
240.     Papadopoulou EL, Valentini P, Mussino F, Pompa PP, Athanassiou A, Bayer IS. Antibacterial bioelastomers with sustained povidone-iodine release. Chemical Engineering Journal. 2018;347:19-26.
241.     Narayanaswamy R, Torchilin VP. Hydrogels and Their Applications in Targeted Drug Delivery. Molecules. 2019;24(3).
242.     Hoare TR, Kohane DS. Hydrogels in drug delivery: Progress and challenges. Polymer. 2008;49(8):1993-2007.
243.     Zhang Y, Ye L, Cui M, Yang B, Li J, Sun H, et al. Physically crosslinked poly(vinyl alcohol)–carrageenan composite hydrogels: pore structure stability and cell adhesive ability. RSC Advances. 2015;5(95):78180-91.
244.     Felfel RM, Gideon-Adeniyi MJ, Zakir Hossain KM, Roberts GAF, Grant DM. Structural, mechanical and swelling characteristics of 3D scaffolds from chitosan-agarose blends. Carbohydr Polym. 2019;204:59-67.
245.     Rivera-Hernández G, Antunes-Ricardo M, Martínez-Morales P, Sánchez ML. Polyvinyl alcohol based-drug delivery systems for cancer treatment. International Journal of Pharmaceutics. 2021;600:120478.
246.     Gao P, Nie X, Zou M, Shi Y, Cheng G. Recent advances in materials for extended-release antibiotic delivery system. The Journal of Antibiotics. 2011;64(9):625-34.
247.     Li J, Mooney DJ. Designing hydrogels for controlled drug delivery. Nat Rev Mater. 2016;1(12):16071.
248.     Pandey S, Mishra SB. Chemical Nanosensors for Monitoring Environmental Pollution. Application of Nanotechnology in Water Research2014. p. 309-32.
249.     Tavakoli S, Klar AS. Advanced Hydrogels as Wound Dressings. Biomolecules. 2020;10(8):1169.
250.     Balakrishnan B, Mohanty M, Umashankar PR, Jayakrishnan A. Evaluation of an in situ forming hydrogel wound dressing based on oxidized alginate and gelatin. Biomaterials. 2005;26(32):6335-42.
251.     Schreml S, Szeimies RM, Prantl L, Karrer S, Landthaler M, Babilas P. Oxygen in acute and chronic wound healing. Br J Dermatol. 2010;163(2):257-68.
252.     Hopf HW, Gibson JJ, Angeles AP, Constant JS, Feng JJ, Rollins MD, et al. Hyperoxia and angiogenesis. Wound Repair Regen. 2005;13(6):558-64.
253.     Kimmel HM, Grant A, Ditata J. The Presence of Oxygen in Wound Healing. Wounds. 2016;28(8):264-70.

254.     Estarabadi H, Atyabi SA, Tavakkoli S, Noormohammadi Z, Gholami MR, Ghiaseddin A, et al. Cold atmospheric plasma induced genotoxicity and cytotoxicity in esophageal cancer cells. Mol Biol Rep. 2021;48(2):1323-33.

255.     Yan D, Xu W, Yao X, Lin L, Sherman JH, Keidar M. The Cell Activation Phenomena in the Cold Atmospheric Plasma Cancer Treatment. Scientific Reports. 2018;8(1):15418.

256.     Oh J-S, Szili EJ, Hong S-H, Gaur N, Ohta T, Hiramatsu M, et al. Mass spectrometry analysis of the real-time transport of plasma-generated ionic species through an agarose tissue model target. Journal of Photopolymer Science and Technology. 2017;30(3):317-23.

257.     Fahr A, Liu X. Drug delivery strategies for poorly water-soluble drugs. Expert Opin Drug Deliv. 2007;4(4):403-16.

258.     Larrañeta E, Stewart S, Ervine M, Al-Kasasbeh R, Donnelly RF. Hydrogels for Hydrophobic Drug Delivery. Classification, Synthesis and Applications. J Funct Biomater. 2018;9(1):13.

259.     Andrews JM. Determination of minimum inhibitory concentrations. Journal of Antimicrobial Chemotherapy. 2001;48(suppl_1):5-16.

260.     Costa RA, Ortega DB, Fulgêncio DLA, Costa FS, Araújo TF, Barreto CC. Checkerboard testing method indicates synergic effect of pelgipeptins against multidrug resistant Klebsiella pneumoniae. Biotechnology Research and Innovation. 2019;3(1):187-91.

261.     Nassar MSM, Hazzah WA, Bakr WMK. Evaluation of antibiotic susceptibility test results: how guilty a laboratory could be? Journal of the Egyptian Public Health Association. 2019;94(1):4.

262.     Miles AA, Misra SS, Irwin JO. The estimation of the bactericidal power of the blood. J Hyg (Lond). 1938;38(6):732-49.

263.     Loo AEK, Wong YT, Ho R, Wasser M, Du T, Ng WT, et al. Effects of Hydrogen Peroxide on Wound Healing in Mice in Relation to Oxidative Damage. PLOS ONE. 2012;7(11):e49215.

264.     Roy S, Khanna S, Nallu K, Hunt TK, Sen CK. Dermal wound healing is subject to redox control. Molecular therapy. 2006;13(1):211-20.

265.     Oh J-S, Szili EJ, Ito S, Hong S-H, Gaur N, Furuta H, et al. Slow Molecular Transport of Plasma-Generated Reactive Oxygen and Nitrogen Species and O$_2$ through Agarose as a Surrogate for Tissue. 2015;5(2-4):125-43.

266.     Patenall B. Novel Applications of Cold Atmospheric Plasma for the Decontamination of Bacterial Biofilm-Associated Wound Infection: University of Bath; 2021.

267.     Mai-Prochnow A, Clauson M, Hong J, Murphy AB. Gram positive and Gram negative bacteria differ in their sensitivity to cold plasma. Scientific reports. 2016;6:38610-.

268.     Hu D, Wang L. Physical and antibacterial properties of polyvinyl alcohol films reinforced with quaternized cellulose. Journal of Applied Polymer Science. 2016;133(25).

269.     World Health Organisation. Alternative drinking-water disinfectants: bromine, iodine and silver2018 21st March 2021. Available from: https://www.who.int/water_sanitation_health/publications/iodine-02032018.pdf?ua=1.

270.     El Kadri H, Costello KM, Thomas P, Wantock T, Sandison G, Harle T, et al. The antimicrobial efficacy of remote cold atmospheric plasma effluent against single and mixed bacterial biofilms of varying age. Food Research International. 2021;141:110126.

271.     Patenall BL, Hathaway H, Sedgwick AC, Thet NT, Williams GT, Young AE, et al. Limiting *Pseudomonas aeruginosa* Biofilm Formation Using Cold Atmospheric Pressure Plasma. 2018;8(3):269-77.

272.     Kvam E, Davis B, Mondello F, Garner AL. Nonthermal atmospheric plasma rapidly disinfects multidrug-resistant microbes by inducing cell surface damage. Antimicrob Agents Chemother. 2012;56(4):2028-36.

273.     Federation. I. Time to act: diabetes and foot care. Brussels: International Diabetes Federation. 2005.

274.     Hartemann-Heurtier A, Robert J, Jacqueminet S, Ha Van G, Golmard J, Jarlier V, et al. Diabetic foot ulcer and multidrug-resistant organisms: risk factors and impact. Diabetic Medicine. 2004;21(7):710-5.

275.     Shahi SK, Kumar A. Isolation and Genetic Analysis of Multidrug Resistant Bacteria from Diabetic Foot Ulcers. Frontiers in Microbiology. 2016;6(1464).

276.    Keidar M, Walk R, Shashurin A, Srinivasan P, Sandler A, Dasgupta S, et al. Cold plasma selectivity and the possibility of a paradigm shift in cancer therapy. Br J Cancer. 2011;105(9):1295-301.
277.    Emmert S, Brehmer F, Hänßle H, Helmke A, Mertens N, Ahmed R, et al. Atmospheric pressure plasma in dermatology: Ulcus treatment and much more. Clinical Plasma Medicine. 2013;1(1):24-9.
278.    Fridman G, Peddinghaus M, Balasubramanian M, Ayan H, Fridman A, Gutsol A, et al. Blood coagulation and living tissue sterilization by floating-electrode dielectric barrier discharge in air. Plasma Chemistry and plasma processing. 2006;26(4):425-42.
279.    Kong MG, Kroesen G, Morfill G, Nosenko T, Shimizu T, Van Dijk J, et al. Plasma medicine: an introductory review. new Journal of Physics. 2009;11(11):115012.
280.    Gardner SE, Hillis SL, Heilmann K, Segre JA, Grice EA. The Neuropathic Diabetic Foot Ulcer Microbiome Is Associated With Clinical Factors. Diabetes. 2013;62(3):923-30.
281.    Sadeghpour Heravi F, Zakrzewski M, Vickery K, D GA, Hu H. Bacterial Diversity of Diabetic Foot Ulcers: Current Status and Future Prospectives. J Clin Med. 2019;8(11).
282.    Malone M, Gosbell IB, Dickson HG, Vickery K, Espedido BA, Jensen SO. Can molecular DNA-based techniques unravel the truth about diabetic foot infections? Diabetes Metab Res Rev. 2017;33(1).
283.    Mai-Prochnow A, Clauson M, Hong J, Murphy AB. Gram positive and Gram negative bacteria differ in their sensitivity to cold plasma. Sci Rep. 2016;6:38610.
284.    Ozer B, Kalaci A, Semerci E, Duran N, Davul S, Yanat A. Infections and aerobic bacterial pathogens in diabetic foot. African Journal of Microbiology Research. 2010;4(20):2153-60.
285.    Kwon KT, Armstrong DG. Microbiology and Antimicrobial Therapy for Diabetic Foot Infections. Infect Chemother. 2018;50(1):11-20.
286.    Clément M-V, Pervaiz S. Intracellular superoxide and hydrogen peroxide concentrations: a critical balance that determines survival or death. Redox Report. 2001;6(4):211-4.
287.    Dubey KK, Indu, Sharma M. Reprogramming of antibiotics to combat antimicrobial resistance. Arch Pharm (Weinheim). 2020;353(11):e2000168.
288.    Weast RC, Astle MJ, Beyer WHe. CRC Handbook of chemistry and physics. Boca Raton: CRC Press; 1983.
289.    Taylor GR, Butler M. A comparison of the virucidal properties of chlorine, chlorine dioxide, bromine chloride and iodine. J Hyg (Lond). 1982;89(2):321-8.

# 8 Appendix

## 8.1 CAP jet
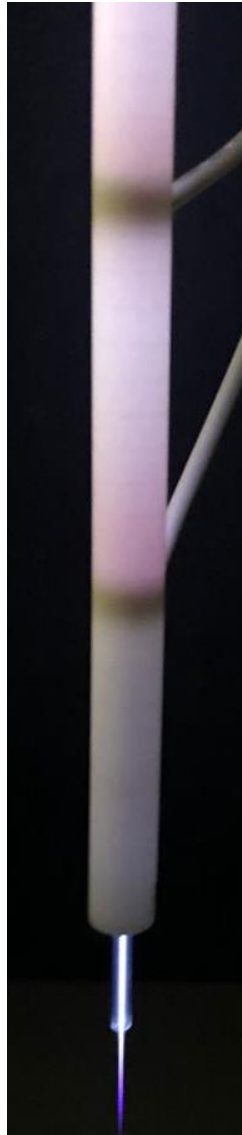


*Figure 8.1: CAP jet ignited under operating conditions. $V_{p-p}$ = 6.96 kV at 23.5 kHz frequency and Ar delivered at 1 SLPM.*

## 8.2 pH

### 8.2.1 PAW
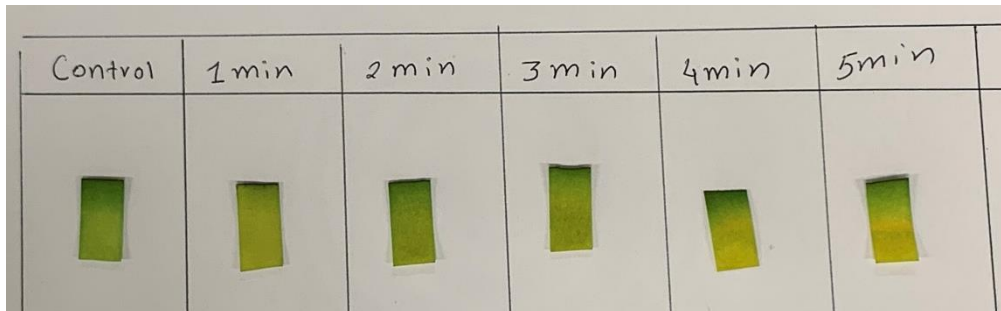


*Figure 8.2: pH of PAW.*



*Figure 8.3: pH Colour Chart. Minimum Inhibitory Concentration*

## 8.2.2 PVP-I

# 8.3 Minimum Inhibitory Concentration
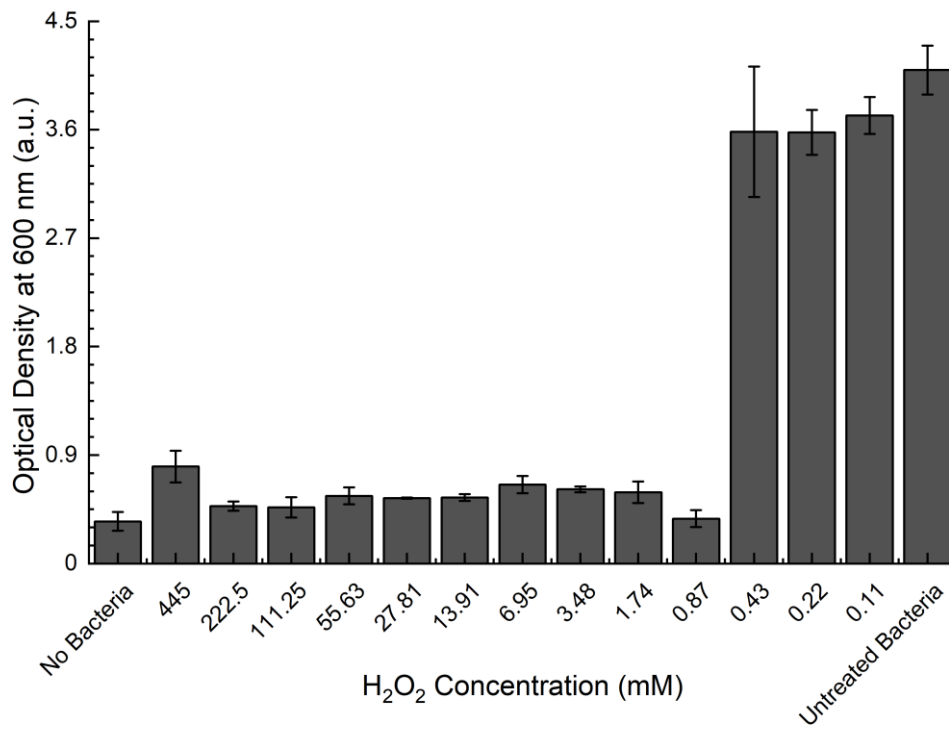
## 8.3.1 H₂O₂ and H560 MIC Optical Density



*Figure 8.4: Optical Density at 600 nm of H560 and H₂O₂ at a variety of concentrations to determine the MIC.*

## 8.3.2  PVP-I and H560 MIC Optical Density
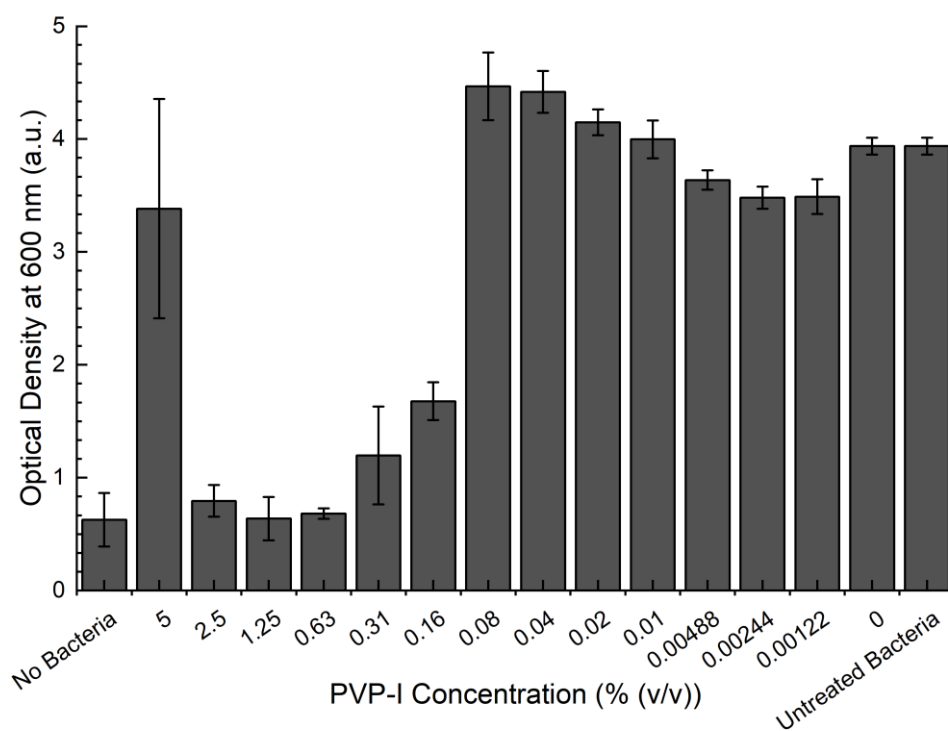


*Figure 8.5 Optical Density at 600 nm of H560 and PVP-I at a variety of percentages for MIC determination.*

## 8.4 Checkerboard Synergy Assay

| A | 50 | 25 | 12.5 | 6.25 | 3.13 | 1.56 | 0.78 | 0.39 | 0.19 | 10 | PVPI MIC | Control |
|---|---|---|---|---|---|---|---|---|---|---|---|---|
| 2.5 | 2.41 | 1.583 | 1.399 | 1.039 | 0.911 | 0.794 | 0.674 | 0.603 | 0.519 | 0.456 | 0.484 | |
| 1.25 | 0.759 | 0.664 | 0.513 | 0.421 | 0.429 | 0.378 | 0.419 | 0.485 | 0.499 | 0.374 | 0.377 | 4.005 |
| 0.625 | 0.351 | 0.603 | 0.55 | 0.497 | 0.54 | 0.537 | 0.592 | 0.549 | 0.363 | 0.4 | 0.409 | 4.021 |
| 0.3125 | 0.479 | 0.562 | 0.561 | 0.502 | 0.48 | 0.513 | 0.494 | 0.471 | 0.398 | 0.434 | 0.59 | 4.014 |
| 0.156 | 0.448 | 0.617 | 0.514 | 0.525 | 0.491 | 0.645 | 1.144 | 1.457 | 1.268 | 1.501 | 1.67 | 0.334 |
| 0.078 | 0.314 | 0.477 | 0.438 | 0.508 | 1.743 | 3.943 | 4.103 | 3.813 | 4.12 | 4.258 | 4.272 | 0.417 |
| 0.039 | 0.545 | 0.36 | 0.398 | 0.411 | 3.922 | 4.111 | 4.106 | 3.941 | 4.111 | 4.284 | 4.164 | 0.257 |
| H2O2 MIC | 0.31 | 0.356 | 0.391 | 3.447 | 4.108 | 4.063 | 4.131 | 3.946 | 4.086 | 4.072 | 3.913 | |

| B | 50 | 25 | 12.5 | 6.25 | 3.13 | 1.56 | 0.78 | 0.39 | 0.19 | 10 | PVPI MIC | Control |
|---|---|---|---|---|---|---|---|---|---|---|---|---|
| 2.5 | 0.945 | 0.633 | 0.665 | 0.499 | 0.613 | 0.885 | 0.697 | 0.769 | 0.783 | 0.778 | 0.603 | |
| 1.25 | 0.557 | 0.525 | 0.447 | 0.394 | 0.426 | 0.508 | 0.456 | 0.461 | 0.462 | 0.381 | 0.427 | 3.858 |
| 0.625 | 0.416 | 0.428 | 0.513 | 0.492 | 0.487 | 0.523 | 0.479 | 0.513 | 0.514 | 0.401 | 0.449 | 4.025 |
| 0.3125 | 0.41 | 0.444 | 0.489 | 0.484 | 0.545 | 0.538 | 0.482 | 0.427 | 0.424 | 0.38 | 0.385 | 3.988 |
| 0.156 | 0.409 | 0.449 | 0.47 | 0.472 | 0.581 | 0.894 | 1.423 | 1.537 | 1.525 | 1.525 | 1.8 | 0.35 |
| 0.078 | 0.425 | 0.39 | 0.408 | 0.453 | 1.022 | 4.032 | 3.803 | 3.699 | 3.272 | 3.36 | 3.599 | 0.48 |
| 0.039 | 0.392 | 0.445 | 0.406 | 0.518 | 3.473 | 4.109 | 4.048 | 3.913 | 3.954 | 4.009 | 4.034 | 0.218 |
| H2O2 MIC | 0.482 | 0.463 | 0.524 | 3.426 | 4.109 | 4.168 | 4.199 | 4.106 | 4.235 | 4.352 | 4.057 | |

| C | 50 | 25 | 12.5 | 6.25 | 3.13 | 1.56 | 0.78 | 0.39 | 0.19 | 10 | PVPI MIC | Control |
|---|---|---|---|---|---|---|---|---|---|---|---|---|
| 2.5 | 2.42 | 1.956 | 1.416 | 1.108 | 0.877 | 0.737 | 0.676 | 0.605 | 0.561 | 0.589 | 0.606 | |
| 1.25 | 0.821 | 0.666 | 0.611 | 0.43 | 0.388 | 0.538 | 0.414 | 0.456 | 0.396 | 0.379 | 0.491 | 4.088 |
| 0.625 | 0.38 | 0.429 | 0.391 | 0.438 | 0.467 | 0.505 | 0.506 | 0.527 | 0.472 | 0.442 | 0.522 | 4.182 |
| 0.3125 | 0.414 | 0.424 | 0.429 | 0.527 | 0.477 | 0.52 | 0.512 | 0.459 | 0.487 | 0.571 | 0.53 | 4.03 |
| 0.156 | 0.418 | 0.426 | 0.437 | 0.452 | 0.5 | 0.597 | 1.6 | 1.392 | 1.567 | 1.569 | 1.685 | 0.352 |
| 0.078 | 0.387 | 0.434 | 0.48 | 0.426 | 0.697 | 1.775 | 4.153 | 3.947 | 4.049 | 3.998 | 3.997 | 0.38 |
| 0.039 | 0.353 | 0.383 | 0.422 | 0.413 | 2.169 | 4.107 | 4.002 | 4.12 | 4.029 | 4.164 | 3.991 | 0.301 |
| H2O2 MIC | 0.5 | 0.474 | 0.427 | 3.557 | 4.561 | 4.501 | 4.254 | 4.351 | 4.085 | 4.362 | 1.822 | |

*Figure 8.6: Checkerboard Synergy Assay Absorbance Values against planktonic H560 with a combination of $H_2O_2$ and PVP-I. Blue boxes represent sub-MIC concentrations of $H_2O_2$ and PVP-I in combination. Green boxes represent where the MIC for each drug lies on its own. Yellow boxes represent sub-MIC concentration in combination but without effect. A-C represent three biological replicates.*

## 8.5  Kirby-Bauer Assay

### 8.5.1  Effect of Povidone-Iodine Concentration on H560
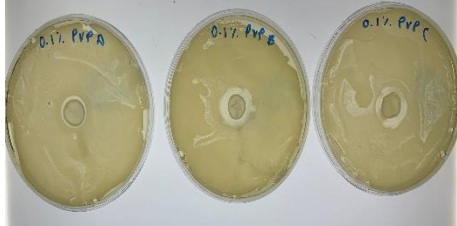
| PVP-I Concentration | Untreated | Plasma Treated |
|---|---|---|
| 0% |  |  |
| 0.1% |  |  |
| 1% |  |  |
| 10% |  |  |

*Figure 8.7: Kirby-Bauer Assay studying the effect of PVP-I concentration on H560. Table shows the agar plates following incubation with triplicate results.*

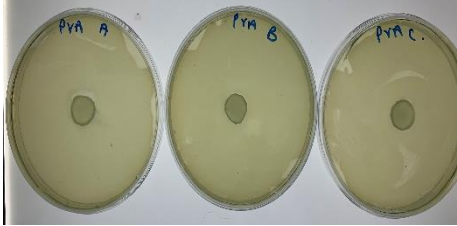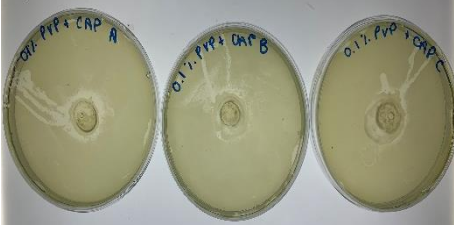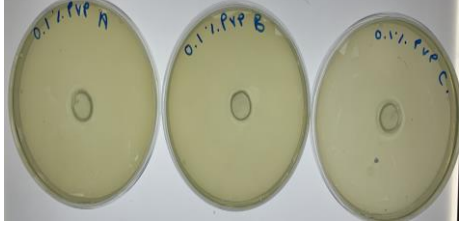## 8.5.2  Effect of Povidone-Iodine Concentration on PAO1
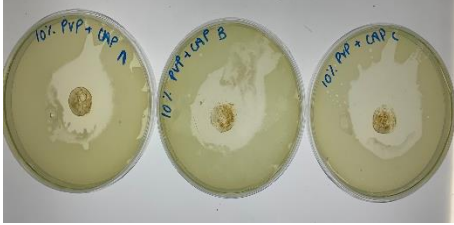
| PVP-I Concentration | Untreated | Plasma Treated |
|---|---|---|
| 0% |  |  |
| 0.1% |  |  |
| 1% |  |  |
| 10% |  |  |

*Figure 8.8: Kirby-Bauer Assay studying the effect of PVP-I concentration on PAO1. Table shows the agar plates following incubation with triplicate results.*

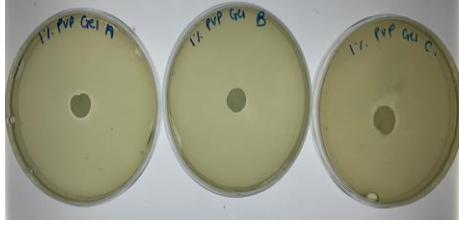## 8.5.3 Effect of Gas Flow on PAO1

| PVP-I Concentration | Without Gas Flow | Gas Flow |
|---|---|---|
| 0.1% | | |
| 1% | | |
| 10% | | |



*Figure 8.9: Kirby-Bauer Assay studying the effect of gas flow on PAO1. Table shows the agar plates following incubation with triplicate results.*